2022

A biologically meaningful evaluation of phenological responses to climate change

Steer, Nicola Carol

Copyright Statement

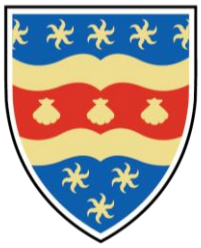

UNIVERSITY OF PLYMOUTH

A BIOLOGICALLY MEANINGFUL EVALUATION OF PHENOLOGICAL RESPONSES TO CLIMATE CHANGE

By

NICOLA CAROL STEER

A thesis submitted to the University of Plymouth in partial fulfilment for the degree of

DOCTOR OF PHILOSOPHY

School of Biological and Marine Sciences

November 2021

For Adeline

Acknowledgements

First and foremost, to my supervisor Dr Miguel Franco. I cannot thank you enough. You are the most knowledgeable person I have ever had the good fortune to meet and you are also one of the kindest, patient and most humble. Your support has been invaluable and we both know that I would not have made it through this without your unwavering belief in me. You gave me confidence when I had lost it in myself and your constructive feedback has made me a better scientist. It was, and will always be, an honour and a privilege to have been your student.

Thank you to Dr Paul Ramsay for it never being good enough. You taught me how to be a better writer and I am grateful for your guidance and impeccably high standards. Thank you also to Dr Chiara Boschetti for being a supervisor and a friend. You gave me a push when I needed it and a hug when I needed that too!

Thank you to the University of Plymouth for funding the studentship and to all of the people and organisations that contributed data, knowledge and expertise to this PhD: Nathan Eastwood, Paola Garcia-Meneses, Jamie Sykes, Pierre Helaouet, Martin Edwards, Ecuadorian Ministry of Environment, La Reserva Ecológica El Ángel, Asociación Ecosistemas Andinos, Huascarán National Park, Marine Biological Association and Japanese Meteorological Agency.

On a more personal note, I would like to express my gratitude to my family and friends. To my husband Lee, thank you for always believing in me and for supporting me on this journey. Thank you also for giving me the time I needed to finish writing after the birth of our beautiful daughter, Adeline. I definitely could not have finished this without you.

Thank you to my parents for supporting my crazy decision to become a mature student and even crazier decision to become a doctoral candidate. And finally thank you to the wonderful people I have met along the way. Emily Churchill, you were the best housemate/surrogate daughter anyone could wish for, Felicity Wynne, your friendship helped me get through some of the hardest times, and Mary Lane, what would I have done without your constant words of encouragement and cemetery walks! I will cherish your friendships always.

Author's declaration

At no time during the registration for the degree of Doctor of Philosophy has the author been registered for any other University award without prior agreement of the Doctoral College Quality Sub-Committee.

Work submitted for this research degree at the University of Plymouth has not formed part of any other degree either at the University of Plymouth or at another establishment.

During the course of this research degree a programme of advanced study was undertaken, which included: Postgraduate Research Skills and Methods module, R Statistics Essential Training (Lynda.com), An Introduction to R, Presenting at Conferences, Research Methods (STEM), An Introduction to Endnote, Presenting to an Audience 1 & 2, Supporting Assessment, Learning & Teaching (SALT), Postgraduate Writing Workshop, Introduction to GIS, GIS Users Workshop, Preparing for the Viva.

Qualifications gained:

Postgraduate Diploma in Academic Practice: Introduction to Teaching and Learning, University of Plymouth, November 2016.

Papers published from the PhD:

Steer, N.C., Ramsay, P.M. & Franco, M. (2019) nlstimedist: An R package for the biologically meaningful quantification of unimodal phenology distributions. *Methods in Ecology and Evolution,* **10,** 1934-1940. DOI: https://doi.org/10.1111/2041-210X.13293

Conferences attended:

British Ecological Society. Bringing the New UKCP18 Climate Projections into Ecology: 18th March 2019. MET Office, Exeter, UK.

British Ecological Society annual meeting: 16-19th December 2018. Birmingham, UK. Oral presentation.

School of Biological and Marine Sciences Showcase: 2nd November 2018. University of Plymouth, UK. Poster presentation.

Climate Change Biogeography. International Biogeography Society meeting: 20-24th March 2018. Évora, Portugal. Oral presentation.

School of Biological and Marine Sciences Showcase: 9th June 2017. University of Plymouth, UK. Poster presentation.

Word count of main body of thesis: 30,027

Signed: 

Date: 29th November 2021

Nicola Carol Steer: *A biologically meaningful evaluation of phenological responses to climate change.*

Abstract

Phenological change is widely regarded as an important biological indicator of contemporary climate change. Increasing global temperatures have been identified as driving changes in the timing of key life-cycle events across a wide range of organisms. Estimates of phenological change are often based on single measure of phenology, such as the date of the first flower to bloom or the first migrant of the season to arrive. However, this approach is unlikely to be representative of the population as a whole and ignores important information regarding, for example, the duration of the phenomenon, its temporal skew, and its shape. A method of analysis that accounts for the variation in the response of individuals and focusses on the population-level dynamics provides a more complete picture of the extent of phenological change. This thesis presents a novel method of analysis that quantifies three essential aspects (or parameters) of the phenological time distribution. It describes an R package produced to automate the fitting of the model to varied phenological datasets and offer researchers a tool to facilitate the standardised comparison of phenological data. The utility of the model is explored using three detailed phenological datasets. The thorough analysis of the germination response of three high-elevation, perennial plant species to temperature demonstrates the accuracy of the model and its ability to quantify subtle variation in the phenology of three closely related species. The capacity of all three parameters to describe the effect of established temperature-mediated processes also demonstrates their biological interpretability. Investigation into the effects of climate change on marine plankton over several decades reveals that successive trophic levels

(or functional groups) are responding differently to changes in sea surface temperature. The advancement of each functional group's bloom phenology is shown to result from the modification of different parameters of the phenological time distribution. Analysis of the parameters reveals that different aspects of sea surface temperature are driving the modification of plankton functional group bloom phenology, both directly and indirectly. Finally, examination of the famous Japanese cherry tree flowering records shows that the novel method of phenological analysis can reliably estimate phenological responses to specific environmental stimuli using first occurrence data occurring along an environmental gradient. A method of phenological analysis that characterises the diversity of the phenological response and quantifies the influence that biological and environmental factors have on the shape of the time distribution provides a detailed understanding of the extent, and potential driving mechanisms, of phenological change.

List of Contents

List of Tables

List of Figures

1 Introduction

The changing composition of the planet's atmosphere over the past two centuries, in particular the increasing concentration of CO_2, and its consequences on the global climate is firmly established (IPCC 2021). A clear, near linear relationship has been observed between the global increase in surface temperature and the concentration of CO_2 in the atmosphere since 1850 (Figure SPM10 in IPCC 2021). This rapidly warming climate and its effects on living organisms is a subject of great scientific and practical interest (Poloczanska *et al.* 2014). One of these effects is the modification of the timing of biological events (Camill 2010). As temperature increases, seasonal events such as migration, recruitment and flowering shift to earlier dates (Walther *et al.* 2002).

The timing of periodically recurring, often seasonal, plant and animal life-cycle events is known as phenology (Walther *et al.* 2002; Schwartz 2003). Typically, the individual events are recorded as sudden changes of biological state such as birth, germination, leaf burst, insect emergence, or arrival at migration sites. Their timing has been shown to change according to environmental cues such as temperature (Menzel *et al.* 2006; Richardson *et al.* 2006b; Estrella, Sparks & Menzel 2007; Fu *et al.* 2018), precipitation (Shen *et al.* 2015; Zhou & Jia 2016), snow melt (Lambert, Miller-Rushing & Inouye 2010; Wipf 2010; Winkler *et al.* 2018) and photoperiod (Basler & Körner 2012; Flynn & Wolkovich 2018). Acting at the level of the individual, the influence of these environmental cues varies depending on the biological characteristics of the organism (Tang *et al.* 2016). Thus, variation in the phenological response of individuals is expressed at the population level as a time

distribution. The interaction between the biology of each individual organism and environmental influences determine how the phenological distribution unfolds through time, including when it begins, its rate of occurrence, its duration and the overall shape of the distribution (Franco 2018).

1.1 The nature of phenological data

The earlier records of phenological phenomena consisted of broad descriptions of, for example, leafing or flowering periods. Natural history observations such as "flowers June-August" or "egg laying in late spring" provided approximate information on when to expect certain phenological phenomena during the annual cycle. As the need for more specific information arose, "point" events such as the date of the first flower (Fitter & Fitter 2002) or the first migrant of the season (Gordo & Sanz 2006) were provided. Furthermore, recognising variation in the timing of the phenomenon encouraged the use of quantitative measures of central tendency and range. An index commonly used is the completion of 50% of cases, such as in the analysis of canopy phenology (Richardson *et al.* 2006b). As useful as they are, these single-point statistics are insufficient to account for the complexity of the phenomenon being described (Clark & Thompson 2011). A more detailed description of a phenology requires collection of a large number of observations to allow characterisation of its start, duration and overall shape of the distribution. Fitting of probability distributions allows quantification of statistical moments, but this requires large sample sizes. Given a sufficiently large sample, the cumulative proportion of individual events plotted against time produces a smoother sigmoid curve (O'Neill et al. 2004) that avoids the need of deciding on time-interval size when looking at a frequency graph of the number of events per time interval.

Some phenologies do not exhibit seasonality or, even if they do, they may occur throughout the whole year, never falling completely to zero. An example of this is births in humans (Lam & Miron 1991; Lam & Miron 1994). Despite evidence of seasonality, whose determinants are complex (Martinez-Bakker *et al.* 2014; Dahlberg & Andersson 2018), this type of phenology does not lend itself to simple analyses by means of a distribution function. The existence of two or more peaks (multimodality) also complicates the analysis. The present study will not consider these complications. Instead, it will concentrate on the quantification of unimodal phenologies.

1.2 Commonly used mathematical functions

A range of mathematical functions have been used to model the cumulative proportion of phenological events such as germination (Forcella et al. 2000; Gabriel y Galán et al. 2015), canopy development (Richardson *et al.* 2006b; Verma *et al.* 2016) and insect emergence (Forrest & Thomson 2011; Emery & Mills 2018). Standardised growth/distribution functions such as the logistic, Gompertz and Richards are often chosen because their sigmoid shapes mimic the time course of a phenology (Verma *et al.* 2016). Their equations describe a gradual transition between three growth phases: (i) an early accelerating phase where the growth rate (slope) gradually increases, (ii) an apparent linear phase where the growth rate decreases to reach a maximum at the curve's point of inflection, and (iii) a saturation phase, where the growth rate decreases towards zero at the curve's upper asymptote (Ratkowsky 1983; Birch 1999; Yin *et al.* 2003). In order to produce this non-linear, monotonically increasing growth pattern, growth functions typically contain three or four parameters which define the shape and position of the curve (Sedmak & Scheer 2015).

1.2.1 Functions with three parameters

Commonly used growth functions with three parameters include the logistic, Gompertz and Weibull distributions (Zeide 1993). The three parameters of the logistic and Gompertz functions are a rate parameter, a time constant and an upper asymptote (Birch 1999). One of the key features of these models is that the maximum rate of the process occurs at the inflection point of the curve. The logistic curve is symmetrical around its point of inflection, which is fixed at half the value of the upper asymptote (Birch 1999; Yin *et al.* 2003; Paine *et al.* 2012). There is no a priori reason for a phenological event to be symmetrical around its mid-point, as it may be right or left skewed. Because of the latter, logistic models fit poorly in cases where data are not near normally distributed and the model is not recommended (Berry, Cawood & Flood 1988; Brown & Mayer 1988).

The Gompertz function suffers from some of the same intrinsic inflexibility of the logistic function, although it is capable of producing asymmetrical sigmoid curves more typical of phenological events (Yin *et al.* 2003). In this function the maximum rate parameter, the point of inflection of the curve, is also fixed although it has a different value to that of the logistic: 1/e (approximately 0.368) times the value of the upper asymptote (Birch 1999; Paine *et al.* 2012).

The Weibull function can also produce asymmetrical sigmoid curves that more closely represent the time course of a phenological event. The three parameters of the Weibull function are a shape (or slope) parameter, a scale parameter and a location parameter. Although this function is not constrained by the inclusion of a parameter with a fixed value, e.g. the inflection point of the curve, the meanings of the parameters in the Weibull function are confounded: the value of one parameter depends on the value of another (Yin *et al.*

2003). The sigmoid curves described by these functions may resemble the time course of a phenology, but they are either severely constrained or confounded. This has led many phenological researchers to opt for equations with additional parameters (Birch 1999).

1.2.2 Functions with four parameters

A four parameter model commonly used in the investigation of phenology is the Richards function. The additional parameter in the Richards function is a shape parameter. This parameter can be varied to allow the point of inflection of the curve to assume any value between the minimum and upper asymptotes (Birch 1999; Damgaard & Weiner 2008). The additional shape parameter enables the Richards function to produce various asymmetrical sigmoid curves and influences the heaviness of the tails of the fitted curve (Stukel 1988). Despite the flexibility of the Richards function, critics have argued that the additional shape parameter has no discernible biological interpretation (Thornley & Johnson 1990; Zeide 1993; Birch 1999; Yin *et al.* 2003). Some have even suggested that the parameter estimates are unstable, which allows the equation to converge regardless of the shape of the data (Ratkowsky 1983; Zeide 1993). The rigidity and lack of biological interpretability of the functions described above make them unsatisfactory for modelling phenological events.

1.3 A distribution tailored to quantify three salient aspects of a phenology

Both biological and environmental factors influence how a phenological distribution unfolds over time, and a more appropriate model would be one that is not only sufficiently flexible to accommodate a range of asymmetrical distributions but also generates physically meaningful parameters. Such a model would allow the influence that both biological and environmental factors have on its parameters to be assessed.

Franco (2018) has developed a distribution function suitable for phenological phenomena whose parameters have clear physical units. The first essential aspect of the phenological time distribution is its rate of occurrence. As described in Franco (2018) a time distribution that occurs at a constant rate would naturally follow an exponential distribution whose cumulative distribution function (*cdf*) would be: $y = 1 - e^{-rx}$. As the time distribution of a phenology does not in general follow an exponential distribution, it can be concluded that the rate of occurrence is not constant. Individual phenological events occur in a probabilistic manner and are conveniently described by the inverse logit (Franco 2018). That is: $r = \frac{r_{max}}{1+e^{-cx}}$. The use of the inverse logit implies the existence of a second parameter (c) determining the rate of change in r as the phenology progresses. Finally, biological processes do not occur instantly, but instead happen sometime after exposure to a specific set of conditions (Wu et al. 2015). This aspect is determined by a third parameter (t), a metabolically-determined time lag, such as an incubation period, resulting in: $r = \frac{r_{max}}{1+e^{-c(x-t)}}$. A model that incorporates these three aspects (parameters) leads to the following cumulative distribution function (Franco, 2018):

$$y = 1 - \left(1 - \frac{r}{1+e^{-c(x-t)}}\right)^{x} \quad (1)$$

where y is the empirically recorded cumulative proportion of events unfolding over time (x); r quantifies the maximum proportional rate at which the process occurs (it is dimensionless and $0<r\leq1$); c is the rate at which r converges on its maximum value and is a measure of the period over which the process happens (units: time^{-1}; $c>0$); and t is an overall measure of the process' time lag (units: time; $t\geq0$). The three parameters of the

model (r, c and t) have clear meanings and units and the influence that each has on the shape of the fitted curve is clear (Fig. 1.1).

A probability density function (*pdf*) can be derived from equation 1 by differentiation:

$$\frac{dy}{dx} = \left(1 - \frac{r}{1+e^{-c(x-t)}}\right)^{x} \left(\frac{rcxe^{-c(x-t)}}{\left(1+e^{-c(x-t)}\right)^{2}\left(1-\frac{r}{1+e^{-c(x-t)}}\right)} - \ln\left(1 - \frac{r}{1+e^{-c(x-t)}}\right)\right) \qquad (2)$$

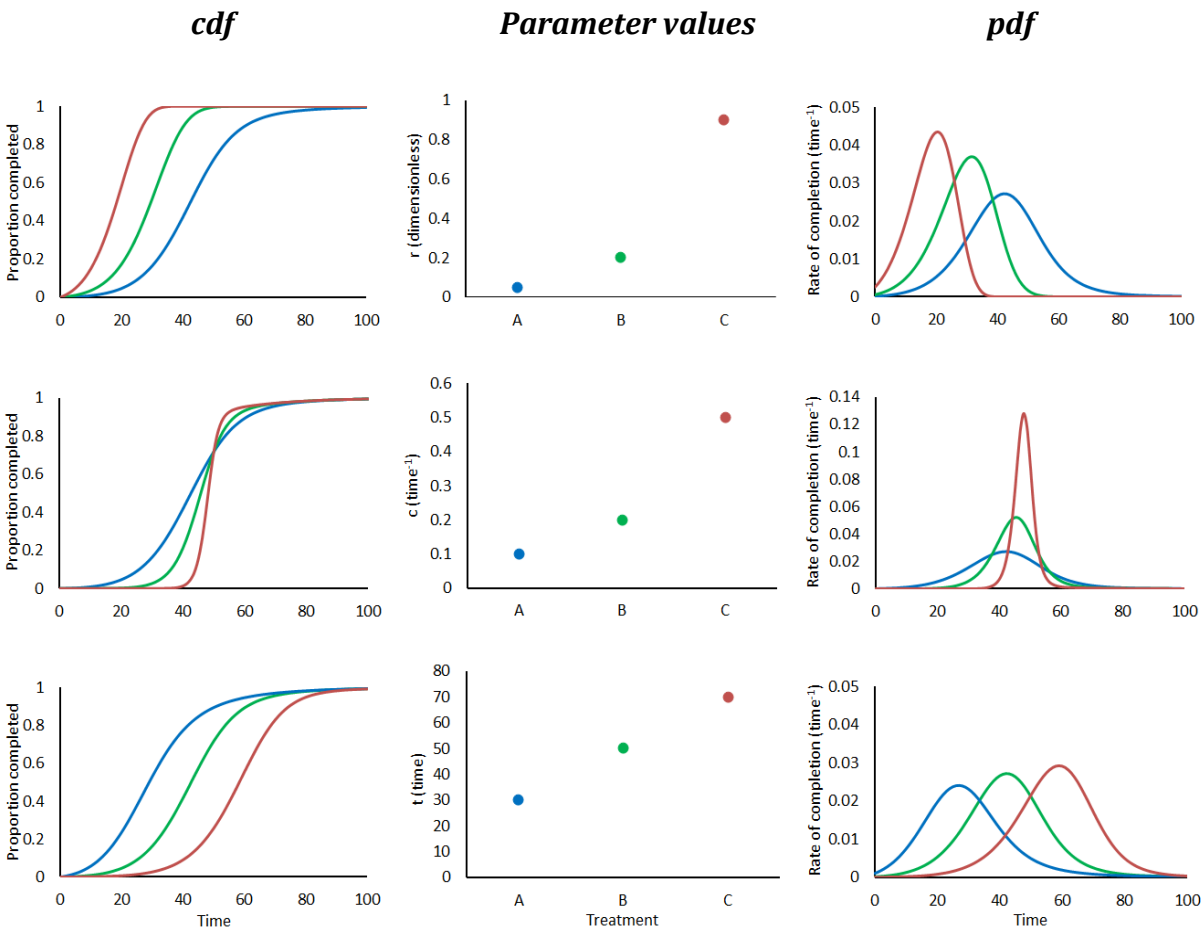

Figure 1.1. The influence of the three model parameters (r, c, and t) on the cumulative distribution function (left panels) and probability density function (right panels). The central panels show how each parameter varies, while the other two are held constant, following the order blue<green<red.

The time course of a phenological event can assume a diverse range of shapes. The *cdf* accurately replicates this range of shapes and the *pdf* defines the changing, population-level rate of the phenological process over time.

In the top row of Figure 1.1, parameter *r* is varied, whilst *c* and *t* remain the same. Parameter *r* determines the rate at which the *cdf* rises: increasing the value of *r* creates an earlier starting point and increases the initial steepness of the curve. In the middle row, parameter *c* is varied whilst *r* and *t* remain the same. Parameter *c* is a measure of the concentration of the time distribution: as the value of *c* is increased, the time span over which the majority of the process occurs is shortened. Finally, in the bottom row, parameter *t* is varied whilst *r* and *c* remain the same. Parameter *t* is a measure of the process' time lag: as the value of *t* is increased, the process is delayed and in an almost parallel fashion moves to the right.

The model is capable of producing a wide range of distributions with varying degrees of skew and kurtosis. However, this model is much more than just a flexible distribution function. The defining feature of this model is that it allows the influence that each parameter has on the shape of the phenological time distribution to be quantified. This quantification can be used to determine the effect that different biological and environmental factors have on each of the three aspects of the time distribution, providing a more detailed understanding of how phenological events are affected and potentially helping to uncover their driving biological and environmental mechanisms.

1.4 Curve-fitting algorithm

The cumulative distribution function (equation 1 above) is fitted to the cumulative number of observed individual phenological events using non-linear least squares regression. Nonlinear least squares methods use an iterative optimisation procedure to gradually update and improve starting parameter values in order to reduce the sum of the squared errors between the function and the observed data (Gavin 2013). To fit the distribution function the model utilises the Levenberg-Marquardt algorithm, also known as the damped least squares method, to find the non-linear least squares minimisation solution. The Levenberg-Marquardt curve-fitting method combines two minimisation procedures, the gradient descent method and the Gauss-Newton algorithm (Marquardt 1963). The gradient descent method is the simplest method for finding the minima in a function, it works by reducing the sum of the squared errors by adjusting the parameters in the direction of the steepest descent (Ranganathan 2004). The Gauss-Newton algorithm presumes that the least squares function is locally quadratic. In this method the sum of squared errors is reduced by finding the minimum of the quadratic (Gavin 2013). Using a combination of curvature and gradient information makes the Levenberg-Marquardt algorithm a resilient and effective method of curve fitting (Lourakis 2005). The algorithm's ability to switch between the two minimisation methods allows the model to cope with starting parameter values that are far away from the optimum. This can be particularly useful when the model is fitted to datasets containing different treatments as these treatments may produce data that have a diverse range of curve shapes.

1.5 Application

By focussing on the parameters of the distribution, the model provides important information about the overall time course of a phenological process. Unlike traditional methods of phenological analysis that only report changes to outliers (such as first and last occurrences), this approach can be used to determine whether entire phenological events are accelerating (higher *r*), spreading over time (lower *c*) or advancing (lower *t*).

The three parameters of the model quantify specific aspects of the distribution with known units and provide a measure of how each of them is affected by biological (e.g., age or sex) or environmental variables (e.g., ambient temperature). The pattern of change in the parameters can then be interpreted with reference to specific biological mechanisms (e.g., differences in metabolism or differential sensitivity to environmental change). This feature sets the model apart from commonly used statistical models, which are often defined by their mean and standard deviation, or their parameter values cannot be interpreted unequivocally (Franco 2018). Each of the parameters is conceptually and numerically different from the distribution's statistical moments. Moreover, the statistical moments and percentiles of the distribution can be extracted from the model and these provide additional relevant information in comparative studies. Analyses of how the different parameters correlate with each other, with particular statistical moments of the distribution and with biological and/or environmental factors, allows specific hypotheses to be tested regarding the possible causes of phenological change.

The model provides a consistent method of phenological analysis that can be used by researchers to facilitate standardised comparisons of phenological data. The model can be used to examine a wide variety of phenological events, including investigations of

reproduction and development (e.g., pollination, gestation, egg-laying, egg-hatching, germination, life stages), seasonal population dynamics (of leaves, flowers, whole organisms, etc.), species interactions (trophic mismatch, predator-prey dynamics, competition, pest outbreaks), migration and dispersal (in relation to cues and invasion dynamics), and mortality in response to environmental challenge (climate change, ecotoxicology).

Understanding how phenological phenomena are responding to a range of biological and environmental variables will allow predictions to be made more accurately regarding possible future changes. Predictions that are more accurate could permit measures to be taken to lessen the impact of future changes in diverse areas including conservation, agriculture, and human health, for example. A greater understanding of phenological changes could also help inform policy by providing valuable evidence of the effect that biological and/or environmental drivers are having on the timing of phenology and its associated consequences.

1.6 Thesis outline

The purpose of this thesis was to explore the utility of the model presented in the previous section. To this end, the first step was to produce a computer package to fit the new distribution presented above to empirical data. Once the package was produced, several reasonably detailed datasets were obtained from available phenological databases and analysed following this methodology. The individual chapters are summarised below. The final chapter is a general discussion to bring together what was learnt throughout this study and suggestions for future work.

- **Chapter 1. Introduction**

  The model to be used throughout the thesis is presented. This model is a function tailored to quantify three different aspects (parameters) of a time distribution. By having specific physical units, the parameters are expected to be controlled by particular physiological mechanisms of the organisms concerned. The potential application of the model is outlined.

- **Chapter 2. nlstimedist: An R package for the biologically meaningful quantification of unimodal phenology distributions**

  A computer package to fit the model to empirical phenological data is developed and its operation is described employing some simple data. This chapter has already been published as a research paper in the journal Methods in Ecology and Evolution.

- **Chapter 3. An introduction to the nlstimedist package: A vignette**

  A short manual or "vignette" accompanying the computer package, which contains more detailed information on its workings, is presented.

- **Chapter 4. Germination response to temperature of three high-elevation Andean *Puya* species**

  A detailed analysis of the germination response of three high-elevation, monocarpic perennial plant species to different temperatures under experimental laboratory conditions is used to illustrate the responses that the model quantifies. These responses are then interpreted in terms of the ecological characteristics of the habitats in which each of the species is found.

- **Chapter 5. Phenological change of four North Sea plankton functional groups over a 56 year period**

  Data from the UK's Continuous Plankton Recorder (CPR) survey for the period 1960-2015 are employed to investigate the changes over that period in the phenology of plankton species grouped into four functional groups. The results are interpreted in light of the trophic levels and ecological attributes of the species in each functional group.

- **Chapter 6. Latitudinal variation in flowering patterns of Japanese cherry trees over seven decades**

  One of the longest running phenological records in the world is that of the first flowering of cherry trees (*Prunus* spp.) at multiple locations across Japan. Records from 83 localities over the period 1953-2018 were analysed to investigate the trend in the model's parameter values across three latitudinal bands (high, mid, and low) over the study period. The results show contrasting flowering responses to climate warming with latitude.

- **Chapter 7. General discussion**

  The final chapter appraises the usefulness of the model, its benefits and limitations, and its prospect as a general time distribution of biological phenomena.

2 nlstimedist: An R package for the biologically meaningful quantification of unimodal phenology distributions

Steer, Ramsay & Franco (2019), *Methods in Ecology & Evolution*, Vol 10: 1934-1940.

2.1 Introduction

Periodically recurring, often seasonal, biological events (phenology) are influenced by environmental factors and interactions between organisms (Lieth 1974). Such phenomena are of particular interest because anthropogenic influences, such as climate change, might alter important ecological processes that are intimately correlated (Forrest & Miller-Rushing 2010). A biologically meaningful description of phenological events is essential to understanding their temporal dynamics, and offers an opportunity to assess the significance of its potential drivers (Rafferty *et al.* 2013).

Certain phenological events are recorded as a binary change from one recognisable state into another, either for a whole organism, as when a winter migrant has arrived for the breeding season (Gordo 2007) or for individual parts, as when individual leaf or flower buds on a plant burst (Cole & Sheldon 2017).

While it is clear that variability of individual events is expressed at the population level as a time distribution, phenological observations are often restricted to recording only extreme events, such as the date of the first flower to bloom (Fitter & Fitter 2002) or the first migrant of the season to arrive (Gordo & Sanz 2006). This approach ignores the population-level dynamics which contains a wealth of information regarding, for example, the duration of the phenomenon, its temporal skew, and its shape. Other scalar values may be conveniently-chosen thresholds (Zhang *et al.* 2003), such as the 50% of completion

commonly used in the investigation of canopy phenology (Richardson *et al.* 2006b), and varying percentage values are a key feature of the BBCH-scale used to identify phenological developmental stages in plants (Meier 2001). All of these approaches result in a single date, which is intended to capture useful information about the phenological process.

When single dates are used to describe the timing of a phenological event, they are often compared across years or linked to changes in an environmental condition, such as temperature, using regression (Sparks & Tryjanowski 2010). As useful as these scalars may be to summarise key features and changes in phenology, they inevitably miss potentially important information about the shape of the overall time course (Clark & Thompson 2011; CaraDonna, Iler & Inouye 2014; Carter, Saenz & Rudolf 2018).

A more thorough assessment should aim to model the entire phenological time distribution (CaraDonna, Iler & Inouye 2014; Carter, Saenz & Rudolf 2018). This is frequently accomplished using classic growth functions, such as the logistic and Richards (Yin *et al.* 2003; Zhang *et al.* 2003; Richardson *et al.* 2006b; Sun & Frelich 2011) as their sigmoid shape resembles the time course of a phenological event. The logistic model is symmetrical around its point of inflection which is always halfway along the asymptotes (Birch 1999), but there is no theoretical basis for a phenological event to be symmetrical around its mid-point. The Richards (or generalised logistic) model is more flexible due to an additional shape parameter but its parameters cannot be interpreted in a meaningful way (Richards 1959; Zeide 1993; Birch 1999; Damgaard & Weiner 2008).

An alternative approach builds on an existing body of work on niche overlap (Pleasants 1980; Fleming & Partridge 1984; Totland 1993; Castro-Arellano *et al.* 2010), and allows species interactions to be compared as measures of temporal overlap (e.g., Carter, Saenz &

Rudolf 2018). These approaches take account of whole phenological distributions through time, accommodating multimodal or skewed responses. Temporal overlap is an outcome of interactions between distributions rather than a direct consideration of their shapes, but is a sensible approach where the comparison focuses on time alone and where there are multimodal, complex probability distributions.

For unimodal phenology distributions, a model that describes the entire phenological time distribution well, is sufficiently flexible to accommodate asymmetrical distributions, and generates biologically interpretable shape parameters would be more useful. In particular, the model should be derived from basic principles applicable to a wide spectrum of biological time distributions. Importantly, goodness-of-fit alone should not be used to justify model selection; it is always preferable to choose a model that has biologically meaningful parameters (Paine *et al.* 2012).

Here, we present a model for describing the temporal dynamics of unimodal phenological events. It has been derived from first principles and generates biologically meaningful parameters that can be compared and used to assess potential driving mechanisms.

2.2 The model

A phenological process of events (y) unfolding over time (x) at a constant rate (r) would follow an exponential distribution (Franco 2018). Phenological processes, however, do not occur at a constant rate (Sparks & Tryjanowski 2010) and individual events are more likely to be distributed according to a probabilistic process described by the inverse logit governed by an additional parameter, c (Franco 2018). Finally, phenological processes do not occur instantly, but happen sometime after exposure to a specific set of conditions (Wu

et al. 2015), which requires a third parameter, the time lag, *t*. By incorporating the lagged form of the inverse logit function into the exponential distribution, a suitable biological time distribution can be derived (Franco 2018). This cumulative distribution function (*cdf*) has the form:

$$y = 1 - \left(1 - \frac{r}{1+e^{-c(x-t)}}\right)^{x} \quad (1)$$

The derivative of this function quantifies the probability density function (*pdf*):

$$\frac{dy}{dx} = \left(1 - \frac{r}{1+e^{-c(x-t)}}\right)^{x} \left(\frac{rcxe^{-c(x-t)}}{\left(1+e^{-c(x-t)}\right)^{2}\left(1-\frac{r}{1+e^{-c(x-t)}}\right)} - \ln\left(1 - \frac{r}{1+e^{-c(x-t)}}\right)\right) \quad (2)$$

which describes the population-level rate at which the phenomenon occurs. Each of the function's parameters has clear meaning and units: *r* quantifies the maximum proportional rate at which the process occurs (it is dimensionless); *c* is the rate at which *r* converges on its maximum value (units: time^{-1}); and *t* is an overall measure of the process' time lag (units: time) (Fig. 2.1). Parameter *t* can also be thought of as a weighted measure of the process' duration – weighted in relation to the values of *r* and *c*, that is. It correlates with, but is not equivalent to any of the distribution's various measures of central tendency.

2.3 The R package

nlstimedist is an R package that provides a convenient way to fit the time course of a unimodal phenological time distribution employing nonlinear regression. *nlstimedist*

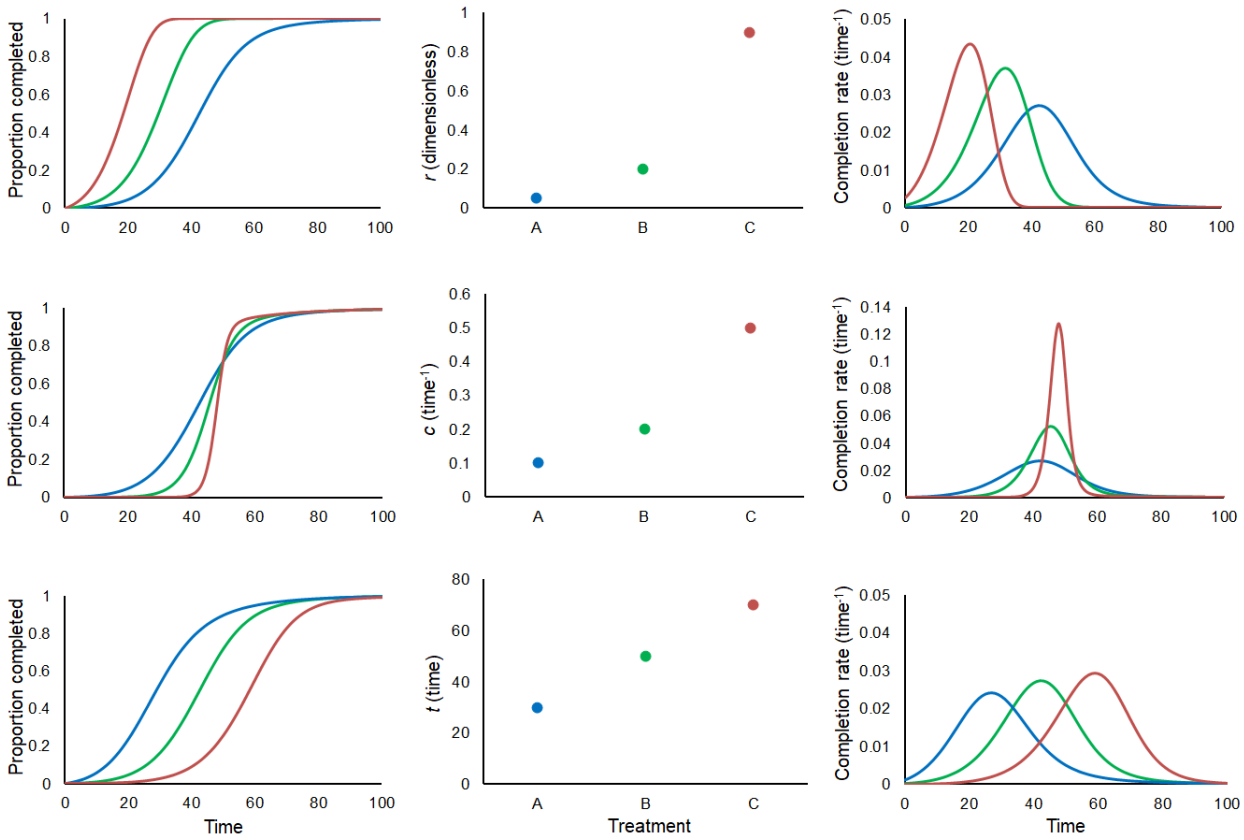

Figure 2.1. The influence of the three model parameters (*r*, *c*, and *t*) on the cumulative distribution function (left panels) and probability density function (right panels). The central panels show how each parameter varies, while the others are held constant.

combines functions for data preparation, model fitting and data visualisation into one complete package, allowing efficient, accurate and meaningful analysis.

The model is fitted to data using the **timedist()** function. The function requires data in the form of the proportion of cumulative number of events through time, together with column identifiers (allowing the analysis of multi-column data) and starting values for *r*, *c* and *t*. If data are in their raw form of counts versus time, they can be cleaned and converted to proportions (range: 0-1) for model use, using the built-in tidy function **tdData()**.

The **timedist()** function returns an object which contains all of the fitted model information. This includes the equation used to fit the estimated time distribution,

estimated values for *r*, *c* and *t*, the model fit's residual sum of squares, and the number of iterations to convergence. The object can be examined with all of the generic *nls* functions, such as **summary(),** and can also be used by packages such as 'nlstools' (Baty *et al.* 2015). Functions and packages such as these can be used to assess how well the model fits the data and the reliability of the parameter estimates. The statistical moments and percentiles of the fitted distribution can be obtained from the model object. The *nlstimedist* package also has two built-in functions for plotting the estimated time distribution as either a cumulative distribution function (*cdf*) **tdCdfPlot(object, ...)** or a probability density function (*pdf*) **tdPdfPlot(object, ...)**.

nlstimedist is based on the framework provided by nlsLM from the *minpack.lm* package (Elzhov *et al.* 2016). nlsLM is a modification of the standard *nls* function that uses the Levenberg-Marquardt algorithm (Marquardt 1963) for model fitting (Elzhov *et al.* 2016). This fitting procedure was chosen because it is considered robust (Lourakis 2005). Because the method of non-linear regression fitting uses an iterative optimisation procedure to converge on the least squares solution, fairly accurate starting values need to be chosen (Ruckstuhl 2010). *nlstimedist* is not a self-starting model, therefore guidelines are provided to assist with the selection of appropriate starting values for the three parameters (see package vignette).

Fitting to the underlying cumulative distribution function (opposed to the more usual practice of fitting a probability density function to binned data) allows datasets with few observations to be analysed. The temporal resolution of the data must be sensible and representative of the whole phenology under investigation. This model cannot be applied to complex, multimodal phenologies.

As shown in Fig. 2.1, each parameter has a unique effect on three different aspects of the distribution's shape. In summary, *r* is a scaled rate of completion (without units), *c* is a measure of its temporal concentration (units: time^{-1}), and *t* is an overall measure of temporal delay (units: time). In combination, these parameters provide insight into potential drivers and mechanisms associated with the phenological process, such as rates of development, climate change, competition between species, genetic diversity, resource availability and environmental heterogeneity. Exploring the relationships between model parameters and statistical moments with biological and environmental variables might offer additional understanding of possible determinants.

2.4 Application of the model

The model can be applied across a wide range of phenological studies, including aspects of reproduction and development (e.g., pollination, gestation, egg-laying, egg-hatching, germination, life stages), seasonal population dynamics (of leaves, flowers, whole organisms, etc.), species interactions (trophic mismatch, predator-prey dynamics, competition, pest outbreaks), migration and dispersal (in relation to cues and invasion dynamics), and mortality in response to environmental challenge (climate change, ecotoxicology). The model has also been fitted successfully to the distribution of reproductive value of perennial plants as a means of quantifying the duration (by parameter *t*) and the speed (parameter *c*) of life (Mbeau-Ache & Franco 2013).

As a worked example, we present data from a controlled seed germination experiment for *Puya raimondii*, a giant rosette plant from the Andes. The experiment tested the effect of temperature on germination along a temperature gradient ranging from 8.4° C to 23.7° C.

We use this example to illustrate how the new function is able to quantify accurately the changing temporal dynamics of a phenological process. We also show how quantification of the models parameters can be used to determine the influence that an environmental factor, in this case temperature, has on seed germination.

The dataset used in this example is available on the Dryad Digital Repository. The file can be read directly into R using the following command.

```
> Puya <- read.csv ("PuyaGermination.csv", header = TRUE, sep = ",")
```

To obtain the estimated parameter values (*r*, *c*, *t*) at each temperature, the model was fitted to each column in the "Puya Germination" dataset separately using the **timedist()** function. Starting values for parameter estimates are dependent on the length of the time course under investigation and as such, starting values were adjusted for each model fit.

```
> Puya1.1 <- timedist (Puya, x = "x", y = "T8.4", r = 0.04, c = 0.5, t = 40)
> Puya1.1

Nonlinear regression model
  model: T8.4 ~ 1 - (1 - (r/(1 + exp(-c * (x - t)))))^x
   data: data
       r        c        t
 0.07347  0.44714 37.36754
 residual sum-of-squares: 0.008334

Number of iterations to convergence: 7
Achieved convergence tolerance: 1.49e-08
```

Fitting accuracy was verified using a range of functions. The reliability of the parameter estimates was obtained for each fit using the generic **summary()** function for *nls* objects. Standard errors of parameter estimates were very small, and model fit was highly significant in all cases ($p < 0.001$; Table 2.1).

```
> summary (Puya1.1, correlation = TRUE, symbolic.cor = FALSE)

Formula: T8.4 ~ 1 - (1 - (r/(1 + exp(-c * (x - t)))))^x

Parameters:
   Estimate   Std. Error t value Pr(>|t|)
r  0.073472   0.005016   14.65   4.51e-11 ***
c  0.447144   0.024582   18.19   1.40e-12 ***
t 37.367538   0.344737  108.39   < 2e-16  ***
---
Signif. codes:  0 ‘***’ 0.001 ‘**’ 0.01 ‘*’ 0.05 ‘.’ 0.1 ‘ ’ 1

Residual standard error: 0.02214 on 17 degrees of freedom

Correlation of Parameter Estimates:
  r      c
c -0.64
t  0.92 -0.82

Number of iterations to convergence: 7
Achieved convergence tolerance: 1.49e-08
```

Nonlinear regression has no direct R^2. However, a pseudo R^2 calculated as $1 - [\sum(y - \hat{y})^2 / \sum(y - \bar{y})^2]$, which defines a similar quantity for nonlinear regression and is able to describe the proportion of variance explained by the model (Kvålseth 1985; Cameron & Windmeijer 1997). Extracting this quantity from each model object provided another measure of how well the model fitted the data. R^2 was over 0.99 for all temperature treatments (Table 2.1), although we recommend caution in the interpretation of this statistic, as it provides an over-optimistic measure of fit (Spiess & Neumeyer 2010).

```
> Puya1.1$m$rss()
[1] 0.99693
```

The statistical moments and the percentiles of the distribution can also be extracted from each model object. These facilitate comparison of different temperature treatments throughout time (Table 2.1).

```
> Puya1.1$m$getMoments()
      mean variance       sd     skew kurtosis  entropy
1 35.66111 34.71189 5.891679 4.156171 36.20471 4.096621
```

Plotting the model fits as both cumulative distribution functions and probability density functions provides a useful summary of how germination is affected across a range of temperatures (Fig. 2.2). These plots provide an informative visual summary of the maximum per capita rate of germination, temporal spread and time delay of seed germination at each temperature.

A key feature of the model is the production of numerically meaningful parameter values. These parameters, when plotted against biological or environmental variables, allow

potential driving mechanisms to be tested. In this example, temperature affected all three parameter estimates in a curvilinear fashion (Fig. 2.3). Parameters *r*, *c* and *t* displayed significant quadratic relationships with temperature, helping to identify the temperature at which germination was fastest, more concentrated and least delayed after sowing. This optimal temperature was remarkably similar for all three parameters: r = 15.6° C, c = 15.5° C and t = 15.9° C.

Table 2.1. Number of seeds germinated (N) and the final percentage of germination (Y_{max} = 100*(N/(number of seeds sown))) in each temperature category, estimated parameter values (with standard errors in parenthesis), *** p < 0.001, proportion of variance explained by the model (R^2) and statistical moments for each of the predicted distributions.

Temp. (°C)	N	y_{max} (%)	*r* (s.e.)	Sig.	*c* (s.e.)	Sig.	*t* (s.e.)	Sig.	R^2	Mean	SD	Skew	Kurtosis	Entropy
8.4	148	74.0	0.073 (0.005)	***	0.447 (0.025)	***	37.368 (0.345)	***	99.7	35.661	5.892	4.156	36.205	4.097
9.3	156	78.0	0.075 (0.003)	***	0.653 (0.032)	***	29.532 (0.158)	***	99.8	29.461	6.334	4.848	37.191	3.823
12.5	161	80.5	0.112 (0.008)	***	0.806 (0.062)	***	22.018 (0.230)	***	99.6	21.421	3.925	4.621	38.424	3.354
13.6	166	83.0	0.158 (0.018)	***	0.696 (0.050)	***	20.449 (0.339)	***	99.8	18.772	2.667	2.177	20.343	3.247
13.8	164	82.0	0.129 (0.004)	***	1.485 (0.083)	***	16.133 (0.071)	***	99.9	16.360	3.571	5.188	39.817	2.748
14.7	160	80.0	0.126 (0.006)	***	1.418 (0.117)	***	15.113 (0.104)	***	99.7	15.580	3.988	4.774	33.338	2.911
16.7	147	73.5	0.134 (0.003)	***	2.230 (0.108)	***	13.992 (0.037)	***	99.9	14.597	3.639	5.116	36.541	2.393
17.6	157	78.5	0.139 (0.005)	***	1.917 (0.158)	***	14.028 (0.074)	***	99.8	14.452	3.418	5.144	37.802	2.500
19.5	159	79.5	0.121 (0.008)	***	0.801 (0.080)	***	15.970 (0.226)	***	99.3	16.061	4.431	3.893	25.498	3.526
20.0	155	77.5	0.090 (0.004)	***	0.487 (0.041)	***	17.896 (0.259)	***	99.4	18.775	7.089	3.218	17.477	4.307
21.7	146	73.0	0.080 (0.003)	***	0.504 (0.025)	***	25.638 (0.212)	***	99.8	25.516	6.712	3.898	26.187	4.154
22.4	144	72.0	0.058 (0.003)	***	0.283 (0.024)	***	30.436 (0.560)	***	99.1	30.989	10.882	3.133	17.629	4.992
23.7	88	44.0	0.052 (0.005)	***	0.201 (0.015)	***	43.426 (0.992)	***	99.2	41.159	11.452	2.641	16.558	5.242

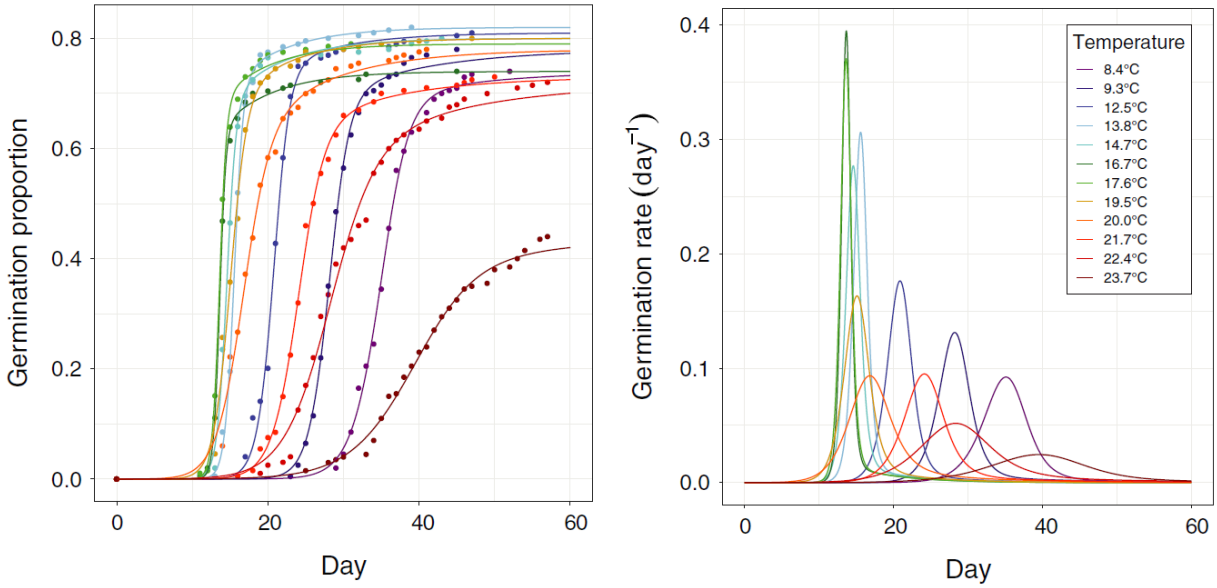

Figure 2.2. Cumulative distribution functions (left) and probability density functions (right) for *Puya raimondii* germination along a temperature gradient ranging from 8.4°C to 23.7°C. Probability density functions describe the population-level rate of germination and the area under the curve is equal to the maximum percentage of germination.

Although the quadratic relationship with temperature was significant and each parameter predicted similar optimal temperatures, there is no reason to expect either a similar optimum for all three parameters or a symmetrical response on either side of the optima. The analysis of other phenological processes may yield different statistical relationships. Temperature was used in this example to illustrate the effect that an environmental factor has on the time course of seed germination. However, the same principles would apply to other environmental conditions that vary on a continuous scale.

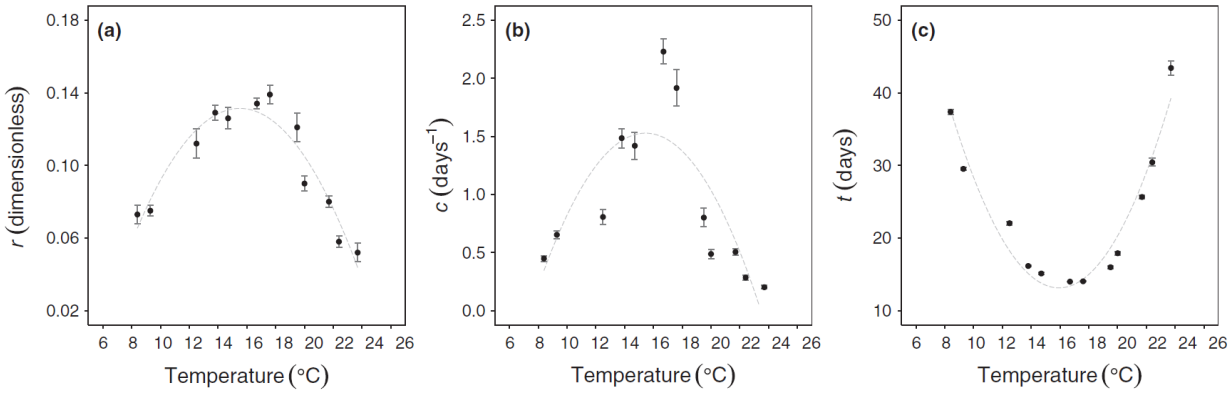

Figure 2.3. The relationship between temperature and the values of parameter estimates produced from each model fit (a) parameter *r*, (b) parameter *c*, and (c) parameter *t*. All three quadratic relationships were significant (a) $R^2 = 0.915$, $p < 0.000$, (b) $R^2 = 0.672$, $p = 0.007$, (c) $R^2 = 0.945$, $p < 0.000$. Error bars represent the standard errors of parameter estimates.

2.5 Conclusions

The *nlstimedist* package was built to facilitate the application of Franco's (2018) distribution function to phenological data. The model adequately describes a unimodal phenological process of events that are usually recorded as completions, i.e., on a binary scale. It is conceptually simple and is able to capture the essence of a phenological process because its three parameters quantify properties of the distribution with known units: a maximum net per capita rate (dimensionless), a rate at which this maximum rate is achieved (units: time^{-1}) and an overall measure of the process' time lag (units: time). Both biological and environmental variables have been shown to affect the individual parameters in a predictable way (Mbeau-Ache & Franco 2013; Franco 2018), and examples provided here. The flexibility of the model in representing various continuous distributions, the interpretability of its parameters and its ability to estimate the underlying statistical distribution of an often highly asymmetrical temporal process make it a useful tool in the analysis of unimodal phenological phenomena.

3 An introduction to the nlstimedist package: A vignette

Steer, Eastwood & Franco (2016) *Cran.nexr.com*

3.1 Introduction

This vignette presents the *nlstimedist* package, a method to fit a new distribution model to the time distribution of a biological phenomenon (Franco, 2018). The model differentiates between three essential aspects of a time distribution: the rate at which the process is expected to occur (parameter *r*), the rate of change of *r* with time, which is reflected in the time concentration of the distribution (parameter *c*), and a measure of the overall distribution time lag (parameter *t*). The fitting method incorporates the nlsLM function from the minpack.lm package (Elzhov et al., 2015) to estimate these three parameters and to plot the estimated time distribution. The *nlstimedist* package also estimates the standard statistical moments. The method can be used to analyse the time distribution of biological events such as germination, phenology, invasion, conclusion of a race, etc. Because parameter values have clear, unique effects on three different aspects of the distribution's shape (and are often correlated but not identical to specific moments), they have clear biological interpretation. This allows the user to further investigate the effect that biological (e.g., species, gender, health, etc.) and environmental factors (e.g., temperature) have on a biological time course. For example, are differences between the sexes in the completion of a marathon race reflected in a particular parameter? If so, what do these differences mean in terms of their size, musculature, aerobic capacity, etc.? If the parameters have a biological interpretation, how are they affected by ambient temperature, hydration, sugar levels, etc.?

3.2 Installation

The package can be installed from any CRAN repository mirror:

```
# Install
install.packages("nlstimedist")

# Load
library(nlstimedist)
```

3.3 Data set up

In the model, time is represented by variable "*x*" and the biological phenomenon is represented by variable "*y*". The values in each "*y*" column should be proportions and should be calculated from the cumulative number of events. This must be completed for each column in a dataset. If data have been set up in this manner, skip ahead to the next section. If the data have not been set up in this format and it is in a raw format of counts vs. time, they must first be cleaned using the **tdData** function.

3.3.1 Cleaning data using tdData

If there is only one column in the dataset, as in the example *Tilia* data, the vector can be converted to the cumulative number of events and proportions by the **tdData** function:

```
# Import data
Tilia <- read.csv("Trees.csv", header = TRUE, sep = ",")
head(tilia)

# Convert data to cumulative
tdTilia <- tdData(Tilia, x = "Day", y = "Trees")
tdTilia
```

If there is more than one column in the dataset, they can be cleaned together and filtered individually for use in the model. You will need to install and load the packages **tidyr** and **dplyr**.

In the *Lobelia* dataset there are different treatment categories ranging from '9.8' to '32.0'. To ensure all of your data are gathered together, replace '9.8:32.0' in the code below with the names of the first and last columns in your dataset and separate these with a colon. The columns in the *Lobelia* dataset are different temperature treatments so they are sorted by 'temp', simply replace each 'temp' in the code below with a category that suits your dataset.

```
# Import your raw data
Lobelia <- read.csv("Lobelia.csv", header = TRUE, sep = ",")
head(Lobelia)

# Convert your data to tidy format
LobeliaTidy <-
  Lobelia %>%
  gather(key = temp, value = y, 9.8:32.0) %>%
  mutate(temp = as.numeric(gsub("y", "", x = .$temp)))

# Start to clean your data (make sure x and y are labelled as they appear in the converted object above).
cleanLobelia <- tdData(LobeliaTidy, x = "Day", y = "y", group = "temp")

# Filter out the first column (place the name of the column you want to filter out after the ==).
9.8 <- cleanLobelia$clean %>%
  filter(temp == 9.8)
```

```
# Filter out the second column.  Continue this process for each column in your dataset.
12.5 <- cleanLobelia$clean %>%
  filter(temp == 12.5)
```

3.4 Fitting the model

The model is fitted by nonlinear regression employing the Levenberg-Marquardt algorithm. This requires three starting values for *r*, *c* and *t*, respectively.

3.4.1 Starting values

Suggestions for appropriate starting values for each parameter are as follows:

r: 1/the period of the time course, e.g., if completion of the process (all individual events) occurred in 25 days, an appropriate starting value for *r* would be around 1/25 = 0.04.

c: This requires some trial and error with your particular dataset. We suggest you start with 0.5 and increase (or decrease) it along a logarithmic scale to get a feel of how it is changing. Increasing values of *c* reduce the spread of the distribution: *c* is a measure of concentration of the distribution.

t: This tends to be close to the mid-point of the monitoring period, but it varies with the skew produced by the combination of parameter values. Nonetheless, as a rule of thumb choose a number near the middle of your time range – if completion of a process (e.g., a marathon race) was closed after 10 hours, choose *t* = 5.

3.4.2 The timedist function

The model is fitted to the data using the **timedist** function.

Fitting the model to data already in the format *x* = time and *y* = proportion of cumulative number of events.

```
LobeliaProp <- read.csv("LobeliaProp.csv", header = TRUE, sep = ",")

head(LobeliaProp)

FrancoLobelia12.5 <- timedist(LobeliaProp, x = "Day", y = "12.5", r = 0.03, c = 0.5, t = 14.5)
```

Print the model

```
FrancoLobelia12.5
```

```
> FrancoLobelia12.5

Nonlinear regression model

  model: y12.5 ~ 1 - (1 - (r/(1 + exp(-c * (Day - t)))))^Day

   data: data

       r        c        t

 0.08339  0.62678 12.09364

 residual sum-of-squares: 0.03901


Number of iterations to convergence: 16

Achieved convergence tolerance: 1.49e-08
```

Fitting the model to data sorted using the tdData function (as seen in section 5.3.1).

```
FrancotdLobelia12.5 <- timedist(data = y12.5, x = "Day", y = "propMax", r = 0.03, c = 0.5, t = 14.5)
```

Print the model

```
FrancotdLobelia12.5
```

```
> FrancotdLobelia12.5

Nonlinear regression model
```

```
  model: propMax ~ 1 - (1 - (r/(1 + exp(-c * (Day - t)))))^Day

   data: data

       r        c        t

 0.08339  0.62678 12.09364

 residual sum-of-squares: 0.03901


Number of iterations to convergence: 16

Achieved convergence tolerance: 1.49e-08
```

The output from the model provides you with the equation used to fit the distribution and the three parameter values: *r*, *c* and *t*.

3.5 Fixing starting values

On rare occasions the model may fail to converge within 50 iterations. This may occur if a very small dataset is used. It is possible to overcome this issue by fixing or setting upper and lower bounds for one of the starting values. The parameter *r* is the most appropriate parameter to do this with. It is suggested that you calculate the starting value for *r* as in section 5.4.1 and set the upper and lower bounds around this figure (see below).

```
# Fixing/constraining starting values
FixedtdLobelia12.5 <- timedist(data = y12.5, x = "Day", y = "propMax", r =
0.03, c = 0.5, t = 14.5, upper = c(0.1, Inf, Inf), lower = c(0.01, -Inf, -
Inf))
```

3.6 Interpreting the fit of the model

To assess how well the model has fit the data, and the reliability of parameter estimates, it

is suggested that the standard errors, correlations of the estimates, and confidence intervals are obtained. In each example we have used the model 'FrancotdLobelia12.5'; simply replace this with the name of the object you have created for your data.

3.6.1 Standard errors

Obtaining the standard errors of the parameter estimates

```
summary(FrancotdLobelia12.5, correlation = TRUE, symbolic.cor = FALSE)
```

```
> summary(FrancotdLobelia12.5, correlation = TRUE, symbolic.cor = FALSE)

Formula: propMax ~ 1 - (1 - (r/(1 + exp(-c * (Day - t)))))^Day)

Parameters:
   Estimate    Std. Error  t value   Pr(>|t|)
r  0.083393    0.006615    12.607    6.99e-08  ***
c  0.626782    0.156122     4.015    0.00203   **
t 12.093637    0.462246    26.163    2.95e-11  ***
---
Signif. codes:  0 '***' 0.001 '**' 0.01 '*' 0.05 '.' 0.1 ' ' 1


Residual standard error: 0.05955 on 11 degrees of freedom


Correlation of Parameter Estimates:
   r      c
c -0.49
t  0.72  -0.52


Number of iterations to convergence: 16
Achieved convergence tolerance: 1.49e-08
```

3.6.2 Correlation of parameter estimates

If a higher level of precision is required, the correlation of parameter estimates can be obtained separately.

Create an object containing the correlations of the parameter estimates (to 7 decimal places).

```
CPE <- vcov(FrancotdLobelia12.5)
```

Print correlations

```
cov2cor(CPE)
```

```
> cov2cor(CPE)
   r          c          t
r  1.0000000 -0.4857904  0.7153296
c -0.4857904  1.0000000 -0.5247586
t  0.7153296 -0.5247586  1.0000000
```

3.6.3 Confidence intervals

To produce accurate confidence intervals for the parameters in a nonlinear regression model fit, it is better to use a package called nlstools.

Install the package nlstools

```
install.packages("nlstools")
```

Load in nlstools

```
library(nlstools)
```

Obtaining the confidence intervals of the parameter estimates.

```
confint2(FrancotdLobelia12.5)
```

```
> confint2(FrancotdLobelia12.5)
```

```
   2.5 %         97.5 %
r   0.06883386    0.09795187
c   0.28316058    0.97040283
t  11.07624152   13.11103293
```

3.6.4 R-squared

There is no direct R-squared for non-linear regression. However, an R-squared value calculated as 1-(Residual Sum of Squares/Corrected Sum of Squares) defines a similar quantity for nonlinear regression, is able to describe the proportion of variance explained by the model, and provides a very good estimate of how well the model fits the data.

Extracting the RSS

```
FrancotdLobelia12.5$m$rss()
```

```
> FrancotdLobelia12.5$m$rss()
[1] 0.9681957
```

3.7 Statistical moments

The following statistical moments for the fitted distribution can be calculated: mean, variance, standard deviation, skew, kurtosis and entropy.

Extracting the statistical moments

```
FrancotdLobelia12.5$m$getMoments()
```

```
> FrancotdLobelia12.5$m$getMoments()
      mean  variance        sd      skew  kurtosis   entropy
1 15.75401  83.02729  9.111931  2.897078  12.17524  4.491001
```

3.8 Percentiles

The percentiles of the distribution can also be calculated. This can be achieved for a single percentile or for a sequence of percentiles.

```
# Extracting a single percentile
tdPercentiles(FrancotdLobelia12.5, n = 0.01)
```

```
> tdPercentiles(FrancotdLobelia12.5, n = 0.01)
      1%
5.913667
```

```
# Extracting a sequence of percentiles from 10% to 90% in steps of 10.
tdPercentiles(FrancotdLobelia12.5, n = seq(0.1, 0.9, 0.1))
```

```
> tdPercentiles(FrancotdLobelia12.5, n = seq(0.1, 0.9, 0.1))
     10%       20%       30%       40%       50%       60%       70%
9.159305 10.382816 11.269057 12.073122 12.918504 13.952189 15.516796
      80%       90%
18.776037 26.446720
```

3.9 Plotting the distribution

The nlstimedist package has two built-in graphing functions for plotting the estimated distribution as both a cumulative distribution function and a probability density function.

3.9.1 Cumulative distribution function (c*df*)

The cumulative distribution function is produced using the function **tdCdfPlot**. This function takes one or more objects produced by the model, a scaling parameter 'S' and

values for the x-axis ‘xVals’ (which includes a value for smoothing the curve), as arguments to produce the *cdf* plot.

The scaling parameter ‘S’ provides a convenient way to scale the curves to the number of completions (n) from a known initial number (N) as their proportion or ration (n/N). Scaling is often appropriate in studies such as germination, egg-hatching, and mortality and is a useful way of visualising differences between groups.

Producing a *cdf* for a single model object

```
tdCdfPlot(FrancotdLobelia12.5, S = 1, xVals = seq(0, 30, 0.01))
```

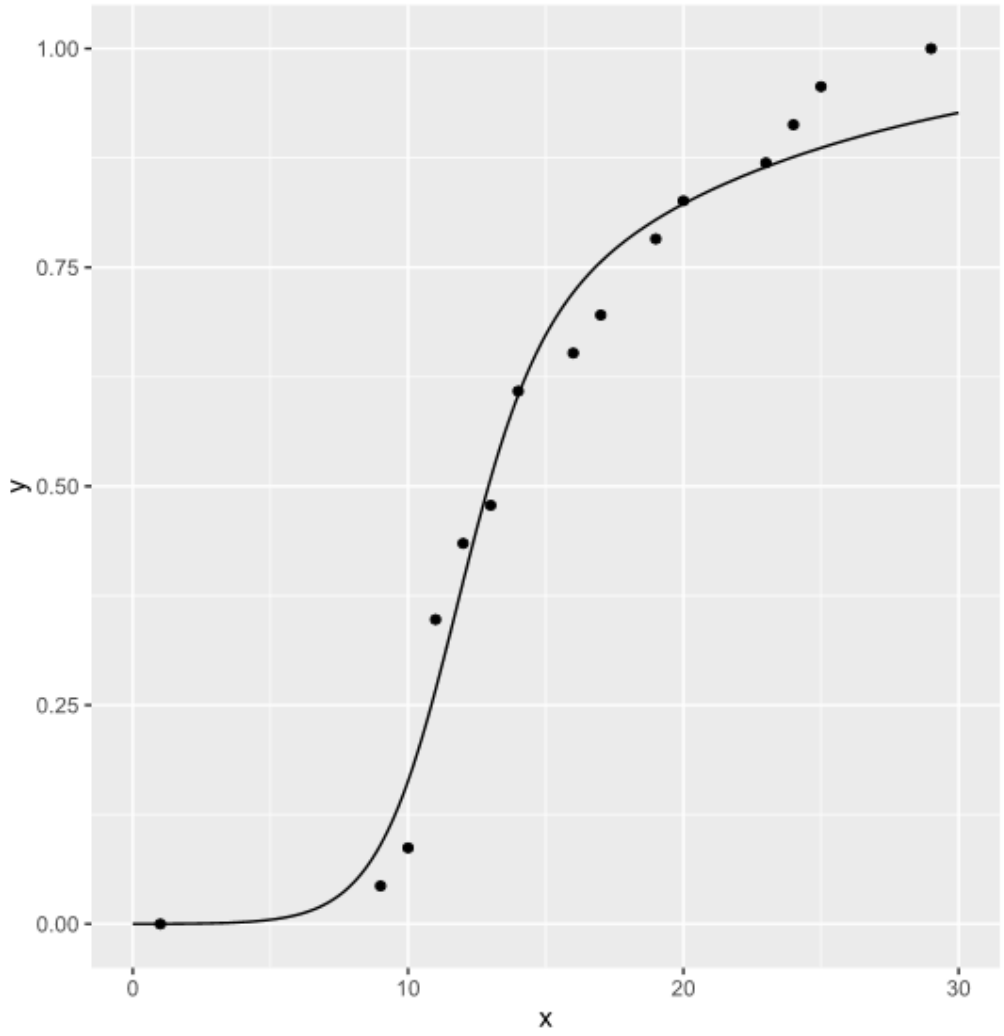

Producing a CDF for multiple model objects with scaling

```
tdCdfPlot(Lobelia1, Lobelia2, Lobelia3, Lobelia4, Lobelia5, Lobelia6,
Lobelia7, S = c(0.213, 0.307, 0.533, 0.707, 0.867, 0.907, 0.840), xVals =
seq(0, 30, 0.001))
```

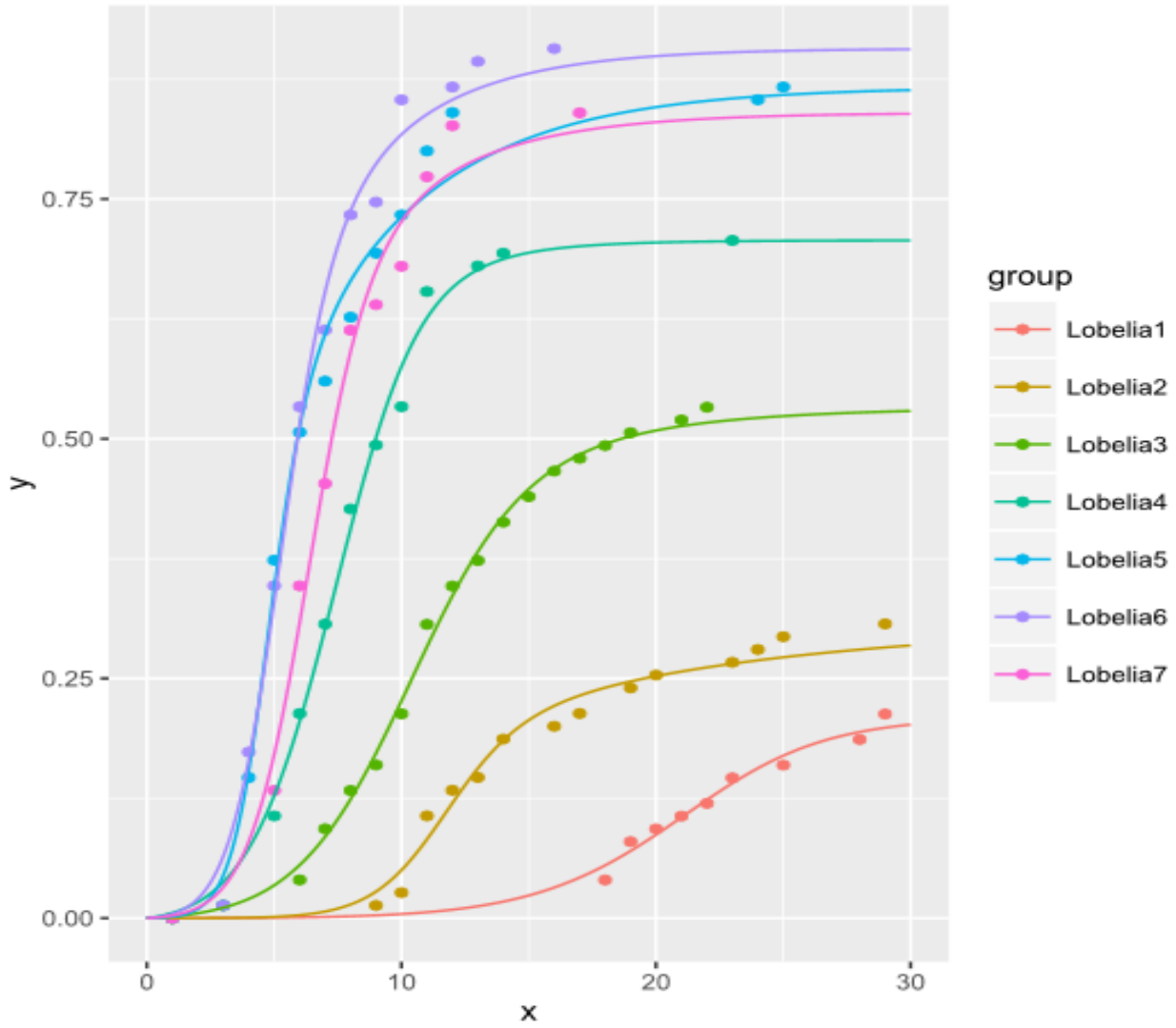

3.9.2 Probability density function (*pdf*)

The probability density function is produced using the function **tdPdfPlot**. This function takes one or more objects produced by the model, a scaling parameter 'S' and values for the

x-axis ‘xVals’ (which includes a value for smoothing the curve), as arguments to produce the *pdf* plot.

Producing a *pdf* for a single model object

```
tdPdfPlot(FrancotdLobelia12.5, S = 1, xVals = seq(0, 30, 0.01))
```

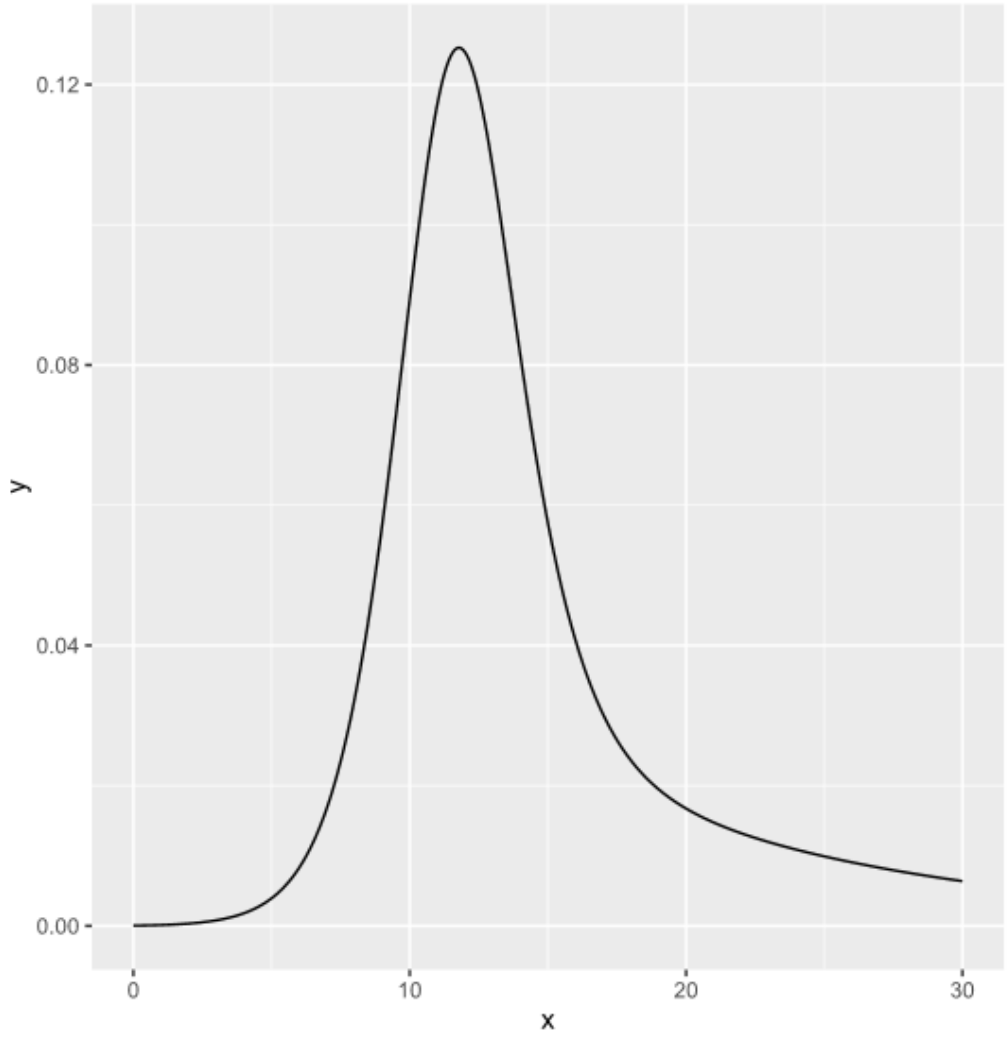

Producing a *pdf* for multiple model objects with scaling once each object has been created using the **timedist** function

```
tdPdfPlot(Lobelia1, Lobelia2, Lobelia3, Lobelia4, Lobelia5, Lobelia6,
Lobelia7, S = c(0.213, 0.307, 0.533, 0.707, 0.867, 0.907, 0.840), xVals =
seq(0, 30, 0.001))
```

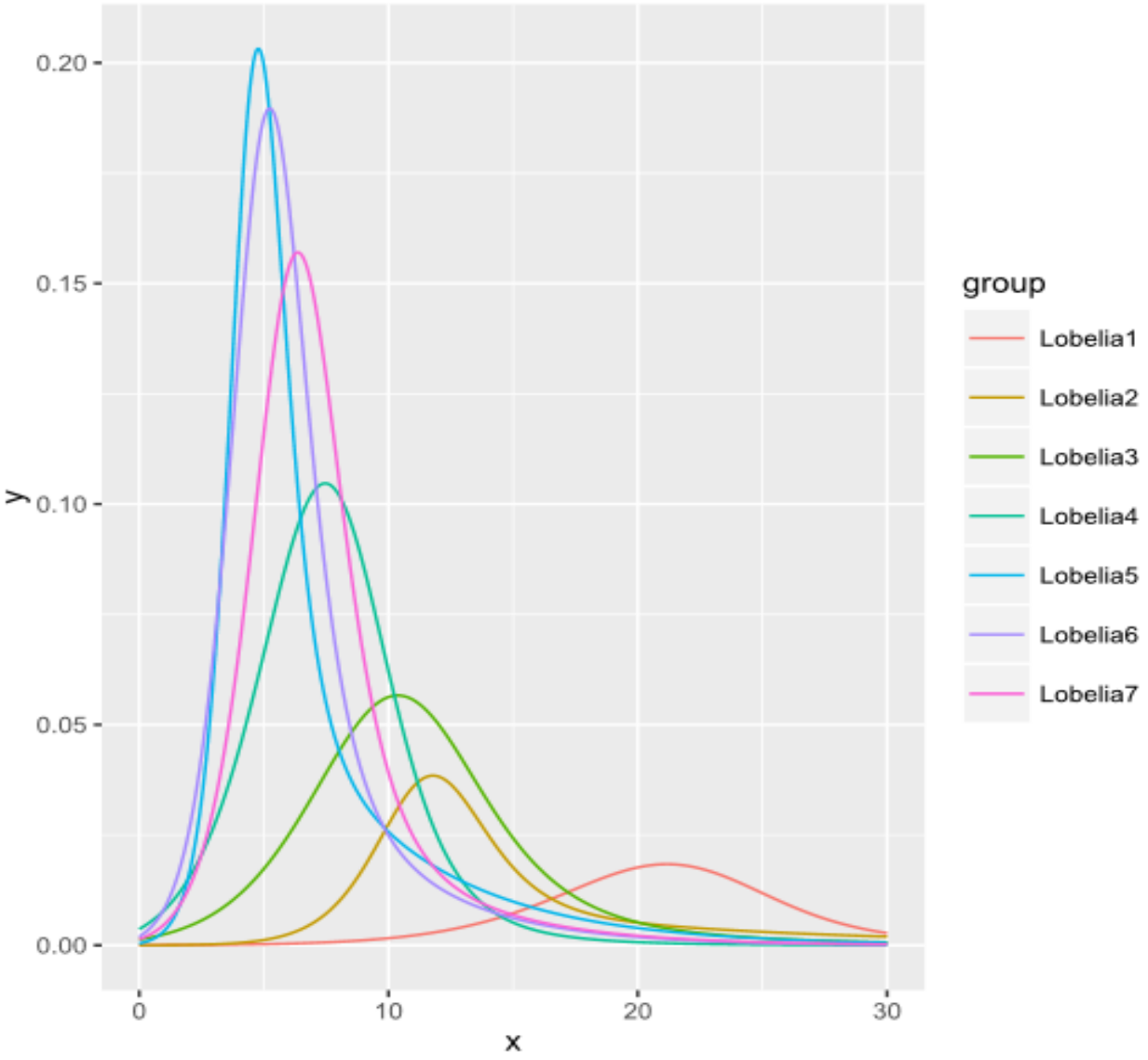

3.9.3 Customising *cdf* and *pdf* plots

Customising the built-in *cdf* and *pdf* graphing functions is easily achieved using **ggplot2** (Wickham 2009).

```
# Install ggplot2
install.packages("ggplot2")

# Load ggplot2
library(ggplot2)

# Save the cdf graphing function to an object
graph1 <- tdCdfPlot(Lobelia1, Lobelia2, Lobelia3, Lobelia4, Lobelia5,
Lobelia6, Lobelia7, S = c(0.213, 0.307, 0.533, 0.707, 0.867, 0.907, 0.840),
xVals = seq(0, 30, 0.001))
```

ggplot2 is fully customisable and allows you to add a theme, axis labels, legend and additional elements to your plot.

```
# Customise your saved object
graph1 + theme_bw() +
  labs(title = "Lobelia", x = "Day", y = "Germination proportion") +
  scale_color_manual("Temperature\n", labels = c("9.8°C", "12.5°C", "16.7°C",
"20.2°C", "24.3°C", "28.5°C", "32.0°C"), values = c("firebrick2",
"darkgoldenrod2", "forestgreen","aquamarine3", "deepskyblue", "blueviolet",
"deeppink" )) +
  theme(axis.text.x = element_text(size = 10), axis.title.x =
element_text(size = 16),
        axis.text.y = element_text(size = 10), axis.title.y =
element_text(size = 16),
        plot.title = element_text(size = 20, face = "bold", color = "black"))
```

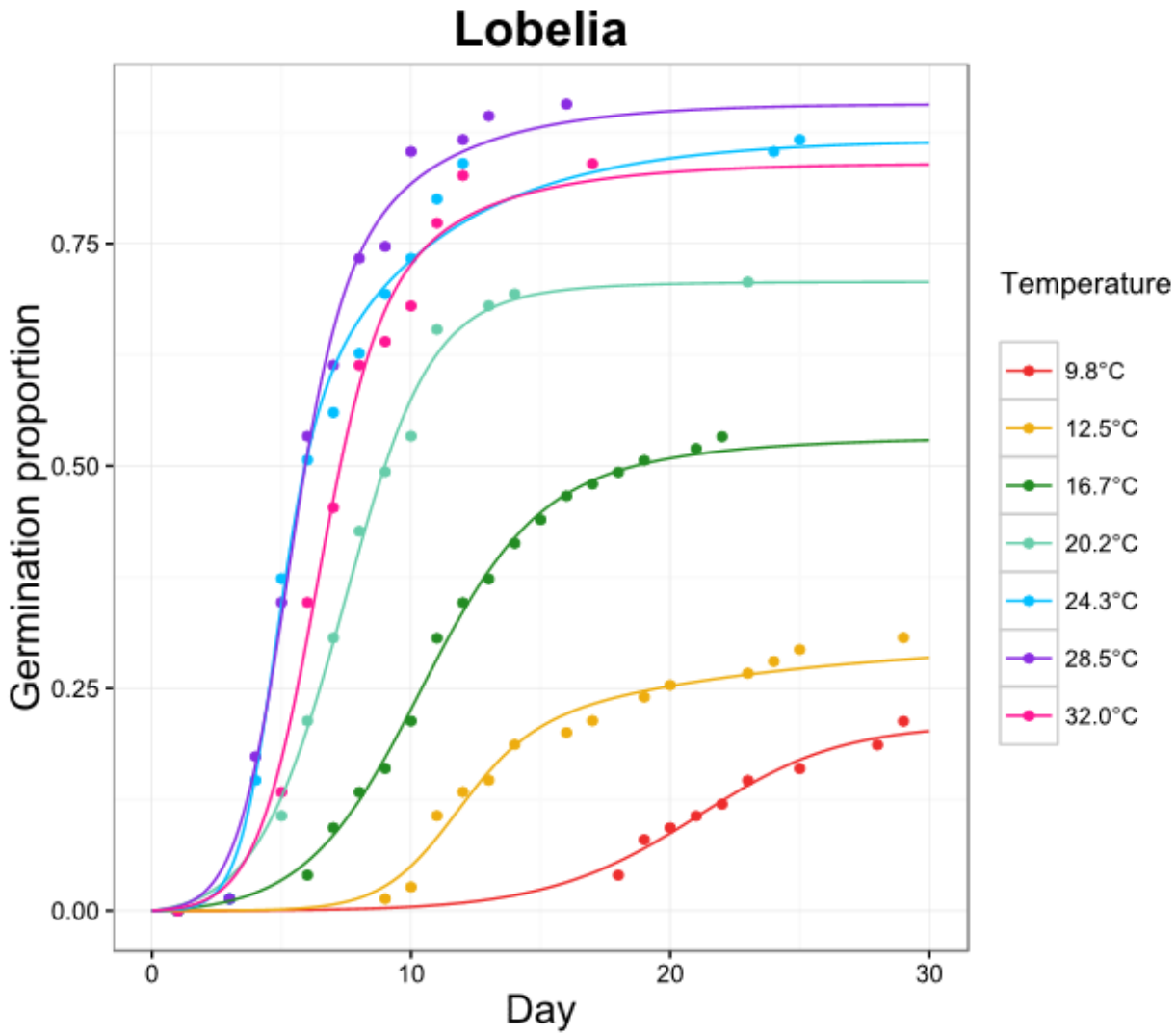

3.10 How to cite the nlstimedist package

Franco, M., Ramsay, P. and Steer, N. (2019). nlstimedist: Non-linear model fitting of time distribution of biological phenomena. R package version 1.1.4.

4 Germination response to temperature of three high-elevation Andean *Puya* species

4.1 Introduction

The climate of the tropical Andes (2°N-18°S) is changing rapidly (Buytaert *et al.* 2010). Climate records for the region show a sustained increase in temperature of 0.13°C per decade for the period 1950-2010 (Urrutia & Vuille 2009; Vuille *et al.* 2015). Model projections of future climatic changes indicate significant tropospheric warming in the tropical Andes (Bradley *et al.* 2006; Vuille *et al.* 2008; Urrutia & Vuille 2009) with a likely mean temperature increase of 3 ± 1.5°C over the current century (Buytaert, Cuesta-Camacho & Tobón 2011). Under a high emission scenario, temperature increases could reach 4.5–5°C by the end of the 21st century (Vuille *et al.* 2008), which would lower the lapse rate (i.e. the decrease in air temperature with elevation), intensifying the trend of greater warming at higher elevations (Urrutia & Vuille 2009; Buytaert *et al.* 2010; Vuille *et al.* 2015). The temperature increases projected for the 21st century have the potential to move temperature regimes, and the species that live within them, upslope by ~600 m (Anderson *et al.* 2011). The ability of species to move in response to climate change is a key consideration in assessing the impact of climate change on biodiversity.

Evidence of range contractions and expansions from palaeoecological records show that plant populations within high-elevation Andean ecosystems are particularly sensitive to changing climatic conditions (van der Hammen 1974; Flantua *et al.* 2019). Distributional changes identified from these records are thought to have been largely regulated by changes in temperature (Madriñán, Cortés & Richardson 2013). Current climatic changes

are occurring much faster than plants in these ecosystems would have experienced in the past. It is therefore uncertain whether they will be able to respond to these changes, either by developing the required adaptations and/or by dispersing sufficiently fast enough to deal with the new climate.

Andean plant species are typically adapted to specific climatic conditions and, as a result, occupy comparatively small altitudinal and latitudinal ranges (Larsen *et al.* 2011). For many species, range changes through time are facilitated by the dispersal of seeds. However, this mechanism is only effective if plants find suitable conditions to complete their lifecycle and reproduce. The temperature of an environment has a strong influence on plant recruitment as it controls many aspects of plant regeneration, in particular seed dormancy and germination (Grubb 1977; Baskin & Baskin 1988; Grime 2002; Walck 2011). To increase the chances of survival, some plants have seeds that become dormant and require specific stimuli before germination is initiated (Baskin & Baskin 2014). Often this evolutionary adaptation promotes the appearance of vulnerable seedlings at appropriate times and in places where establishment is more likely. An understanding of how plant regeneration responds to temperature will be essential to help manage existing communities and predict how individual species might respond to changing climatic conditions.

In high-elevation ecosystems, germination and establishment requirements have been proposed as explanations for the distributional limits of mountain plants (in the general sense), especially the role of low temperatures in setting the upper altitudinal limits of species (Körner & Paulsen 2004; Klimeš & Doležal 2010; Dvorský *et al.* 2017). Most studies investigating the distributional limits of high-elevation plants have been carried out on

temperate species and in mountains with clear seasonality in climate. Alpine plants from seasonal climates go through dormancy in winter and are protected against extreme conditions under snow, or are frost resistant (Grabherr, Gottfried & Pauli 2010). In contrast, plants from tropical mountains, where there is little seasonal variability in temperature, tend to remain in an active state throughout the year (Squeo *et al.* 1991).

Many plant genera in tropical mountains have a temperate origin, such as *Alchemilla, Carex and Ranunculus* which colonised the high mountains of Africa several times (Gehrke & Linder 2009) and *Cerastium, Hypochaeris, Draba*, and *Lupinus* which arrived into the Andean páramo from northern temperate regions (Sklenář, Dušková & Balslev 2011). Others are of tropical origin and evolved alongside the development of the mountain habitats where they live. For example, the adaptive radiations of giant *Lobelia* (Lobeliaceae) in the East African mountains (Hedberg 1969; Knox & Palmer 1998; Masao 2012; Zhao *et al.* 2016) and *Puya* (Bromeliaceae) during the Andean uplift (Varadarajan 1990; Jabaily & Sytsma 2013). Owing to the differing evolutionary histories of tropical mountain plants and the lack of germination studies conducted on plants from tropical mountain regions, it is unclear whether they respond to temperature in a similar way to that of temperate mountain plants. It is also not clear how much the upper altitudinal limit of some plants might reflect their germination temperature requirements.

Puya is an interesting genus to consider for the investigation of tropical mountain plant germination as it has undergone considerable adaptive radiation linked to the isolation of populations on mountains and, potentially, niche expansion into new kinds of environment (Jabaily & Sytsma 2013). Because of its evolutionary history, *Puya* species occupy different altitudes and latitudes and are subject to different temperature regimes. This tropical

genus is a flagship species of high-elevation Andean páramo and puna, yet despite its ecological importance, little is known about how climate warming will affect the ability of *Puya* species to persist at high elevations. *Puya* appears to have a germination response to temperature and it has been repeatedly suggested that *Puya* are limited by suitable germination sites (Miller & Silander 1991; Laegaard 1992; Ramsay & Oxley 1996). This is particularly important because many high-elevation *Puya* species are semelparous ("big bang" reproduction only at the end of their lives) and disperse their non-dormant seeds relatively short distances from the mother plant (García-Meneses 2012). Many *Puya* species are dependent on reproduction from seed. Their persistence in habitats and their ability to expand into new territory is likely limited by seed dispersal and germination.

Germination requirements are also likely to be relevant to the heterogeneous, fine-scale habitat mosaics that typify tropical mountains (Körner 2003). The availability of suitable microsites ("safe sites") for seed germination could be fundamental to a species' persistence in mountain landscapes (García-Camacho, Iriondo & Escudero 2010; Scherrer & Körner 2011; Frei, Scheepens & Stöcklin 2012). Microsites are essential for the survival of many plant species in challenging mountain environments as they provide appropriate temperature and soil moisture conditions within an otherwise inhospitable landscape (Forbis 2003; Körner 2003). Few studies have been conducted in the Andes, but it is clear that several species are sensitive to fine-scale microclimates (Miller & Silander 1991; Laegaard 1992; Ramsay & Oxley 1996; Cavieres *et al.* 2007; Rada, García-Núñez & Rangel 2011). These studies show that recruitment in high-elevation environments tends to be patchy and suggest links to temperature. Changing climatic conditions and human land use could alter the availability of suitable seedling safe sites over relatively short time scales

and are likely to affect plant species recruitment at and beyond their range edges (Kroiss & HilleRisLambers 2015).

This study assesses the germination responses of three species of *Puya* across a range of temperatures. We aim to compare broad germination responses of the three species. We also consider the potential for germination temperature limitations to explain *Puya* distribution patterns in the field both within microhabitat mosaics and at their upper altitudinal limits. Finally, we consider the consequences of these findings for the potential future distribution of these species.

4.2 Materials and Methods

4.2.1 Study species

The genus *Puya* Molina (Bromeliaceae) comprises approximately 200 species most of which are restricted to South America but with distinct altitudinal ranges up to > 4500 m elevation (Benzing 2000; Hornung-Leoni & Sosa 2005). *Puya hamata* L.B. Smith*, Puya clava-herculis* Mez & Sodiro and *Puya raimondii* Harms are three species of giant rosette-forming bromeliads belonging to the subfamily Pitcairnioideae (Jabaily & Sytsma 2010). Their distributional ranges and selected reproductive characteristics are summarised in Table 4.1.

P. hamata commonly occurs in the high-altitude páramo grasslands in parts of Ecuador, Colombia and Peru (Garcia-Meneses & Ramsay 2014). *P. clava-herculis* is common in the páramo regions of Ecuador and Colombia. Although there is some overlap in the distributional range of these two species, in regions where they co-occur, they are largely parapatric. *P. hamata* occupies lower elevation sites and is most often found at altitudes

between 3350 m and 3700 m, whilst *P. clava-herculis* occupies higher elevation sites and is most often found between 3650 m and 4125 m (Miller & Silander 1991). Finally, *P. raimondii* has a restricted distribution and is only found in a few isolated locations in the high-altitude humid puna grasslands of Peru and the west of Bolivia (Smith & Downs 1974; Waite 1978; Hornung-Leoni *et al.* 2013). *P. raimondii* commonly occurs between 3800 m and 4500 m but its range probably extends to even higher altitudes (Lambe 2009; Hornung-Leoni, Gonzalez-Gomez & Troncoso 2013; Montesinos-Tubee, Cleef & Sykora 2015).

Table 4.1. Location and reproductive characteristics of three *Puya* species.

	P. hamata	*P. clava-herculis*	*P. raimondii*
Geographic range	Ecuador, Colombia & Peru	Ecuador & Colombia	Peru & Bolivia
Core altitudinal range (m) above sea level	3350–3700	3650–4125	3800–4500
Reproductive schedule	Semelparous	Semelparous	Semelparous
Inflorescence height (m)	3–4	1–1.5	8–10
Seed type	Winged	Winged	Winged
Approximate no. of seeds per plant	700,000*	23–28,000**	6–12 million***
Dispersal ability	Poor	Poor	Poor

*Garcia-Meneses and Ramsay (2012); **Miller (1986); ***(Vadillo, Suni & Cano 2004).

4.2.2 Seed collection

Seed sampling details are summarised in Table 4.2. All fruits were collected from randomly selected reproductive plants. After collection, seeds were carefully removed from their seedpods, cleaned by hand and stored in paper bags. Predated or damaged seeds were

discarded and only undamaged seeds with a visibly developed embryo were retained for use in the experiment. The seeds were kept at room temperature until germination trials were carried out within eight months of collection.

In order to characterise the thermal microenvironments in the seed collection sites, a series of temperature measurements were taken at the soil surface and at 10 cm depth. iButton data loggers (iButtons DS1922L, Maxim Integrated, USA) were placed in six locations on Volcán Chiles at 3600–3800 m altitude for *P. hamata,* and in another six locations at 4000–4200 m altitude for *P. clava-herculis*. These locations were unshaded, with no vegetation directly above them, which is where *Puya* seedlings are more likely to be found (P. Ramsay's personal observation; see also Discussion section). Temperatures were recorded every three minutes from 10:00 to 15:00 from 29 March to 2 April 2013 (1800 measurements for each datalogger). For *P. raimondii*, temperatures were recorded at the soil surface at Pachapaqui (3800–4000 m) with a Krisbow KW06-559 dual laser infrared thermometer and at 10 cm depth with a Signstek 6802 II Dual Channel Digital Thermometer for 320 different locations from 14–20 March 2017.

4.2.3 Effect of temperature on seed germination

Puya seeds were sown in 0.8% bacteriological set water agar, in 9 cm diameter petri dishes, arranged across a temperature gradient (Table 4.2). Water agar was used due to its ability to retain moisture (Ellis, Hong & Roberts 1985) and was autoclaved at 120°C for 15 minutes to sterilise it (Fuller & Fuller 1995). The seeds were not sterilised. To create a temperature gradient, two Grant thermostatic water baths (one cold and one hot), were linked by an aluminium plate. Petri dishes were placed at intervals along the aluminium plate and temperatures across each petri dish were measured with DS-1922L *i*-button data

loggers (Maxim Integrated, USA). Due to the continuous nature of the temperature gradient, a small range of temperatures was experienced across the width of each petri dish. To control for this variation, and to ensure that seeds were germinated at a constant temperature, petri dishes were subdivided vertically according to the temperatures recorded across each dish. Seeds were placed into these subdivisions in columns. Cool white fluorescent lighting was provided by two 55-Watt bulbs in a 12-hour light/12-hour dark photoperiod. For the purpose of this experiment, a seed was said to have germinated

Table 4.2. Origins of the seeds used in this study and experimental design of germination trials along temperature gradients for three *Puya* species.

	P. hamata	*P. clava-herculis*	*P. raimondii*
Seed collection			
Locality	Reserva Ecológica El Ángel, Ecuador	Volcan Chiles, Ecuador	Pachapaqui, Peru
Coordinates	0.7552° N 77.9053° W	0.8169° N 77.9372° W	9.9583° S 77.0953° W
Altitude (m)	3600	4150	4000
No. of plants	40	6	10
No. of fruits per plant	10	10	10
Date seeds collected	July-Oct 2009	Jan-April 2014	Jan-April 2014
Germination trials			
Date experiment conducted	Jan-March 2010	Sept-Nov 2014	Sept-Nov 2014
Total no. of seeds	700	1800	3600
Temperature gradient min (°C)	10.8	0.3	3.4
Temperature gradient max (°C)	31.6	26.2	26.3
No. of temperature intervals	35	18	18
No. of seeds per treatment	20	100	200

upon radical emergence from the seed coat (Salisbury & Ross 1992). Germinated seeds were counted daily. All trials were run until no further seeds germinated for a period of 72 hours.

4.2.4 Data analysis

Analysis of the effect of temperature on seed germination was performed using a novel model of phenological dynamics (Steer, Ramsay & Franco 2019). The Franco model was fitted to each cumulative germination curve (the proportion of germinated seeds through time). This method was chosen as it quantifies different components of the cumulative germination distribution and allows biologically meaningful comparisons between treatments.

The model has the form:

$$y = 1 - \left(1 - \frac{r}{1+e^{-c(x-t)}}\right)^{x} \quad (1)$$

where y is the empirically recorded proportion of germination over time (x), r quantifies the maximum proportional rate at which germination occurs (it is dimensionless), c is the rate at which r converges on its maximum value and is inversely proportional to the temporal spread of the distribution (units: time^{-1}), and t is an overall measure of the time lag of the response (units: time) (Steer, Ramsay & Franco 2019). The model can be scaled by y_{max} which represents the observed final percentage of germinated seeds.

The derivative of equation 1 provides the probability density function (*pdf*):

$$\frac{dy}{dx} = \left(1 - \frac{r}{1+e^{-c(x-t)}}\right)^{x} \left(\frac{rcxe^{-c(x-t)}}{\left(1+e^{-c(x-t)}\right)^{2}\left(1-\frac{r}{1+e^{-c(x-t)}}\right)} - \ln\left(1 - \frac{r}{1+e^{-c(x-t)}}\right)\right) \quad (2)$$

which describes the changing population-level rate of germination with time. The statistical moments and percentiles of the fitted distribution can be extracted from the *pdf* facilitating the comparison of different temperature treatments through time. The final percentage of germinated seeds (y_{max}) was obtained directly from the data, while parameters *r*, *c* and *t* and the statistical moments were estimated using the *nlstimedist* R package (Franco, Ramsay & Steer 2019; Steer, Ramsay & Franco 2019).

4.3 Results

4.3.1 Field temperatures

Of the three species, *P. clava-herculis* seeds were collected from the coolest location, with average soil temperatures at the surface and at 10 cm depth of just over 6°C (Fig. 4.1). Surface temperatures at the *P. hamata* site were around 12°C compared with the *P. raimondii* site which reached >16°C on average, despite it being approximately 400 m higher in elevation. However, at 10 cm depth, the soil temperatures of both *P. hamata* and *P. raimondii* sites was similar. At the *P. hamata* and *P. raimondii* collection sites, temperature varied considerably through time, at times reaching 30°C on sunny days, even at 10 cm depth. This was less true of the *P. clava-herculis* site, where surface temperatures occasionally approached 20°C and never exceeded 8°C at 10 cm depth.

4.3.2 Laboratory germination experiments

A relatively broad range of temperatures produced high germination percentages (y_{max}) for each species. Within this optimum range, germination percentages exceeded 70% for both *P. hamata* and *P. raimondii* but were lower (around 50%) for *P. clava-herculis* (Fig. 4.2). *P. hamata* had the warmest optimum temperature range for germination with maximum

germination percentages occurring between 15.7°C and 25.5°C. The optimum temperature range for germination was cooler for both *P. clava-herculis* and *P. raimondii,* 11.0°C–23.2°C and 9.3°C–20.0°C, respectively. For all three species, the highest germination percentages occurred within a 10-12°C window.

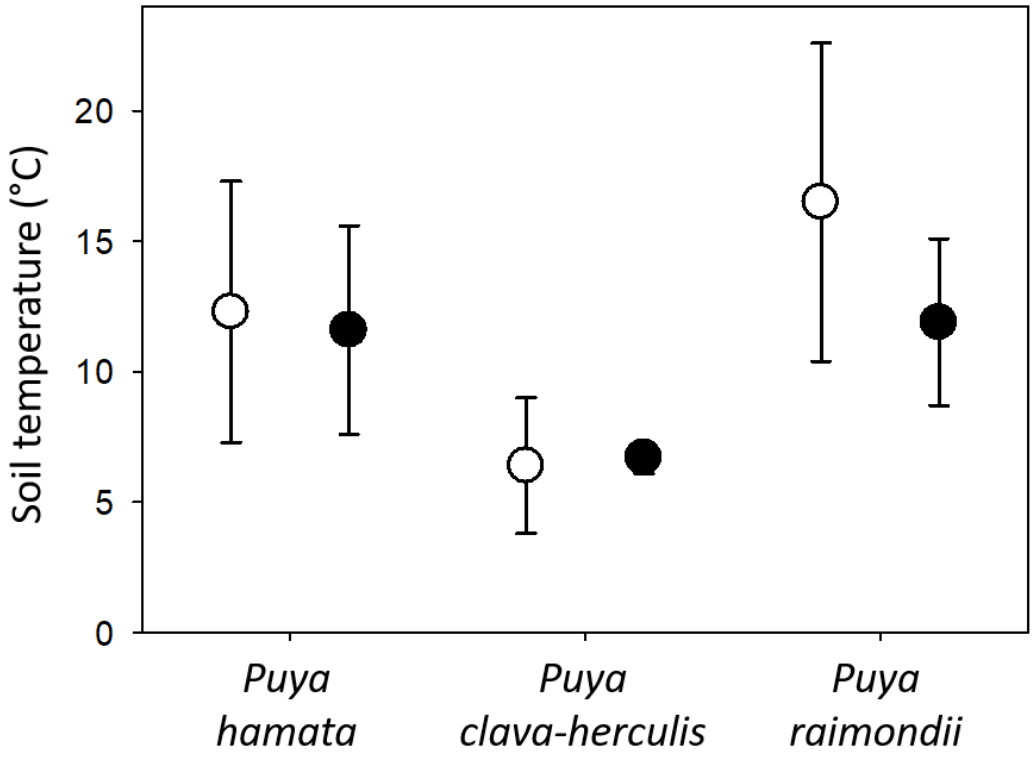

Figure 4.1. Mean soil temperature at the surface (white symbols) and at 10 cm depth (black symbols) for the locations of seed collection for each of the three *Puya* species. Error bars represent one standard deviation from the mean.

There was a steep decline in germination percentages on either side of each species optimum temperature range until no germination was observed and the minimum and maximum temperature thresholds were identified. The minimum threshold for germination for *P. hamata* was 13.9°C and was much lower for *P. clava-herculis* and *P. raimondii*, 7.5°C and 4.6°C, respectively. The maximum temperature threshold for

germination was again higher for *P. hamata* (28.5°C) than it was for *P. raimondii* (24.3°C). No upper threshold was identified for *P. clava-herculis* as the temperature range employed did not reach it.

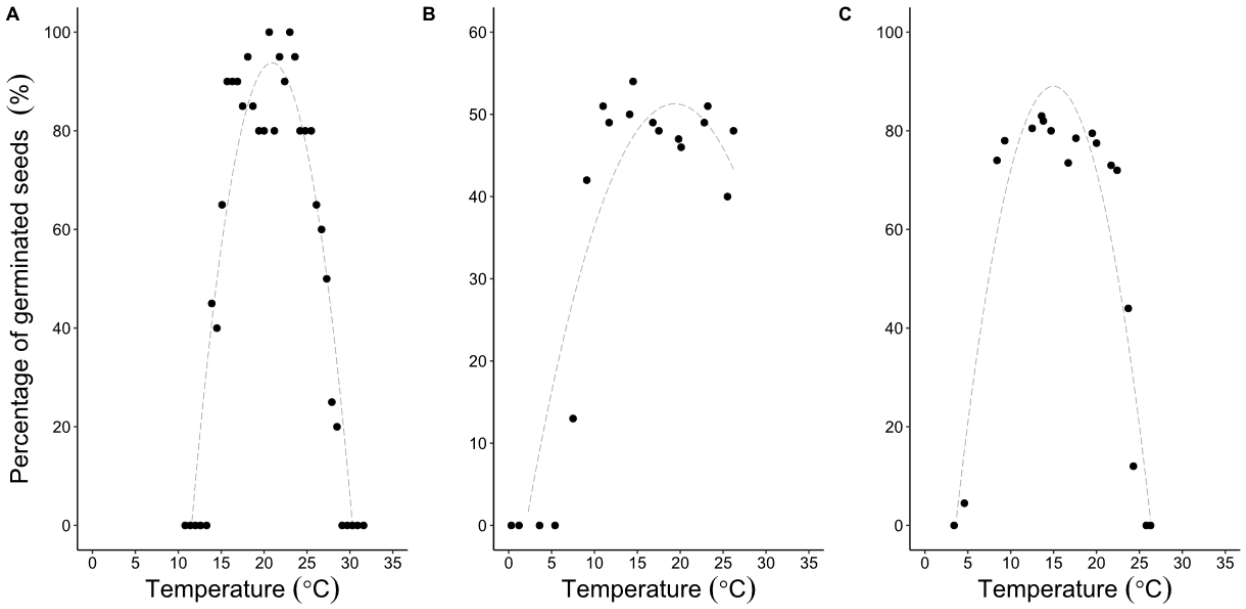

Figure 4.2. The percentage of germinated seeds of (A) *Puya hamata*, (B) *Puya clava-herculis*, and (C) *Puya raimondii* along an experimental temperature gradient. The dashed grey line is a quadratic fit to the germination percentage data.

The model successfully fitted the germination time course of 35 temperature treatments (10 for *P. hamata*, 11 for *P. clava-herculis*, and 14 for *P. raimondii*) (Fig. 4.3). In the remaining treatments, either no germination occurred, or germination occurred very rapidly (over a period <5 days) and not enough data points were produced to allow germination curves to be fitted. The cumulative distribution functions (*cdfs*) and the population-level rate of germination, represented as probability density functions (*pdfs*), provide an informative visual summary of how germination was affected across a range of temperatures (Fig. 4.3). The form produced is typical of germination curves and shows

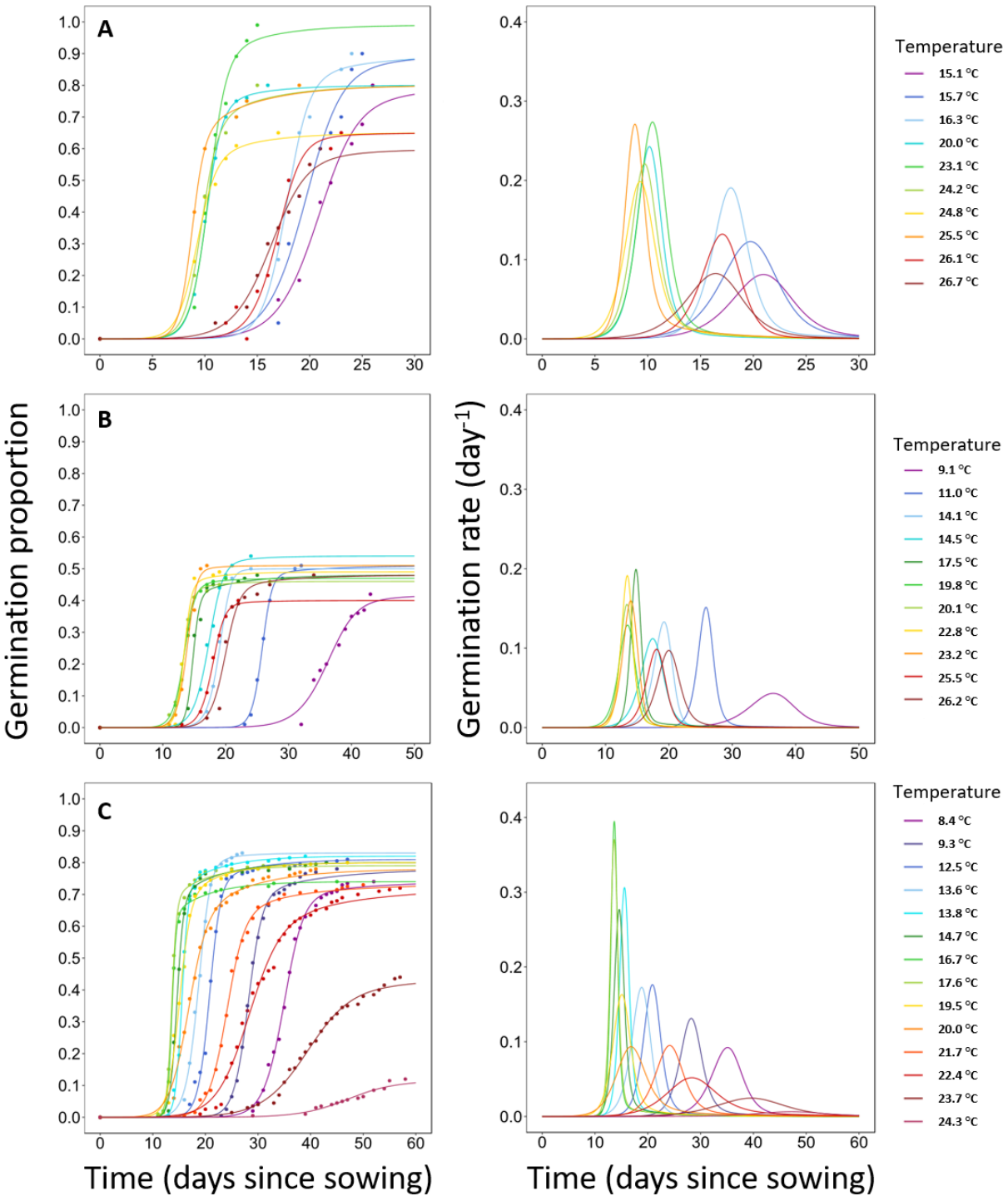

Figure 4.3. Cumulative distribution functions (left) and corresponding probability density functions (right) for each species, scaled by the total germination percentage (y_{max}): (A) *Puya hamata*, (B) *Puya clava-herculis*, and (C) *Puya raimondii*. Probability density functions describe the population-level rate of germination and the area under each curve is equal to the maximum percentage of germination.

that, for each species, when temperatures were outside of the optimum, the start of germination was delayed and occurred over a longer period. This pattern is examined in more detail using the parameters produced by the model.

In each of the *Puya* germination experiments, temperature affected all three model parameters in a curvilinear fashion (Fig. 4.4). For each species, the relationship between

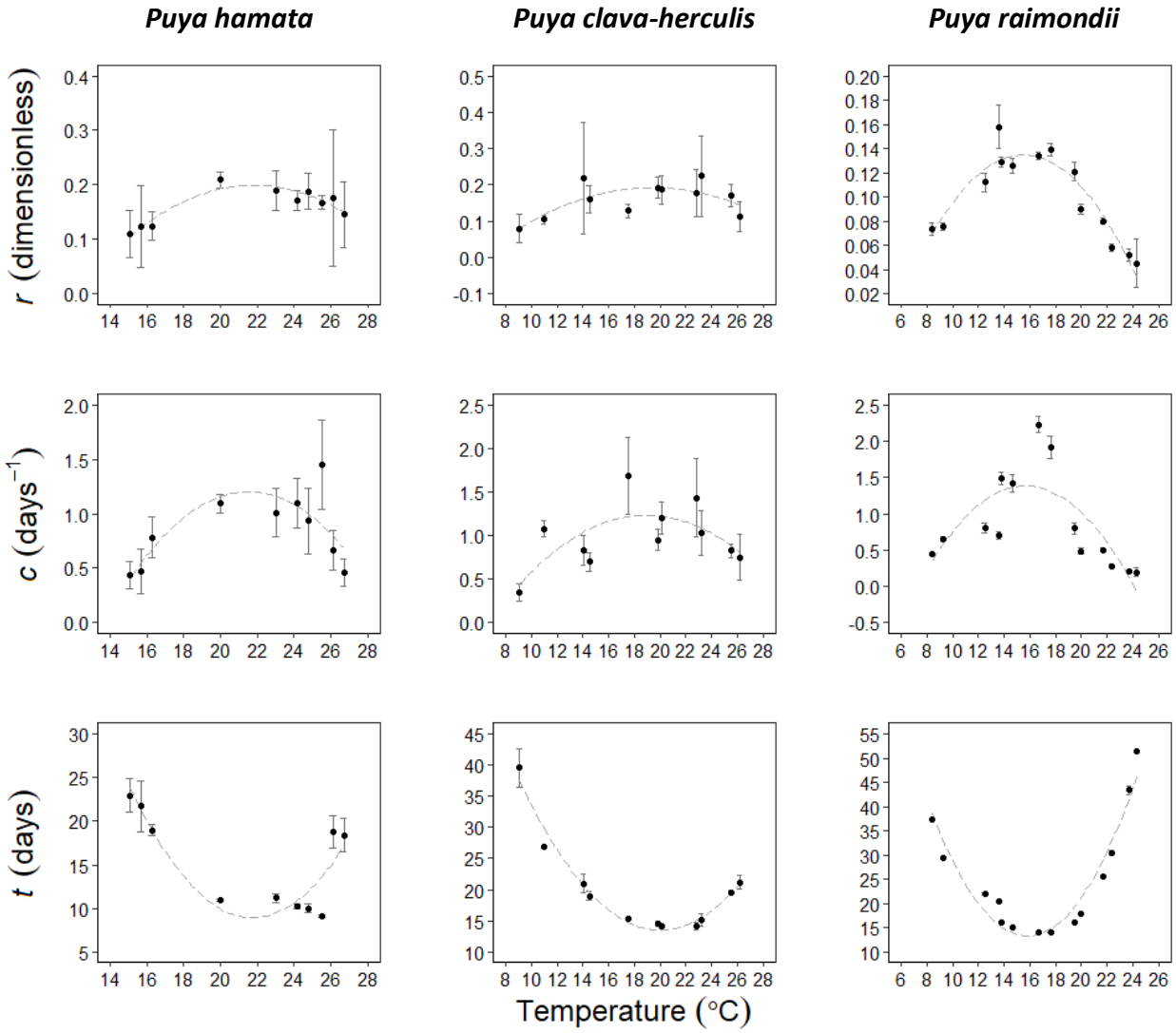

Figure 4.4. The quadratic relationships between the values of the parameter estimates produced from each model fit and temperature for each species. *Puya hamata*: (*r*) R^2 = 0.887, p < 0.001; (*c*) R^2 = 0.588, p = 0.045; (*t*) R^2 = 0.833, p = 0.002); *Puya clava-herculis*: (*r*) R^2 = 0.538, p = 0.045; (*c*) R^2 = 0.453, p = 0.090; (*t*) R^2 = 0.971, p < 0.001); *Puya raimondii*: (*r*) R^2 = 0.886, p < 0.001; (*c*) R^2 = 0.595, p = 0.007; (*t*) R^2 = 0.931, p < 0.001). Error bars represent the standard errors of the parameter estimates.

temperature and parameters *r* (the maximum proportional rate of germination) and *c* (the temporal spread) was convex, whereas the relationship between temperature and parameter *t* (the time lag of the response) was concave. The highest proportion of seeds germinated coincided with the highest rate of germination and narrowest temporal spread (parameters *r* and *c*) and the shortest time lag (parameter *t*). Away from these temperature optima all three species had a lower rate and a greater temporal spread of germination with longer response times. For each species, the model parameters identified similar optimum germination temperatures even though each parameter has a unique effect on the three different aspects of the distribution's shape. These optima were: *P. hamata r* = 21.8°C, *c* = 21.5°C and *t* = 21.7°C; *P. clava-herculis*: *r* = 20.2°C, *c* = 19.0°C and *t* = 20.0°C; and *P. raimondii r* = 15.6°C, *c* = 15.7°C and *t* = 15.8°C. The reliability of the parameter estimates and therefore the accuracy of each fitted curve was evidenced by the small standard errors of the estimates produced by the model. Out of a total of 105 parameter estimates for the 35 cumulative germination curves, 98 had $p \leq 0.05$ (see Appendix A).

4.4 Discussion

The germination of all three species responded similarly to the temperature gradient. Germination percentages increased markedly once the minimum temperature threshold for germination was exceeded. Optimum germination occurred across a relatively broad range of temperatures within which germination percentages (y_{max}) remained high. A generally rapid decline in germination percentages occurred at around 25°C. The rapid increase and decline in germination percentages on either side of the optimal temperature range indicates that the germination of each species is highly sensitive to temperature. This is unsurprising as temperature strongly influences the physiological and biochemical

processes involved in germination and species typically have a range of temperatures at which germination will occur and within which seedling establishment is possible (Bewley & Black 1982; Bradbeer 1988).

The temporal dynamics (rate, concentration and time lag) of the germination response also displayed a similar pattern for all three species. The parameter estimates produced by the fitted cumulative distribution functions show that temperature affected the proportional rate of occurrence (parameter *r*), temporal spread (parameter *c*) and time delay (parameter *t*) of germination in all three species in a curvilinear fashion. The generally high quadratic relationships with temperature (weaker for parameter *c* of *P. clava-herculis*), revealed the standard effect that temperature had on the temporal distribution of seed germination in each species. Metabolic processes, including enzymatic reactions, can only take place between certain temperature limits and are known to proceed more rapidly as temperatures increase above the minimum required for their activation (Kozlowski 1972; Bewley & Black 1982). Metabolic processes continue to increase until a certain temperature is reached. Once this temperature has been exceeded, any further increase will cause these processes to slow before they cease completely at their upper thermal limit (Kozlowski 1972). Protein denaturation and enzymatic inactivity have been identified as key processes inhibiting germination at high temperatures (Bewley & Black 1982; Hills, Van Staden & Thomas 2003; Fenner & Thompson 2005). For many seeds, germination stops when temperatures exceed the maximum favourable temperature for germination (Hills, Van Staden & Thomas 2003). The rapid acceleration and deceleration of metabolic processes are likely to explain the curvilinear relationships identified between each set of parameter estimates and temperature. These relationships allowed the temperature at

which germination was fastest (parameter *r*), more concentrated (parameter *c*) and least delayed after sowing (parameter *t*) to be identified for each species.

Although each parameter measures a different aspect of the statistical distribution of germination over time, each set of parameters produced very similar temperature optima which indicates that temperature-mediated metabolic processes influence all three parameters in all three species. The reliability of the parameter estimates, and therefore the accuracy of each model fit, is evidenced by the small standard errors of the estimates evident in most cases. The error of parameter estimates is a consequence of sample size and it is not surprising that the "poorer" fits occurred in treatments where fewer seeds germinated (such as the minimum germination temperature).

Differences in the germination response of each species were most evident at minimum germination temperatures and make sense in relation to local environmental temperatures in seed collection localities. Each species experiences a particular range of environmental conditions, due to its latitudinal and elevational position, and germination physiology is generally adapted to these same conditions (Thompson 1970; Bewley & Black 1982).

The minimum germination temperature for both *P. hamata* and *P. clava-herculis* corresponded closely with the mean daytime temperature recorded for the upper limits of their respective elevational ranges. Of the three species *P. clava-herculis* inhabits the coolest location, with a mean soil temperature at its upper limit of 6°C, and its minimum germination temperature of 7.5°C reflects this (no germination was recorded at the next lower temperature interval of 5.4°C). The lower elevation species *P. hamata* inhabits a location with a mean soil temperature at its upper limit 6°C warmer than that of *P. clava-*

herculis and has a minimum germination temperature of 13.9°C, approximately 6°C warmer than that of *P. clava-herculis*.

The minimum germination temperature for *P. raimondii* seeds was 8.4°C. Baskin and Baskin (2014) noted that if germination trial periods exceed a reasonable length, germination may be promoted due to seeds receiving sufficient warm stratification. For this reason, we excluded the small proportion (< 5% of seeds) of outlier germination that occurred at 4.6°C between days 47 and 54 for *P. raimondii*. The mean daytime soil temperature recorded at the *P. raimondii* site was 12°C. However, this temperature was recorded towards the lower limit of its elevational range (approx. 4,000 m). *P. raimondii* is able to inhabit much higher, cooler elevations (>4,500 m). Assuming a lapse rate of 0.6°C per 100 m (Goldstein, Meinzer & Rada 1994), seeds towards the upper limit of its elevational range will experience mean daytime soil temperatures of approximately 9°C which is in line with their minimum temperature threshold for germination.

These results suggest that the upper elevational limit for each of the *Puya* species sampled is largely determined by low soil temperature. A similar conclusion was reached by Perez (1987) for *Coespeletia* (Asteraceae), an unrelated species of giant rosette-forming species in the páramo. There are a number of reasons why seeds may fail to germinate at unsuitably low soil temperatures. Whilst imbibition may still be possible, low temperatures may damage embryos and prevent embryo growth (Bradbeer 1988). Damage sustained at low temperatures may be due to changes in membrane fluidity or from the denaturation of proteins (Bewley & Black 1982; Mayer & Poljakoff-Mayber 1982; Fenner & Thompson 2005).

With temperature ranges specific to each species, the germination pattern observed is likely to apply to other *Puya* species from the páramo and puna. Similar results identifying a decline in *Puya* germination percentages at higher temperatures have previously been reported. Smith and Downs (1974) found that germination percentages of *P. berteroniana,* a high elevation Chilean species, were highest at 15°C and declined as temperatures increased up to 25°C. Vadillo et al. (2004) reported that germination percentages of *P. raimondii* declined as temperatures exceeded 21°C and Choquecahua-Morales (2013) found that germination percentages for this species were highest at temperatures between 10°C and 17°C and were much reduced above 24°C. This is approximately the same optimum temperature range and temperature at which germination began to decline for *P. raimondii* in our experiment.

Each species had a slightly different optimum temperature range for germination. *P. clava-herculis* and *P. raimondii* inhabit cooler, higher elevations than *P. hamata* and their cooler optimum temperature ranges reflect their elevational positions. The differences in optimum temperature ranges identified in these species can be attributed to habitat characteristics (Baskin & Baskin 2014) and suggests that natural selection has exerted selection pressure on their germination phenology (Tudela-Isanta *et al.* 2018b). High elevation *Puya* species occupy complex, heterogeneous environments. Due to the complexity of these mountain environments, *Puya* are often found in small isolated populations where selection for adaptation at a local scale often occurs (Nevado *et al.* 2019). Given the level of environmental heterogeneity within mountains this adaptation cannot be too narrow. The ability to germinate across a relatively broad range of temperatures, as observed for the three species of *Puya* in this paper, has been identified as a survival strategy which can allow alpine plants to persist in unpredictable environmental

conditions (Kigel 1995; Tudela-Isanta *et al.* 2018a). Species with broader regeneration niches (Grubb 1977) are likely to have more establishment opportunities, both spatial and temporal, which may enhance seedling recruitment in areas composed of different microhabitats (Thompson & Ceriani 2003; Tudela-Isanta *et al.* 2018a).

High elevation tropical environments present particular challenges to seeds and seedling establishment due to intense solar radiation, extreme daily temperature fluctuations, ice crystal formation and solifluction (Balslev & Luteyn 1992). The challenging conditions, and the ability of *Puya* species to germinate at temperatures higher than those generally found within their elevational ranges, suggests that fine-scale microclimates may be key to their persistence and may control their subsequent distribution at high elevations by providing safe sites for seedling establishment. In a comprehensive review, Baskin and Baskin (2014) suggest that alpine species require warmer temperatures for germination compared with species from lower elevations (Baskin & Baskin 2014). The requirement for warmer temperatures allows species to avoid unfavourable conditions and prevents them from germinating too early or too late in the year (Baskin & Baskin 2014; Walder & Erschbamer 2015). Although this is true of species that inhabit temperate alpine regions, it is unclear whether this principle also applies to species that inhabit tropical alpine areas and further investigation is required.

The temperature that seeds experience during their development and maturation is known to strongly influence germinability in both temperate and tropical seeds: higher parental temperatures result in a faster loss of dormancy and higher germination (Fenner 1991). Seeds of *Puya* are contained high up on the parent plant in seed pods which can experience greatly elevated daytime temperatures before they are dispersed. There is evidence that

higher parental temperatures influence the phenotypic plasticity of seeds (Huang *et al.* 2018; Fernández-Pascual, Mattana & Pritchard 2019). It has been suggested that phenotypic plasticity, resulting from the thermal history of the plant's recent ancestors, allows individuals to adapt to their environments and permits greater regeneration opportunities (Fernández-Pascual, Mattana & Pritchard 2019). This may be particularly important within the thermally complex high-elevation environments of the tropical Andes. Phenotypic plasticity of seeds and a wide thermal range for germination have also been identified as important factors in high-elevation species inhabiting the Himalaya-Hengduan Mountains (Peng *et al.* 2017) and the Qinghai-Tibet Plateau (Peng *et al.* 2019). Studies of *Rheum* and *Saussurea* revealed that these species are adapted to low temperatures but were able to germinate relatively well at temperatures much higher than the ambient temperatures recorded within their elevational ranges.

In high elevations environments, warmth is generated by solar radiation. *Puya* seeds are positively photoblastic (Vadillo, Suni & Cano 2004). However, seeds lying unprotected on the surface of the soil are likely to experience unfavourably high levels of solar radiation which have an inhibitory effect on seed germination, even in positively photoblastic seeds (Fenner & Thompson 2005). If seeds receive too little warmth, in the form of solar radiation, it is unlikely that the minimum threshold for germination would be reached. The balance between too much and too little solar radiation may help to explain the patchy distribution of *Puya*.

Puya recruitment has been associated with microenvironments, such as tussock grass edges, edges of wetlands, and burned habitat, which allow just the right amount of light to reach the soil surface (Garcia-Meneses & Ramsay 2014). Some *Puya* species have been

shown to have a strong association with tussock grass edge habitat (Miller & Silander 1991). These microenvironments might provide protection from the intense solar radiation, which is characteristic of high elevation environments, whilst affording seeds the light and subsequent warmth required for germination. Protection from strong diurnal temperature fluctuations, organic matter and moisture is also provided by tussock grass edge habitat. Despite their strong association with tussock grass edge habitat, *Puya* species are out-competed in areas where tussock grasses and sclerophyllous shrubs are dominant (Miller & Silander 1991). One aspect of competition that could affect *Puya* germination is the cooling of the soil underneath dense vegetation canopies. Shade from vegetation can cool the soil by about 5°C in these habitats (equivalent to an increase in elevation of approx. 800 m) (P. Ramsay, personal observation).

Burning of the páramo at lower elevations for grazing and cultivation removes large swathes of dense tussock grass cover and promotes more tussock grass edge habitat. Lower elevation species, such as *P. hamata*, benefit from regular burning as the removal of vegetation allows more light to reach the surface and elevates temperatures which facilitates germination (Laegaard 1992; Albano 2000; Garcia-Meneses & Ramsay 2014). Other areas in which tussock grasses are restricted and *P. hamata* can increase in dominance are páramo mire habitats (Miller & Silander 1991). These waterlogged areas have been shown to have soil temperatures which are 2°C warmer than those of neighbouring areas with free draining soils (Ramsay 2001). The combination of reduced competition and increased soil temperatures provide favourable conditions for *Puya* germination, and as our results demonstrate, a few degrees difference can greatly affect the probability of *Puya* germination and establishment.

Changing climatic conditions are likely to affect the germination ecology and alter the distribution of *Puya* in the tropical Andes. Temperature increases of 3–5°C are projected for the region, depending on the emission scenario, by the end of the 21st century (Vuille *et al.* 2008; Buytaert, Cuesta-Camacho & Tobón 2011). Assuming a lapse rate of 0.6°C/100 m, these increases are likely to move temperature regimes upslope between 500 m and 800 m, an extent greater then the entire elevational range of most *Puya* species. The upper elevational limits of the *Puya* species in this study appear to be restricted by low temperatures, therefore temperature increases at high elevations have the potential to facilitate their upward range expansion. However, *Puya* species possess characteristics, such as slow growth, a long juvenile stage and poor seed dispersal ability, which are likely to cause a dispersal lag (sensu Alexander *et al.* 2018) preventing *Puya* from keeping pace with rapidly changing climatic conditions. This dispersal lag has the potential to be more acute for *P. raimondii* as this species is estimated to take 120 years to reach reproductive maturity (Ruiz 1978). Even if *Puya* were able to disperse to areas above their current ranges, and temperatures became more conducive to their germination requirements, their initial establishment probability would more than likely be very low due to the paucity of suitable germination sites at the highest elevations. Poorly developed alpine soils, particularly those on recently deglaciated slopes, have low nutrient availability and low water-retaining capacity (Alexander *et al.* 2018). Although precipitation is projected to increase north of 11°S (Vuille *et al.* 2008), the extreme porosity of high elevation soils might constrain the range expansion of the highest elevation species, *P. clava-herculis* and *P. raimondii*.

The same dispersal and establishment issues will not hinder many lower elevation species from moving up the altitudinal gradient and some *Puya* could experience displacement by

species currently inhabiting lower elevations as the climate changes. Increases in temperatures and precipitation are expected to facilitate the upslope movement of woody species from lower elevations and increase the abundance of rapidly growing species (Young, Young & Josse 2011). Climate change may also make the lower margins of páramo and puna environments more suitable for agriculture (Anderson *et al.* 2011). These factors, combined with poor expansion at higher elevations, have the potential to cause range contractions by reducing the total available area suitable for *Puya* germination and establishment. The increasing abundance of rapidly growing species has been shown to eliminate establishment sites in *P. dasylirioides* (Augspurger 1985) and determine the lower elevational limit of *P. clava-herculis* (Miller & Silander 1991). The amount and type of ground cover appears to be particularly important in determining the distribution of *Puya* at lower elevations. Due to the shape of mountains and the reduced land area at higher elevations, it is also possible that *Puya* species already inhabiting areas near the tops of mountains could get "pushed off" mountain tops locally by warming temperatures. This is particularly important for a genus with high diversity following adaptive radiation on isolated mountaintops. Because many *Puya* species are endemic, their potential upward movement could result in their extinction.

In conclusion, all three *Puya* species showed similar germination responses across temperature gradients, with differences related to local conditions in the areas where the seeds came from. The regeneration niche is crucial to *Puya*. Their vulnerability to climate change is likely to be expressed through the regeneration niche and attention should be given to this in future conservation efforts. Other mountain species are likely to show similar vulnerabilities to changing recruitment from seed as temperatures warm, an issue that merits wider consideration than just *Puya* species.

5 Phenological change of four North Sea plankton functional groups over a 56 year period

5.1 Introduction

Phenology, the seasonal timing of biological events, is widely regarded as an important biological indicator of climate change (Parmesan & Yohe 2003; Root *et al.* 2003; Menzel *et al.* 2006; Scranton & Amarasekare 2017; Garonna *et al.* 2018). Increasing global temperatures have been identified as driving changes in the timing of key life-cycle events such as reproduction, emergence, and migration across a wide range of organisms (Crick & Sparks 1999; Roy & Sparks 2000; Cotton 2003; Dickey, Gauthier & Cadieux 2008; Melaas, Sulla-Menashe & Friedl 2018; Orellana Macías *et al.* 2020). Although an overall trend of phenological advancement in response to rising global temperatures has been detected, the extent and pattern of phenological responses are far from uniform (Parmesan 2007; Thackeray *et al.* 2010; Thackeray *et al.* 2016).

Differing rates of phenological change between interacting species have the potential to cause phenological mismatches between trophic levels (Cushing 1990). Trophic mismatches often occur when the environmental cue (frequently temperature) used by organisms in one trophic level changes at a different rate than the cue used by those in another trophic level (Thackeray *et al.* 2016; Visser & Gienapp 2019). Warming trends, as a result of climate change, have been seasonally heterogeneous and when different trophic levels respond to temperatures in different parts of the year, trophic mismatches are likely to ensue (Straile, Kerimoglu & Peeters 2015; Visser & Gienapp 2019). Mismatches between plants and pollinators, and consumers and resources have been shown to negatively

impact reproduction (Kudo & Ida 2013), recruitment (Régnier, Gibb & Wright 2019), and nutrient cycling (Beard *et al.* 2019) and are predicted to have significant implications for population dynamics and ecosystem function (Edwards & Richardson 2004; Durant *et al.* 2007; Miller-Rushing *et al.* 2010; Thackeray *et al.* 2016; Renner & Zohner 2018).

As the references above show, variation in phenological responses to a changing climate, with possible trophic mismatch, is being investigated in a variety of systems and settings. Plankton represents an attractive study subject because it does not only contain species belonging to different trophic levels (or functional groups), but their generally small body size, which correlates with short life-cycles, makes them highly sensitive to environmental change (Hays, Richardson & Robinson 2005). Initiated in 1931, the Continuous Plankton Recorder (CPR) survey (Richardson *et al.* 2006a) is one of the longest running, large-scale, biological surveys in the world and as such allows investigation into the effects of climate change on marine plankton over several decades. Links between climate change and changes in plankton abundance, geographic range and phenology have been identified using data from the CPR survey (Edwards & Richardson 2004; Hays, Richardson & Robinson 2005; Ji *et al.* 2010; Chiba *et al.* 2012; Hinder *et al.* 2012; Edwards *et al.* 2013; Chivers, Walne & Hays 2017).

Here, a 56-year time series (1960-2015) from the CPR survey was used to examine phenological changes in marine plankton functional groups. The new method of phenological analysis described in previous chapters quantifies three key aspects of the phenological time distribution (Franco 2018; Steer, Ramsay & Franco 2019). Investigating whether and how each of the three aspects of the distribution's shape are influenced by environmental change is a first step in exploring specific biological attributes, such as

physiological processes, that may be responsible for them (Steer, Ramsay & Franco 2019). By itself, however, the model cannot possibly provide specific answers to these questions, which must be the subject of additional research.

Specifically, the aims of this study were: (i) to quantify the phenology of abundance of four functional groups of plankton in the central North Sea for the period 1960-2015, (ii) to contrast the variation in the values of the parameters as a function of time and changing sea surface temperature, and (iii) based on the results, to hypothesise on the possible influence of biological attributes of the groups in question on the observed responses.

5.2 Materials and Methods

5.2.1 Plankton abundance data

The plankton abundance data used in this study was collected by the Continuous Plankton Recorder (CPR) survey and was provided by the Sir Alister Hardy Foundation for Ocean Science (SAHFOS). The CPR survey has been operating on a routine monthly basis in the North Sea since 1946, and is the longest running, large-scale plankton survey in the world (Warner & Hays 1994; Edwards & Richardson 2004). The CPR survey is a near surface plankton-monitoring programme and is operated at a standard depth of approx. 6.5 m (Warner & Hays 1994; Batten *et al.* 2003). The CPR machines are towed voluntarily behind "ships of opportunity" (SOOPs) along their normal operating routes (Batten *et al.* 2003). Using SOOPs provides a measure of standardisation and consistency to the monthly sampling as the normal operating routes act as transects (McQuatters-Gollop *et al.* 2015). Plankton are collected on a continuously moving band of filtering silk, with mesh size of 270 µm, which is rolled up and stored in formaldehyde, ready for analysis (Batten *et al.*

2003). Although the sampling technique is semi-quantitative in nature, only larger and chain-forming species are captured, the method of analysis has remained unchanged since 1958 and therefore direct comparison between samples can be made from this year onwards (Warner & Hays 1994). Despite the potential biases that exist in the collection and analysis of the plankton abundance data (see McQuatters-Gollop *et al*. 2015 & Edwards & Richardson, 2004), it is still regarded as a consistent and comparable method that is able to reveal important changes in the abundance, distribution, and specific composition of the plankton (Beaugrand, Ibañez & Lindley 2003; Hays, Richardson & Robinson 2005).

5.2.2 Sampling area

The plankton abundance data used in this study originated from CPR standard areas C1 and C2, located in the central North Sea (55°–58° N) (Fig. 5.1), and were from the period 1960-2015. This area was chosen because it provides the most comprehensive data set in the entire CPR survey, having been sampled every month from 1958 (see Edwards & Richardson, 2004).

5.2.3 Study species

Thirty-nine taxa from 20,985 CPR records were used in the study. The taxa were selected due to their inclusion in the Edwards and Richardson (2004) study and were originally chosen by the authors due to their occurrence in more than 1% of all samples taken from the region. As with the study by Edwards and Richardson (2004), taxa were assigned to four functional groups (dinoflagellates, copepods, non-copepod holozooplankton, and meroplankton) based on differences in trophic levels, physiology and life cycle stages. The taxa assigned to each functional group were as follows: **Dinoflagellates** – *Ceratium furca, Ceratium fusus, Ceratium horridum, Ceratium lineatum, Ceratium longipes, Ceratium*

macroceros, Ceratium tripos, Dinophysis spp., *Prorocentrum* spp., and *Protoperidinium* spp.; **Copepods** – *Acartia* spp. (unidentified), *Calanus finmarchicus, Calanus helgolandicus, Candacia armata, Centropages hamatus, Corycaeus* spp., *Harpacticoida* Total Traverse, *Labidocera wollastoni, Metridia lucens, Oithona* spp., *Para-Pseudocalanus* spp., *Pseudocalanus* spp. Adult Atlantic, and *Temora longicornis*,; **Non-copepod holozooplankton** – *Chaetognatha, Clione limacine, Cumacea, Euphausiacea* (total), *Evadne* spp., *Gammaridea, Hyperiidea* (total), *Podon* spp., *Polychaete* larvae (unidentified), and *Tomopteris* spp.; and **Meroplankton** – Cirripede larvae, Cyphonautes, Decapoda larvae, Echinoderm larvae, fish eggs, and fish larvae.

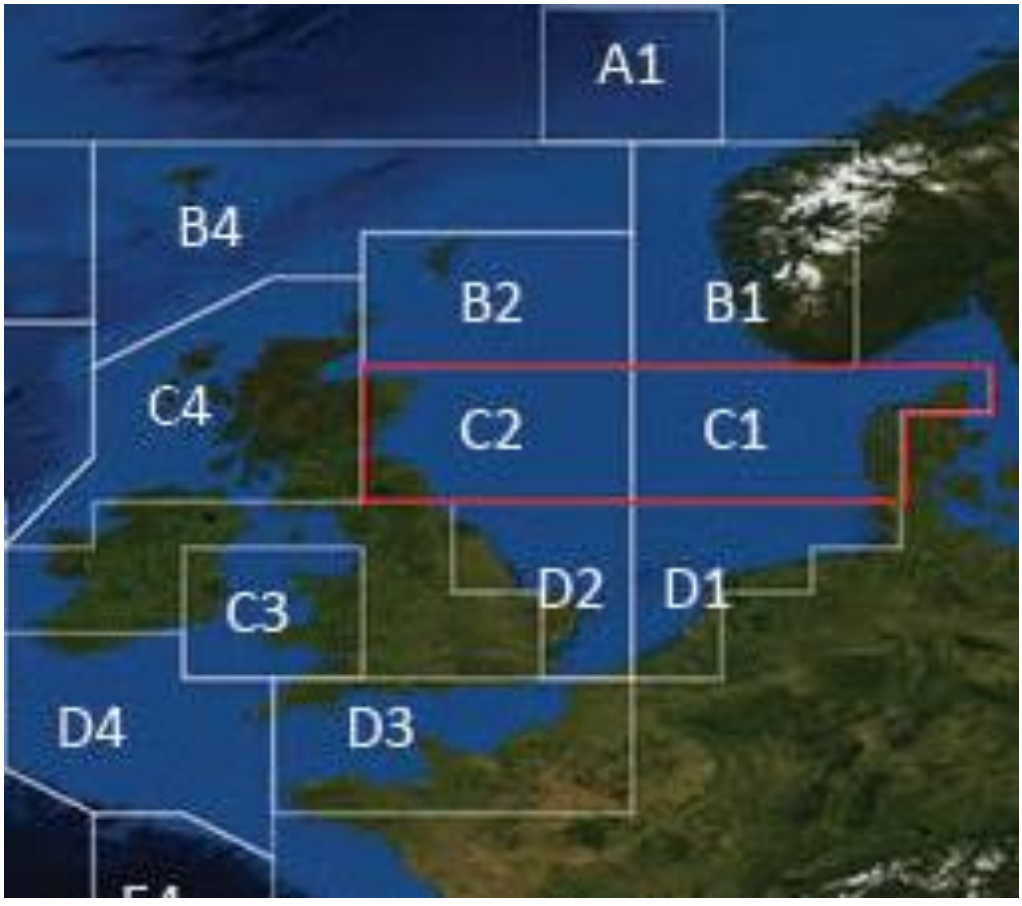

Figure 5.1. Continuous Plankton Recorder standard areas C1 and C2, located in the central North Sea (55°–58°N).

5.2.4 Sea surface temperatures

Sea surface temperature (SST) was used as the environmental variable of interest because temperature was identified as an environmental driver of phenological change on a previous analysis of this dataset for the period 1958-2002 (Edwards & Richardson 2004). Monthly mean SST (°C) measurements for the central North Sea were obtained from the Hadley Centre of the UK Meteorological Office (http://www.metoffice.gov.uk/hadobs/hadisst/) (Rayner *et al.* 2003). SST data was extracted and recompiled by Dr Pierre Helaouet (Marine Biological Association) to ensure that the measurements corresponded with the same geographic area that the samples originated from, standard areas C1 and C2. From this dataset, mean decadal SST, mean decadal spring (March-May) SST, the change in mean decadal spring (from March to May) SST, and mean decadal summer (June –August) SST were calculated to identify which had the greatest effect on the parameter estimates produced from each model fit.

5.2.5 Statistical analysis

The initial aim of the study was to quantify the three aspects (parameters) of the annual distribution of abundance of taxa employing the model described below. However, it was decided to pool the monthly abundance data over ten-year intervals, except for the final interval, which for reasons of delay in the analysis of samples ended in 2015 (1960-69, 1970-79, 1980-89, 1990-99, 2000-09, 2010-2015; see Appendix B: Table B1, for abundance values for each taxa per decade). The reasons for this decision were: (a) year to year variation in abundance is likely to obey other factors in addition to changes in temperature, (b) the likely existence of unknown and varying time lags in the response of individual species to changing temperatures, (c) the low abundance observed in many species and samples does not allow a reliable fit of the model to many, if not most of them, and (d)

some species show two peak abundances (spring and autumn blooms; Edwards & Richardson, 2004). It was reasoned that this procedure would smooth their influence, thus providing comparable seasonal trends for each functional group. This is equivalent to, say, monitoring the seasonal development of leaf area in a diverse deciduous forest. The model was fitted to each of the six decadal cumulative abundance curves for each functional group, i.e., 24 phenology distributions. We expected that, by virtue of measuring the aspects of initiation (r), speed (c) and duration (t) of the distributions, the parameters of the model would allow a more meaningful interpretation of the biological differences between the four functional groups.

The model has the form:

$$y = 1 - \left(1 - \frac{r}{1+e^{-c(x-t)}}\right)^{x} \quad (1)$$

where y is the empirically recorded cumulative proportion of plankton functional group abundance over time (x(months January to December)= 1, 2, …12), r quantifies the maximum proportional rate of increase in abundance (it is dimensionless), c is the rate at which r converges on its maximum value and is inversely proportional to the temporal spread of the distribution (units: time^{-1}), and t is an overall measure of the time lag of the phenology (units: time) (Steer, Ramsay & Franco 2019). Each parameter measures a specific aspect of the shape of the distribution (Chapter 2) and, although correlated with some statistical moments, they are not equivalent to them. They quantify important aspects of the time distribution's dynamics.

The derivative of equation 1 provides the probability density function (*pdf*):

$$\frac{dy}{dx} = \left(1 - \frac{r}{1+e^{-c(x-t)}}\right)^{x} \left(\frac{rcxe^{-c(x-t)}}{\left(1+e^{-c(x-t)}\right)^{2}\left(1-\frac{r}{1+e^{-c(x-t)}}\right)} - \ln\left(1 - \frac{r}{1+e^{-c(x-t)}}\right)\right) \quad (2)$$

which describes the population-level change in abundance (blooming rate) over the course of the average decadal year. Parameter *r, c* and *t* and the statistical moments were estimated using the *nlstimedist* R package (Franco, Ramsay & Steer, 2019; Steer, Ramsay & Franco, 2019).

Analysis of covariance (ANCOVA) was used to identify the effect that functional group had on the parameter estimates (*r*, *c*, *t* and *median*) while controlling for mean decadal SST, mean decadal spring SST, change in mean decadal spring SST, mean decadal summer SST, and time (decade). Estimated marginal means were manipulated to understand the effect that different aspects of SST had on each functional group. Finally, pairwise comparisons based on estimated marginal means were used to detect significant differences (using Bonferroni adjustment for multiple comparisons) between functional groups.

5.3 Results

5.3.1 Sea surface temperatures

The annual mean SST for the geographic areas C1 and C2 was relatively stable from 1960 to the late 1980s, followed by rapid ocean warming until the late 2000s when slight ocean cooling was evident (Fig. 5.2A). The pattern of a relatively static period followed by rapid ocean warming from the late 1980s is also apparent for mean annual spring SST (Fig. 5.2B) and mean annual summer SST (Fig. 5.2D). In contrast, the change in mean annual March to May SST shows a steady increase from the 1970s onwards (Fig. 5.2C).

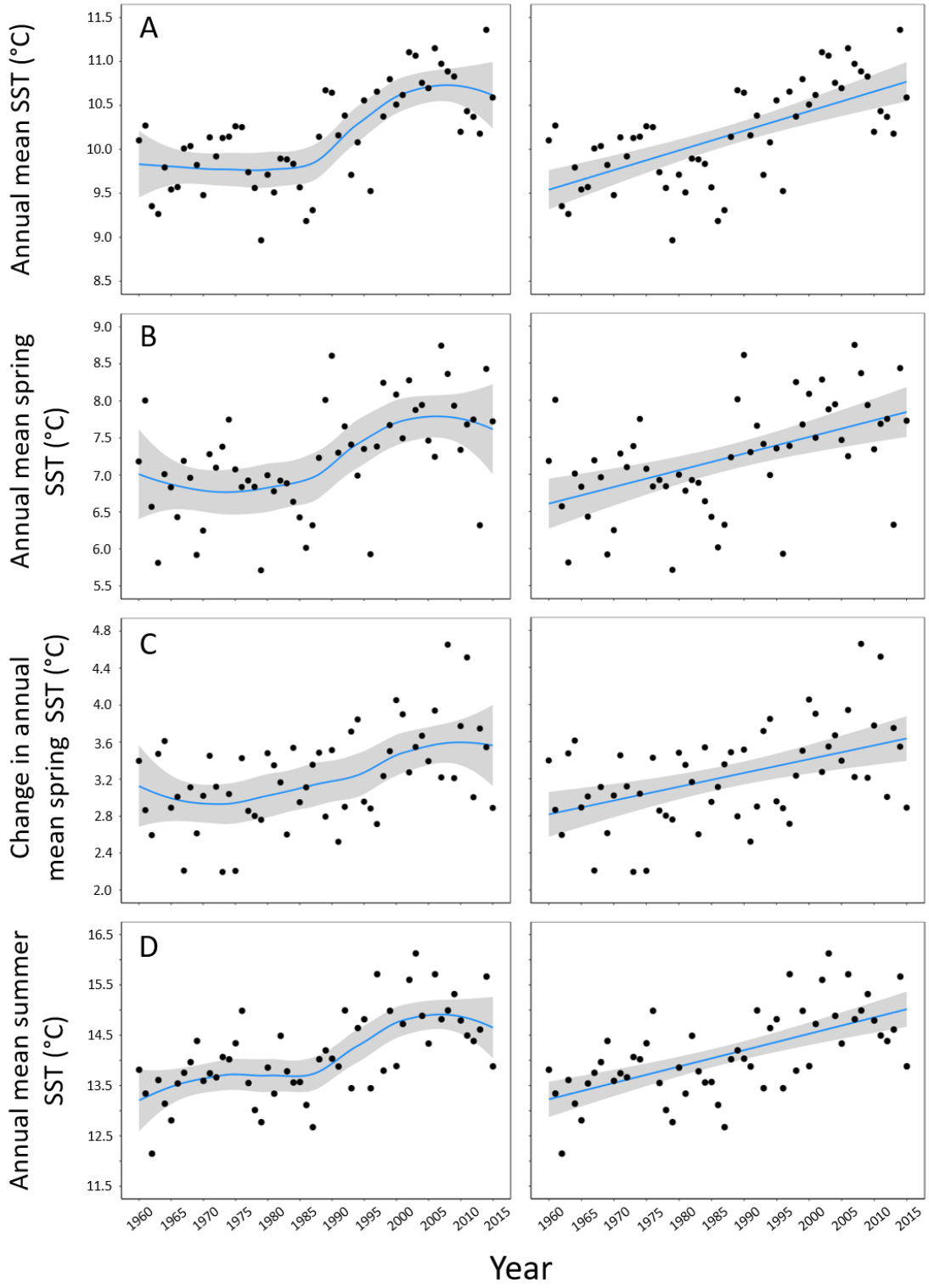

Figure 5.2. Sea surface temperatures from 1960 to 2015. (A) Annual mean sea surface temperature (SST), (B) Annual mean spring SST, (C) Change in annual mean spring (March to May) SST, (D) Annual mean summer SST. Loess (locally weighted regression) smoothers (left panel) with 95% confidence interval in grey. Linear regression (right panel) with 95% confidence interval in grey (A) $F_{1,54} = 40.823$, $p < 0.001$, $R^2 = 0.431$; (B) $F_{1,54} = 18.297$, $p < 0.001$, $R^2 = 0.253$; (C) $F_{1,54} = 15.554$, $p < 0.001$, $R^2 = 0.224$; (D) $F_{1,54} = 35.253$, $p < 0.001$, $R^2 = 0.395$.

Simple linear regression showed consistent positive linear relationships with Pearson's correlation coefficients of 0.656, 0.503, 0.473, and 0.628, respectively, with low type-1 error ($p<0.001$). The slope coefficients showed that, on average, SST increased between 0.015°C and 0.033°C for each year of the study period. The relatively low R^2 values reflect the wide inter-annual variation in sea surface temperatures.

5.3.2 Model fits

The pooling together of monthly species data by decade within each functional group produced distributions more closely representing unimodal trends of development and decline throughout the year (see Appendix B: Fig. B1), and the model successfully fitted each time course (Fig. 5.3). The time sequences of both *cdf*s and *pdf*s reflect the periods of stability (1960s-1980s) and increase (1990s-2010s) observed in sea surface temperature described above. The curves for these two periods tending to occur together within each of the four functional groups, though not always in the expected temporal order. The curves also reveal that the pattern of seasonal change in abundance differed for each functional group, but these patterns are better described by the change in the values of the distributions' parameters (Appendix B: Table B2) with both time and SST.

5.3.3 Correlations between parameter estimates and both time and SST

Simple linear regression was used to explore the relationships between the parameter estimates (*r*, *c*, and *t*, and the statistical moment *median*) and (a) mean annual SST, (b) mean annual spring SST, (c) change in mean annual March to May SST, (d) mean annual summer SST, and (e) time (Fig. 5.4; Appendix B: Table B3). Despite small sample size (N=6), there were consistent trends in the values of model parameters over time and with increasing measures of SST for all functional groups. Stronger ($p <0.05$) linear

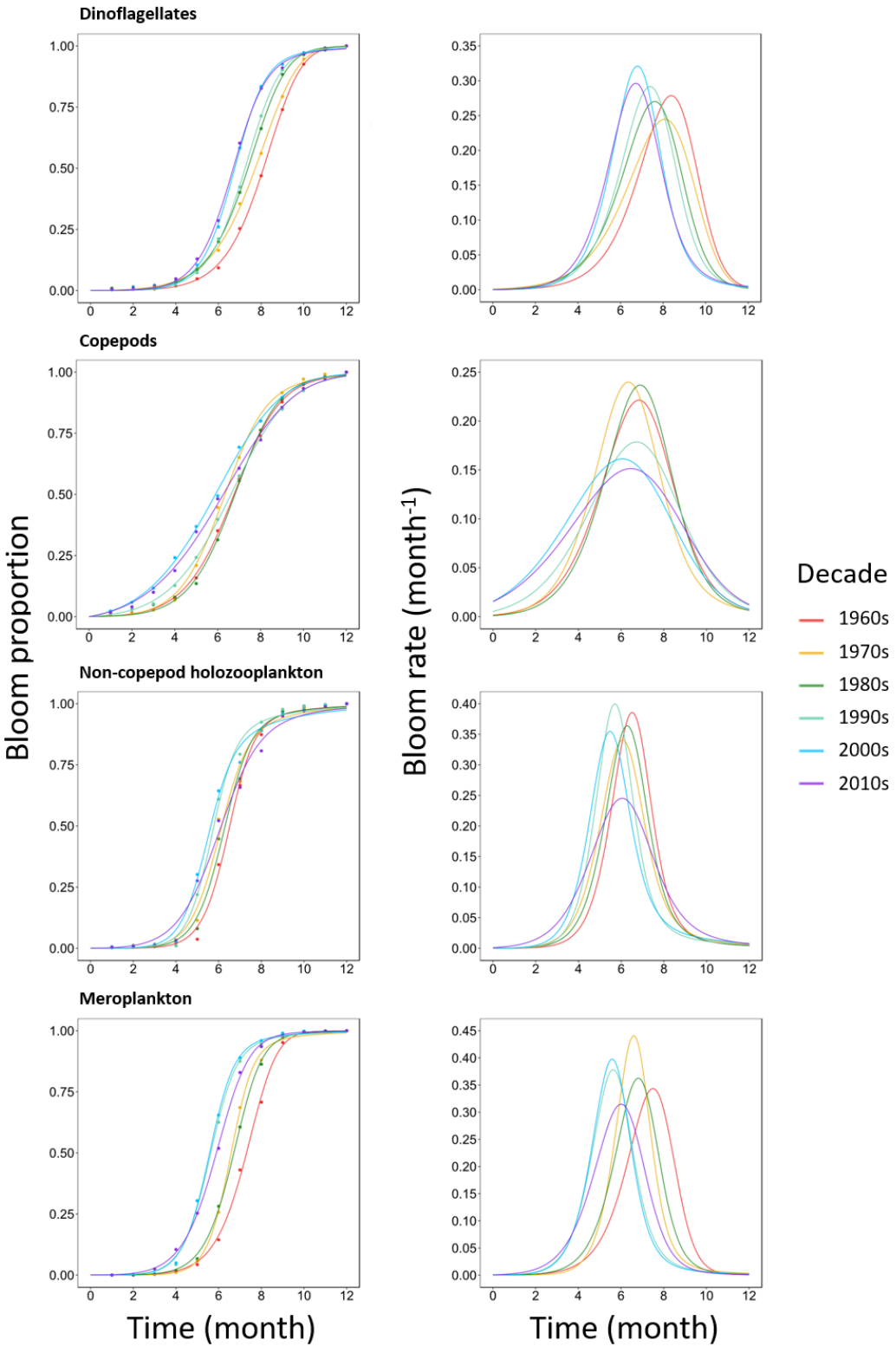

Figure 5.3. Cumulative distribution functions (left) and corresponding probability density functions (right) of plankton functional group (dinoflagellates, copepods, non-copepod holozooplankton and meroplankton) abundance for each decade: 1960-69 (red), 1970-79 (yellow), 1980-89 (dark green), 1990-99 (light green), 2000-09 (blue) and 2010-2015 (purple). Probability density functions describe the population-level rate of abundance through time.

relationships with sea surface temperature were found in dinoflagellates and copepods. The strength of the relationships between the parameter estimates and SST for each functional group varied with the aspect of SST employed, but the direction of the relationships (or lack of relationship) was consistent among them. Functional groups differed in the measure of SST to which they responded more strongly. Dinoflagellates displayed the strongest linear relationships with the change in mean decadal March to May SST (all parameters); copepods with both the change in mean decadal March to May SST (parameters *r* and *t*) and mean decadal SST (parameters *c* and *median*); non-copepod holozooplankton with both mean decadal summer SST (parameter *r*) and mean decadal spring SST (parameters *t* and *median*); and meroplankton with mean decadal summer SST (parameters *t* and *median*). Parameters *t* and *median* showed strong negative correlations with aspects of SST in the non-copepod holozooplankton and meroplankton groups (Fig. 5.4; Appendix B: Table B3). With weak or no correlation between *r* and SST (all measures), non-copepod holozooplankton had the lowest values of *r*, while meroplankton's were intermediate between dinoflagellates and copepods, which followed significant opposite trends. Similarly, with weak or no correlation between *c* and SST (all measures), non-copepod holozooplankton and meroplankton had similar and higher values of *c* than dinoflagellates and copepods.

The significant linear relationships of parameter estimates *r* (the maximum proportional rate of plankton bloom, which would produce an earlier rise at constant values of *c* and *t*), *c* (the temporal concentration), and *t* (the time lag of the distribution), *versus* SST indicate that the dinoflagellate bloom rate is decreasing (parameter *r*), its temporal spread is narrowing (increasing parameter *c*) and its time lag (parameter *t*) is shortening as SST temperatures increase (Table 5.1). The opposite pattern was identified for copepods, i.e.

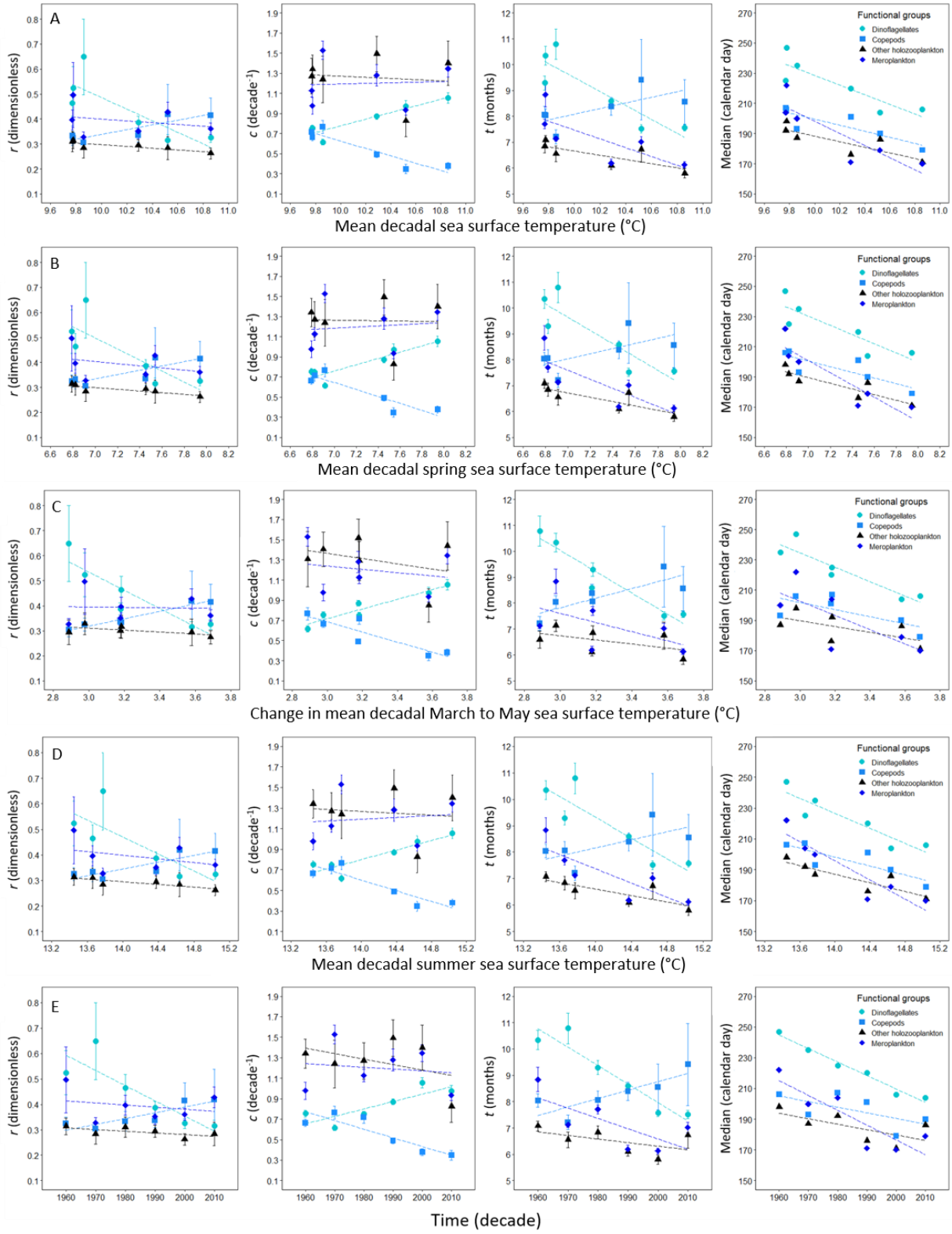

Figure 5.4. Linear relationships between the values of the parameter estimates (*r*, *c*, *t* and *median*) produced from each model fit and four aspects of SST: (A) Mean decadal SST, (B) Mean decadal spring SST, (C) Change in mean decadal March to May SST, (D) Mean decadal summer SST, and (E) Time. Functional groups are plotted separately: dinoflagellates (circle), copepods (square), non-copepod holozooplankton (triangle), and meroplankton (diamond). Error bars represent the standard error of the parameter estimates. For regression analysis, see Appendix B: Table B3.

the rate of bloom is increasing, its temporal spread is widening, and its time lag is lengthening with increasing SST. The signal is less clear in the non-copepod holozooplankton and meroplankton groups. Although the rate of the holozooplankton bloom is decreasing slightly, only the time lag (parameter *t*) shows a marked decline with increasing temperatures in both groups.

Table 5.1. Summary of strength and direction of change in parameter values with both time and measures of sea surface temperature. The strength of positive and negative correlation is indicated by the number of these symbols, with one symbol indicating a weak correlation and two symbols indicating a strong correlation. Zero identifies trends with a <0.05; 0- indicates weak or no correlation depending on SST measure.

Functional group	***r***	***c***	***t***	***Median***
Dinoflagellates	--	++	--	--
Copepods	++	--	++	-
Holozooplankton	0-	0	--	-
Meroplankton	0-	0	--	--

Assuming 30 days per month, the statistical moment *median* was used to estimate the number of days that each distribution has shifted in the intervening six decades of study. All four functional groups showed advancement in the median point of their temporal distribution. The largest advancement was identified in dinoflagellates (43 days) and meroplankton (43 days), followed by copepods (15 days) and non-copepod holozooplankton (12 days) (Fig. 5.4; Appendix B: Tables B2 & B3).

5.3.4 Analysis of Covariance

A one-way ANCOVA was conducted to ascertain differences between dinoflagellates, copepods, non-copepod holozooplankton and meroplankton on the parameter estimates *r*, *c*, *t* and *median*, controlling for mean decadal SST, mean decadal spring SST, change in mean decadal March-May SST, mean summer SST, and time. The assumption of homogeneity of variance was not met for parameter *r*. However, as this method of analysis is considered to be robust to violations of this assumption when sample sizes are equal (Olejnik & Algina 1984; Keppel 1991), the results of the ANCOVA are still informative. Significant interactions were identified between functional group and each aspect of SST, and time, for parameters *r* and *t* (Appendix B: Table B4). This is unsurprising as dinoflagellates and copepods displayed opposing relationships between the parameters (*r*, *c*, and *t*) and SST. A significant difference was identified between the functional groups for parameters *c* and *median*, whilst adjusting for each aspect of SST, and time. The partial η^2 values indicate moderate to large effect sizes (following Cohen's guidelines: 0.2 – small effect, 0.5 – moderate effect, 0.8 – large effect) (Appendix B: Table B4). The covariates, mean decadal SST, mean decadal spring SST, change in mean decadal March to May SST and mean decadal summer SST, and time, were significantly related to the parameter *median* (Mean SST $F_{1,4} = 39.551$, $p < 0.001$, $\eta_p^2 = 0.675$; Spring SST = $F_{1,4} = 44.232$, $p < 0.001$, $\eta_p^2 = 0.700$; Change SST = $F_{1,4} = 20.773$, $p < 0.001$, $\eta_p^2 = 0.522$; Summer SST $F_{1,4} = 52.279$, $p < 0.001$, $\eta_p^2 = 0.733$).

To explore the effects of the covariates on parameters *r* and *t*, the estimated marginal means were examined. The estimated marginal means adjust for the mean value of the covariate to identify if the factor still has an effect, beyond the effect of the covariate. By adjusting the estimated marginal means by the lowest and highest value of each covariate,

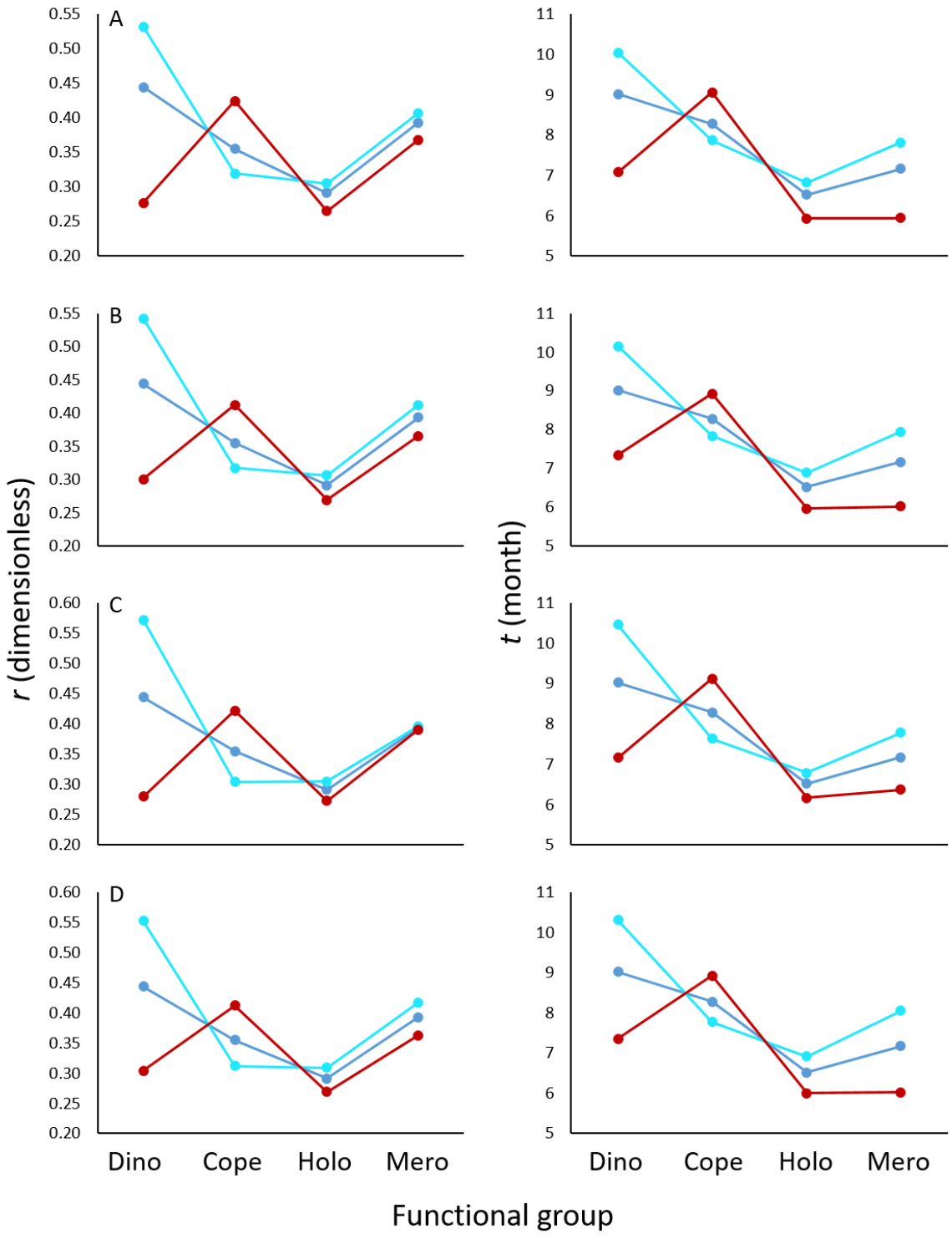

Figure 5.5. Comparison of adjusted estimated marginal means of parameters *r* (proportional rate of increase) and *t* (time lag) for the plankton functional groups dinoflagellates, copepods, non-copepod holozooplankton and meroplankton. Estimated marginal means were calculated at low (light blue), mean (darker blue) and high (red) values of the four SST covariates: (A) Mean decadal SST – low 9.8°C/mean 10.2°C/high 10.8°C, (B) Mean decadal spring SST – low 6.8°C/mean 7.2°C/high 7.9°C, (C) Change in mean decadal March to May SST – low 2.9°C/mean 3.2°C/high 3.7°C, and (D) Mean decadal summer SST – low 13.5°C/mean 14.2°C/high 15.0°C

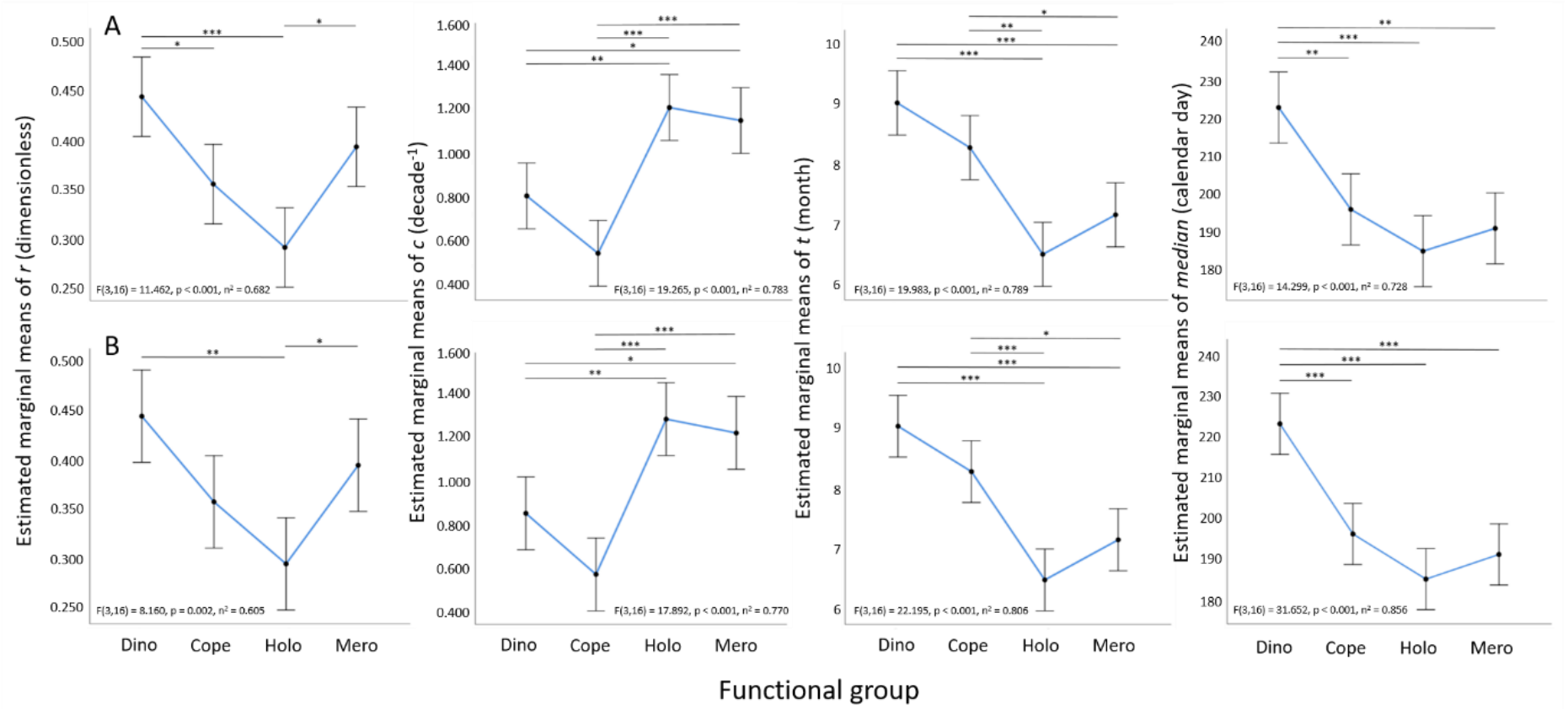

Figure 5.6. Estimated marginal means of parameters *r* (proportional rate of increase), *c* (temporal spread), *t* (time lag), and *median* (calendar day) for the plankton functional groups dinoflagellates, copepods, non-copepod holozooplankton and meroplankton. Estimated marginal means were calculated using the mean value of (A) Change in decadal March to May SST, and (B) Decadal summer SST. Significant pairwise comparisons between groups were made using Bonferroni adjustment (* p <0.05, ** p <0.01, *** p <0.001).

it was possible to see the effect that each had on the parameter estimates. The covariates with the greatest effect on parameters *r* and *t* were change in mean decadal March to May SST (for dinoflagellates and copepods) and mean decadal summer SST (for non-copepod holozooplankton and meroplankton) (Fig. 5.5). Post hoc pairwise comparisons of the estimated marginal means, adjusted for the mean value of the two covariates that had the greatest effect on the parameter estimates, revealed that there were significant differences between the functional groups for parameters *r*, *c*, *t*, and *median* with moderate to large effect sizes (Fig. 5.6; Appendix B: Tables B5, B6).

5.4 Discussion

An overall trend of earlier blooming (shorter measures of central tendency) with time was evident in the four functional groups examined. This confirmed the shift in the peak of the phenologies observed by Edwards and Richardson (2004) employing the peak blooming month. This result indicates that the mismatch identified by Edwards and Richardson (2004) between successive plankton trophic levels has continued to increase. Significantly, the results presented here indicate that the general advance of the *median* (and other measures of central tendency) was produced through different responses of the individual parameters of the model in each functional group (Table 5.1). The results from the model indicate that the observed advance in phenology was achieved through modification of different parameters. Other things being equal, an advancing phenology would be achieved either by an increase in the maximum rate of blooming (larger *r*), a decrease in the rate at which the rate of blooming reaches its maximum value (smaller *c*), or a shift in the distribution to occur earlier in the year (smaller *t*) (Fig. 2.1). The reality was more complex and could even be achieved when some of the parameters went in the opposite direction to

the one expected if only one parameter varied. Thus, (i) the only functional group whose *r* increased with time/temperature was the copepods, (ii) the only functional group in which *c* decreased with time/temperature was also the copepods, and (iii) except for copepods, in the other three groups *t* decreased with time/temperature.

Following a period of little change between 1960 and the late 1980s, sea surface temperatures in the central North Sea rose abruptly before reaching a peak in the mid-2000s (Tinker *et al.* 2020). Each functional group responded to the sudden increase in SST in the late 1980s. However, both the magnitude and the nature of the response differed between functional groups. The effect that the quite dramatic increase in SST had on the bloom characteristics of each functional group is reflected in the changing position and shape of their decadal distributions from the 1990s onwards.

The shape of the dinoflagellate decadal distributions prior to the sharp rise in SST of the late 1980s were negatively skewed and platykurtic showing that historically (1960s-1980s) the dinoflagellate bloom built slowly and extended over a relatively long period of time. From the 1990s onwards the decadal bloom distributions became positively skewed and leptokurtic revealing that the bloom characteristics had shifted to both building and terminating more rapidly. The strongest linear relationships were identified between the parameter estimates (*r*, *c*, *t*, and *median*) produced by the fitted cumulative distribution functions, and the change in mean decadal March-May SST. These relationships show that, of all the aspects of SST examined, the increase in spring SST is likely the most important driver of phenological change for the dinoflagellate functional group. As spring SST has increased, the dinoflagellate bloom has become more concentrated (higher *c*) and has started earlier (shorter *t*). Counterintuitively, the advance has resulted despite both a

decrease in *r* and an increase in *c*. Dinoflagellates, along with diatoms and flagellates, form part of the spring bloom which is initiated by vertical mixing and stratification of the water column (Johns & Reid 2001). The seasonal abundance of plankton in temperate waters typically changes from diatoms to dinoflagellates when stratification intensifies and nutrients become depleted (Mann & Lazier 2013). Warmer spring temperatures have been shown to affect the onset and strength of vertical stratification (Sharples *et al.* 2006; Li & Glen Harrison 2008; Ji *et al.* 2010; Chiba *et al.* 2012), while an increase in the abundance of diatoms over the last three decades has caused a more rapid reduction of nutrients in the near-surface zone (Chiba *et al.* 2012; Hinder *et al.* 2012). Both of these factors likely promote the earlier occurrence of dinoflagellates due to their ability to move to access alternative nutrient sources. A more intense spring thermocline, as a result of warmer spring temperatures, has previously been recognised as a key factor determining the initiation of dinoflagellate blooms (Xie *et al.* 2015; Chivers, Edwards & Hays 2020). Warming spring temperatures may also trigger the earlier termination of the dinoflagellate bloom through increased grazing pressure from over-wintering zooplankton (Winder *et al.* 2012; Winder & Sommer 2012; Hjerne *et al.* 2019) and fungal parasites (Frenken *et al.* 2016). The earlier occurrence and an overall narrowing of the dinoflagellate temporal distribution is likely due to the indirect effects of warming spring temperatures.

Warming spring temperatures were also identified as an important driver of phenological change for the copepod functional group. Of all the functional groups, the copepods displayed the most radical change in the shape of their decadal distributions following the sharp rise in SST of the late 1980s. From the 1990s onwards the copepod decadal bloom distributions changed from being relatively normally distributed to platykurtic, revealing that the copepod bloom was happening over a longer period of time. This change is

reflected in the lower values of parameter *c* (larger temporal spread) and, counterintuitively, larger *t* (temporal delay) for the last three decades. As mentioned above, copepods were the only group with a larger *r* at increasing time/SST. The extreme change in the length of the decadal distributions between the 1980s and 1990s coincide with the regime shift that was detected in the North Sea in the late 1980s (Beaugrand 2004; deYoung *et al.* 2008; Beaugrand *et al.* 2015). Increases in SST, that contributed to the regime shift, were shown to have changed the composition and diversity of copepods in the North Sea (Beaugrand 2004; Beaugrand & Ibanez 2004). For example, the abundance of the warm-water species *Calanus helgolandicus* has increased while the colder-water species *Calanus finmarchicus* has decreased (Reid *et al.* 2003; Beaugrand 2004). These two important copepod species occupy different thermal niches and show distinct differences in their patterns of seasonal abundance, with *C. helgolandicus* peaking significantly later in the year than *C. finmarchicus* (Wilson, Speirs & Heath 2015). The increase in abundance of warm-water species that have their seasonal peak later in the year is likely to explain why the copepod decadal bloom distribution widened following the hydroclimatic changes of the late 1980s. The length of the copepod bloom window suggests that copepod species are responding to SSTs across a large part of the year which may explain why the strongest linear relationships were identified between mean decadal SST and parameters *c* and *median*. The importance of summertime, as well as winter-spring temperatures for understanding the mechanisms of change in plankton productivity was discussed by Chiba *et al.* (2006) in their study of copepod phenology in the North Pacific. Copepods were found to be responding to changes in decadal hydroclimatic conditions and a lengthening of the optimal productive season was detected after the regime shift of the late 1980s. Warmer winter-spring temperatures were suggested by Chiba *et al.* (2006) to be responsible for the

earlier initiation of the copepod bloom. This study found that the rate of warming in spring (the change in decadal March-May SST) had the greatest effect on the bloom's proportional rate of increase (parameter *r*) and time delay (parameter *t*). The positive relationship between parameter *t* and SST may reflect the physiological and developmental lag times that occur between the triggering cue (the change in mean decadal March-May SST) and the adaptive response (Mackas *et al.* 2012) while the rate of spring warming is likely to affect copepod bloom dynamics by enhancing developmental rates, up-regulating metabolic processes, reducing food availability, shortening the maximum potential diapause duration, and increasing the survival of the early ascending cohort (Mackas, Goldblatt & Lewis 1998; Chiba *et al.* 2006; Saumweber & Durbin 2006; Mayor *et al.* 2015; Wilson *et al.* 2016). Each of these factors may contribute to the earlier occurrence and slow but sustained increase of the copepod bloom. Copepods demonstrate that, despite a temporal delay of the distribution (larger *t*) in later decades and at increasing temperatures, an earlier *median* is reached through a higher *r* and a smaller *c*.

The blooms of the non-copepod holozooplankton and meroplankton functional groups were also found to be happening earlier and more pronounced changes were again found to have occurred after the sharp rise in SST of the 1980s. Parameters *r* and *c* were largely independent of the different aspects of SST and time. The lack of a relationship could be explained by the larger heterogeneity in the biology (feeding mechanism, life history, physiology) of these two functional groups. A detailed analysis of members of the non-copepod holozooplankton and meroplankton functional groups based on feeding guilds or life history, may yield a better understanding of how increasing temperatures affects the seasonal abundance of these important links in the food web. Both the non-copepod holozooplankton and meroplankton functional groups showed a reduction in the time

delay (parameter *t*) and a consequent advancement (*median*) of their blooms. Strong negative relationships between both parameters *t* and *median*, and mean decadal spring SST were identified for the non-copepod holozooplankton group and suggest that increasing spring temperatures might be driving the phenological advancement of this functional group. For the meroplankton functional group, parameters *t* and *median* were found to be more closely correlated with mean decadal summer SST. Warmer spring temperatures have been shown to influence gametogenesis, spawning and larval survival of echinoderms, which has led to an earlier peak in their abundance and their domination in the plankton during the summer months (Lindley & Batten 2002; Kirby *et al.* 2007). The large proportion of echinoderm larvae in the meroplankton functional group may explain the phenological advancement and strong negative relationships with mean decadal summer SST that were identified for this group.

Controlling for the effects of the different aspects of SST revealed that the parameter estimates differed significantly between functional groups. This is unsurprising as these differences probably reflect the diverse life histories of the species that make up each assemblage. Pairwise comparisons revealed greater similarities between non-copepod holozooplankton and meroplankton for parameters *c* (temporal spread) and *t* (time lag). This may be due to these groups sharing more similar physiological attributes, such as respiration, reproduction, and embryonic development, and the comparable way that these attributes respond to changing SSTs (Edwards & Richardson 2004). Across all functional groups, spring and summer SSTs were found to have the largest effect on the timing of peak abundance (*median*). The influence that spring and summer SSTs have on the temporal dynamics (rate, concentration and time lag) of each functional group's bloom distribution

is clear from the examples described above. These influences combine and result in the overall phenological advancement of each functional group.

The extent of phenological advancement differed considerably between functional groups. The dinoflagellates and meroplankton groups displayed the greatest amount of advancement, each moving forward by 43 days over the 56-year study period. The copepod and non-copepod holozooplankton groups moved forward by 15 days and 12 days, respectively. These large phenological advancements have resulted following an increase in mean SST of 1.25 °C (estimated from regression) during the same period. A recent study by Chivers, Edwards and Hays (2020) estimated that the advancement of the dinoflagellate group was approximately 39 days (between 1958 and 2016), which is very close to the estimate in this study. Differences between the two methodologies must account for this relatively small difference.

In conclusion, by quantifying three different aspects of the temporal dynamics of the phenology of four different functional groups of plankton, the model allowed us to go beyond the effects of global warming on statistical moments of the temporal distribution and begin the exploration of possible biological reasons for the differing responses shown by each parameter: a measure of maximal developmental capacity, a rate of realisation of this capacity as it unfolds with time, and an overall measure of the distribution's time delay. A full account of these biological reasons, however, would require experimental investigation of how temperature affects the population dynamics of individual species through changes in physiological processes. The model itself cannot possibly provide these answers, but by quantifying the influence of each of the parameters on the temporal distribution under a particular set of conditions, it would help us to focus on crucial

biological processes (e.g., gonadal development, incubation period, egg hatching, larval development and survival, etc.) potentially influencing each of the aspects of the distribution. The variation in the response of individual parameters across the different functional groups indicates that these likely respond via different biological mechanisms or processes. A shifting phenology contains more information than a standard distribution, defined by its first two statistical moments, provides.

6 Latitudinal variation in flowering patterns of Japanese cherry trees over seven decades

6.1 Introduction

In mid and high latitudes, the seasonal timing of plant life-cycle events (phenology) is highly dependent on air temperature (Linkosalo *et al.* 2000; Badeck *et al.* 2004; Chmielewski, Müller & Bruns 2004). Air temperatures in the Northern Hemisphere have risen dramatically since the beginning of the 1980s, with more rapid warming observed in late winter and early spring and at higher latitudes than at lower latitudes (IPCC 2014). Numerous studies have described the earlier onset of spring events (bud burst, leafing and flowering), in response to warming temperatures (Menzel 2000; Abu-Asab *et al.* 2001; Fitter & Fitter 2002; Parmesan & Yohe 2003; Root *et al.* 2003; Menzel *et al.* 2006; Schwartz, Ahas & Aasa 2006; Cleland *et al.* 2007; Miller-Rushing & Primack 2008; Zhang *et al.* 2013; Ge *et al.* 2014). Importantly, these studies demonstrate that changes in spring phenology match the Northern Hemisphere warming pattern. For example, in a comprehensive study of European plant phenology, Menzel *et al.* (2006) found that early spring phases showed the strongest response to warming temperatures, advancing up to 4.6 days $°C^{-1}$ between 1951 and 1999. Similarly, Miller-Rushing and Primack (2008) reported that first flowering dates in Concord, Massachusetts had advanced by 3.1 days $°C^{-1}$ between 1852 and 2006, and were likely due to rising winter and spring temperatures. In an extensive review of phenological records spanning 86 years and 42.6 degrees of latitude, Post, Steinman and Mann (2018) found that rates of phenological advance increased significantly with latitude. A similar pattern of latitudinal variation was described by Cheng, Li and Yan (2021) who

found that leaf-unfolding dates of woody species located between 23-49°N latitude in eastern China had advanced more in regions above 30°N.

Estimates of phenological advancement, such as those described above, are often based on historical datasets describing first occurrences. Traditionally, first occurrences were recorded to identify changes in seasonal rhythms and to help guide agricultural decisions (Schwartz 2003; Piao *et al.* 2019). The practice of recording first occurrences has continued in recent years and long-term datasets have provided valuable information on the phenological response of plants to changing climatic conditions (Wenden *et al.* 2016).

One of the longest-running phenological records of first occurrences is for flowering of Japanese cherry trees (*Prunus* spp.). The popularity and huge cultural significance of cherry blossom festivals has resulted in the extensive recording of cherry tree flowering dates from multiple locations across Japan. The Somei-yoshino (*Prunus* × *yedoensis*) is the most widely planted cherry tree in Japan and specimen trees, used for ecological purposes, are maintained by the Japanese Meteorological Agency at the majority of their stations (Primack, Higuchi & Miller-Rushing 2009). *P.* × *yedoensis* trees are clones of a single individual and are therefore genetically identical (Innan *et al.* 1995). Japan's extended latitudinal range and diverse climatic conditions, provide a unique opportunity to assess the effects of temperature on the flowering phenology of genetically similar individuals (Ohashi *et al.* 2012).

The Japanese cherry tree dataset presented an exciting opportunity to test whether the new method of phenological analysis, described in previous chapters, could use first occurrence data to identify phenological trends along an environmental gradient. First flowering records, from 83 locations across Japan, were assigned to latitudinal bands and

were used to examine changes in cherry tree flowering phenology during the period 1953–2018. The new method of phenological analysis quantifies three key parameters of the phenological time distribution (Franco 2018; Steer, Ramsay & Franco 2019). Relationships between the parameters and different aspects of temperature were explored to identify which aspects of temperature, if any, had the greatest influence on cherry tree flowering phenology for each latitudinal band.

The aims of this study were (i) to test whether first flowering data occurring across an environmental gradient could be analysed as a time distribution, (ii) to quantify cherry tree first flowering phenology across three latitudinal bands in Japan for the period 1953–2018, (iii) to contrast the variation in the values of the parameters as a function of time and of changing air temperature, and (iv) based on the results, to evaluate whether the model can be used to uncover phenological trends not revealed by standard distribution functions defined by their first two statistical moments.

6.2 Materials and Methods

6.2.1 Phenological data

The first flowering records used in this study were collected by the Japanese Meteorological Agency (JMA) and were obtained from their website (https://www.data.jma.go.jp/sakura/data/index.html). The JMA has been observing first flowering dates of specimen *Prunus* spp. trees, located at World Meteorological Organisation (WMO) stations, since 1953. The JMA define the date of cherry blossom flowering as the first day when five to six or more flowers are open on the specimen tree (Japanese Meteorological Agency 1988). The flowering dates of the ornamental cherry tree

Prunus × *yedoensis* were observed in all of the meteorological stations, apart from those located in the northernmost region of the island of Hokkaido. *P.* × *yedoensis* does not grow in the sub-arctic climate of northern Hokkaido, therefore *P. sargentii* and P. *nipponica var. kurilensis* are observed in its place (see Appendix C: Table C1, for species information per location).

Meteorological stations across mainland Japan were selected based on the criteria that a minimum of 45 years of phenological data were available within the period 1953-2018. Consequently, 83 meteorological stations were selected and a total of 5,092 *Prunus* first flowering records were used in the study. First dates are obviously insufficient to investigate how the flowering phenology develops throughout each season. However, a sufficiently large sample of first dates must themselves follow a time distribution within certain geographical confines. Thus, in order to test the hypothesis that sufficient first flowering data occurring across an environmental gradient could be analysed as a time distribution, stations were allocated to latitudinal bands: 28 stations located between 30.574-34.975°N were allocated to the low latitudinal band, 39 stations located between 35.013-39.717°N were allocated to the mid latitude band, and 16 stations located between 40.500-45.415°N were allocated to the high latitude band (Fig. 6.1). This assumes that longitudinal variation (e.g., altitudinal range) is similar across latitude, particularly if latitudinal bands are wide and, inevitably, few.

6.2.2 Climatic data

Air temperature was used as the environmental variable of interest as earlier studies have shown that the flowering date of *Prunus* is influenced by the air temperature 1-2 months before flowering starts (Omoto & Aono 1989; Miller-Rushing *et al.* 2007; Ohashi *et al.*

2012). Monthly mean air temperatures (°C) from 83 WMO stations were obtained for the period 1953-2018 from the Japanese Meteorological Agency website (https://www.data.jma.go.jp/obd/stats/data/en/smp/index.html). The WMO stations correspond with the location of the *Prunus* specimen trees (Fig. 6.1). From this dataset, (i)

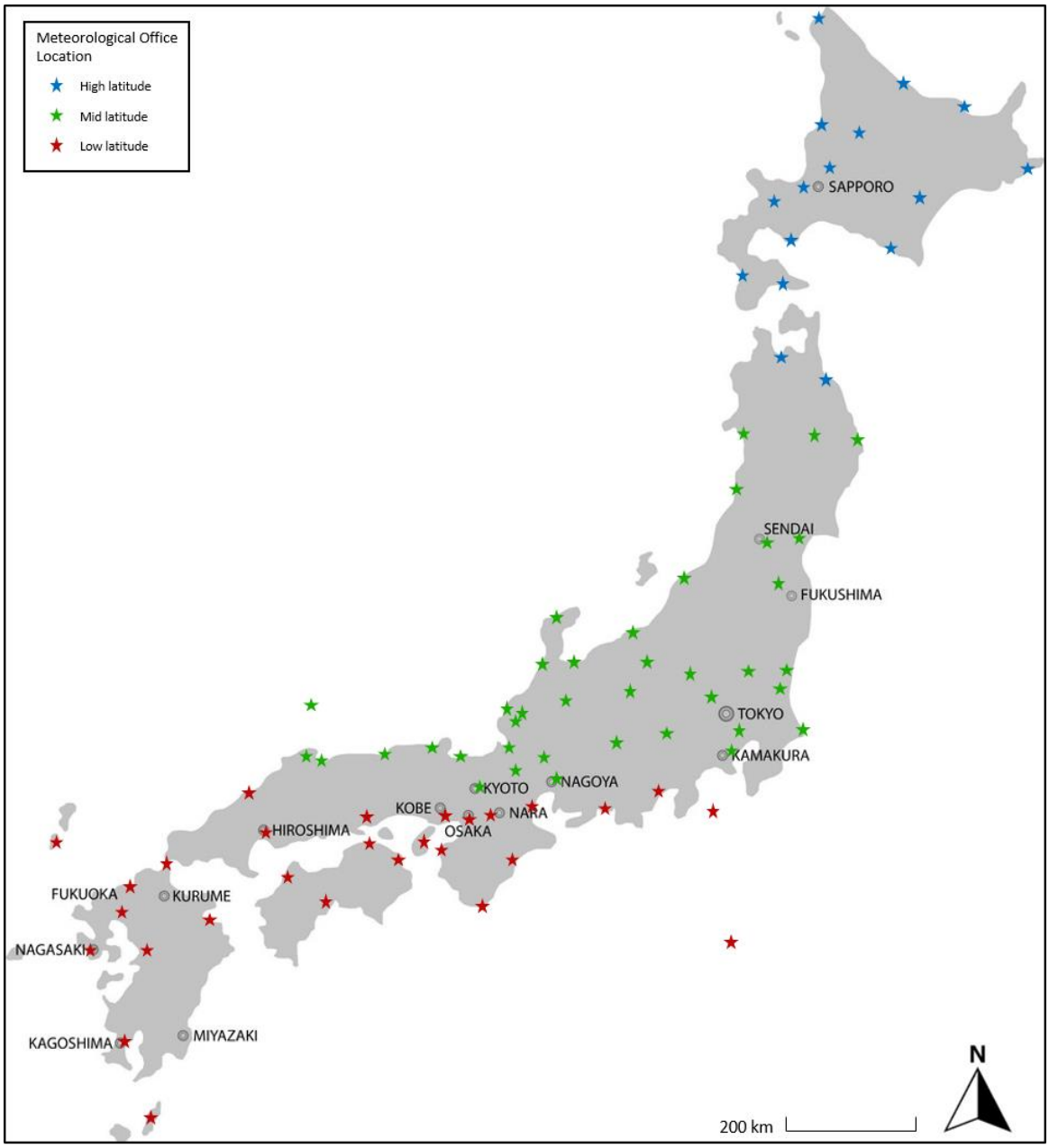

Figure 6.1. Japanese Meteorological Agency WMO local office locations. Low latitude locations between 30.574-34.975°N (red), mid latitude locations between 35.013-39.717°N (green), and high latitude locations between 40.500-45.415°N (blue).

mean decadal temperatures for the individual months of January, February, March, and April, (ii) the change in winter (December-February), (iii) the change in mid-winter/early spring (January-March), (iv) the change in late winter/mid-spring (February-April), (v) the average of February and March, and (vi) the average of March and April were calculated for each latitudinal band (low, mid and high) to identify which had the greatest effect on the parameter estimates produced from each distribution model fit.

6.2.3 Distribution model fits

In order to ensure sufficient data were available to produce reliable model fits, flowering data were pooled by decade (1953-59, 1960-69, 1970-79, 1980-89, 1990-99, 2000-09, 2010-18). Pooling the data also permitted the overall pattern of gradual phenological change to be detected as it dampened short-term interannual variation. The model was fitted to each of the seven decadal cumulative first occurrence curves for each of the three latitudinal bands, producing a total of 21 phenology distributions. Quantifying the three different parameters measuring proportional maximum completion, speed, and duration of the cumulative first occurrence distributions allowed identification of differences between latitudinal bands.

The model has the form:

$$y = 1 - \left(1 - \frac{r}{1+e^{-c(x-t)}}\right)^{x} \qquad (1)$$

where y is the empirically recorded cumulative first occurrence of *Prunus* flowering over time (x(calendar days)), r quantifies the maximum proportional rate of increase in occurrence (it is dimensionless), c is the rate at which r converges on its maximum value and is inversely proportional to the temporal spread of the distribution (units: time^{-1}), and

t is an overall measure of the time lag of the phenology (units: time) (Steer, Ramsay & Franco 2019). Each parameter measures a specific aspect of the shape of the distribution (Chapter 2) and, although correlated with some statistical moments, they are not equivalent to them. They quantify important aspects of the time distribution's dynamics.

The derivative of equation 1 provides the corresponding probability density function (*pdf*):

$$\frac{dy}{dx} = \left(1 - \frac{r}{1+e^{-c(x-t)}}\right)^{x} \left(\frac{rcxe^{-c(x-t)}}{\left(1+e^{-c(x-t)}\right)^{2}\left(1-\frac{r}{1+e^{-c(x-t)}}\right)} - \ln\left(1 - \frac{r}{1+e^{-c(x-t)}}\right)\right) \quad (2)$$

which describes the population-level change in occurrence (first flowering rate) over the course of the average decadal year. Parameter *r, c,* and *t* and the statistical moments were estimated using the *nlstimedist* R package (Franco, Ramsay & Steer, 2019; Steer, Ramsay & Franco, 2019).

Finally, regression methods were employed to investigate the relationships between model parameters (*r*, *c*, *t* and median) and either time (decade) or the different aspects of temperature mentioned in the previous section.

6.3 Results

6.3.1 Air temperature

Annual mean air temperatures for all three latitudinal band showed a slight cooling trend (more pronounced at low and mid latitudes) from 1953 until the late 1970s/early 1980s, followed by more consistent warming. Despite the initial cooling and regular short-term fluctuations, an overall positive linear trend was evident from 1953 to 2018 for all months

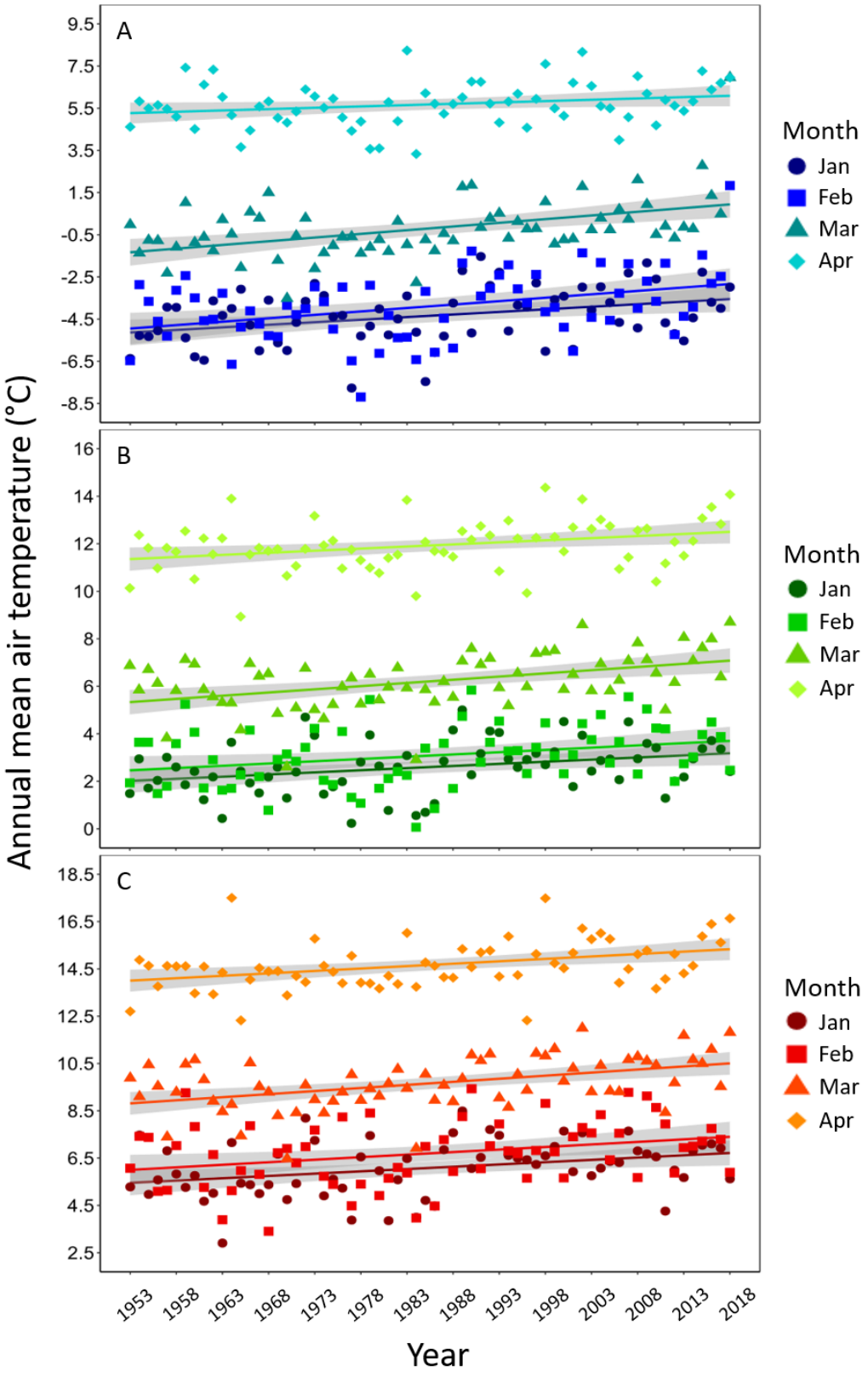

Figure 6.2. Annual mean air temperatures from 1953 to 2018 for January (circle), February (square), March (triangle), and April (diamond) at three latitudinal bands: (A) high latitude sites between 40.500-45.415°N (blue), (B) mid latitude sites between 35.013-39.717°N (green), and (C) low latitude sites between 30.574-34.975°N (red).

Table 6.1. Regression analysis of the relationship between annual mean air temperatures for the months January, February, March, and April, and time (year) for three latitudinal bands: high (40.500-45.415°N), mid (35.013-39.717°N), and low (30.574-34.975°N) crossing mainland Japan, and time (1953-2018), * p < 0.05, ** p < 0.01, *** p < 0.001, Unst. Coeffs. B is the estimated linear trend (°C per year).

Latitude	Month	Sum of Squares	df1	df2	F	Sig.	R^2	Pearson's R	Unst. coeffs. B
High	January	14.334	1	64	9.015	0.004**	0.123	0.351	0.024
	February	13.552	1	64	6.782	0.011*	0.096	0.310	0.024
	March	18.784	1	64	16.909	0.000***	0.209	0.457	0.028
	April	3.832	1	64	3.646	0.061	0.054	0.232	0.013
Mid	January	7.722	1	64	7.310	0.009**	0.103	0.320	0.018
	February	8.735	1	64	5.869	0.018*	0.084	0.290	0.019
	March	17.313	1	64	15.496	0.000***	0.195	0.442	0.027
	April	7.462	1	64	7.401	0.008**	0.104	0.322	0.018
Low	January	9.013	1	64	7.630	0.007**	0.107	0.326	0.019
	February	11.063	1	64	6.414	0.014*	0.091	0.302	0.021
	March	16.205	1	64	16.686	0.000***	0.207	0.455	0.026
	April	10.007	1	64	10.995	0.002**	0.147	0.383	0.020

at all latitudes (Fig. 6.2). The month of March showed the strongest and most consistent warming trend at all three latitudes (Table 6.1, Fig. 6.2). The high latitudinal band displayed the greatest overall warming, with the months of January, February and March all warming more rapidly than their mid and low latitude counterparts (annual mean air temperatures rose by 1.6 °C, 1.5 °C and 1.8 °C (estimated from regression) respectively, between 1953 and 2018). The relatively low R^2 values reflect the wide inter-annual variation in air temperatures.

6.3.2 Model fits

Pooling together the first flowering dates by latitude and decade allowed the model to estimate successfully the time distribution of first flowering dates (Fig. 6.3). The time sequences of both *cdfs* and *pdfs* closely reflect the periods of cooling and warming described above for each latitudinal band. Cooler periods (relative to the 1950s) resulted

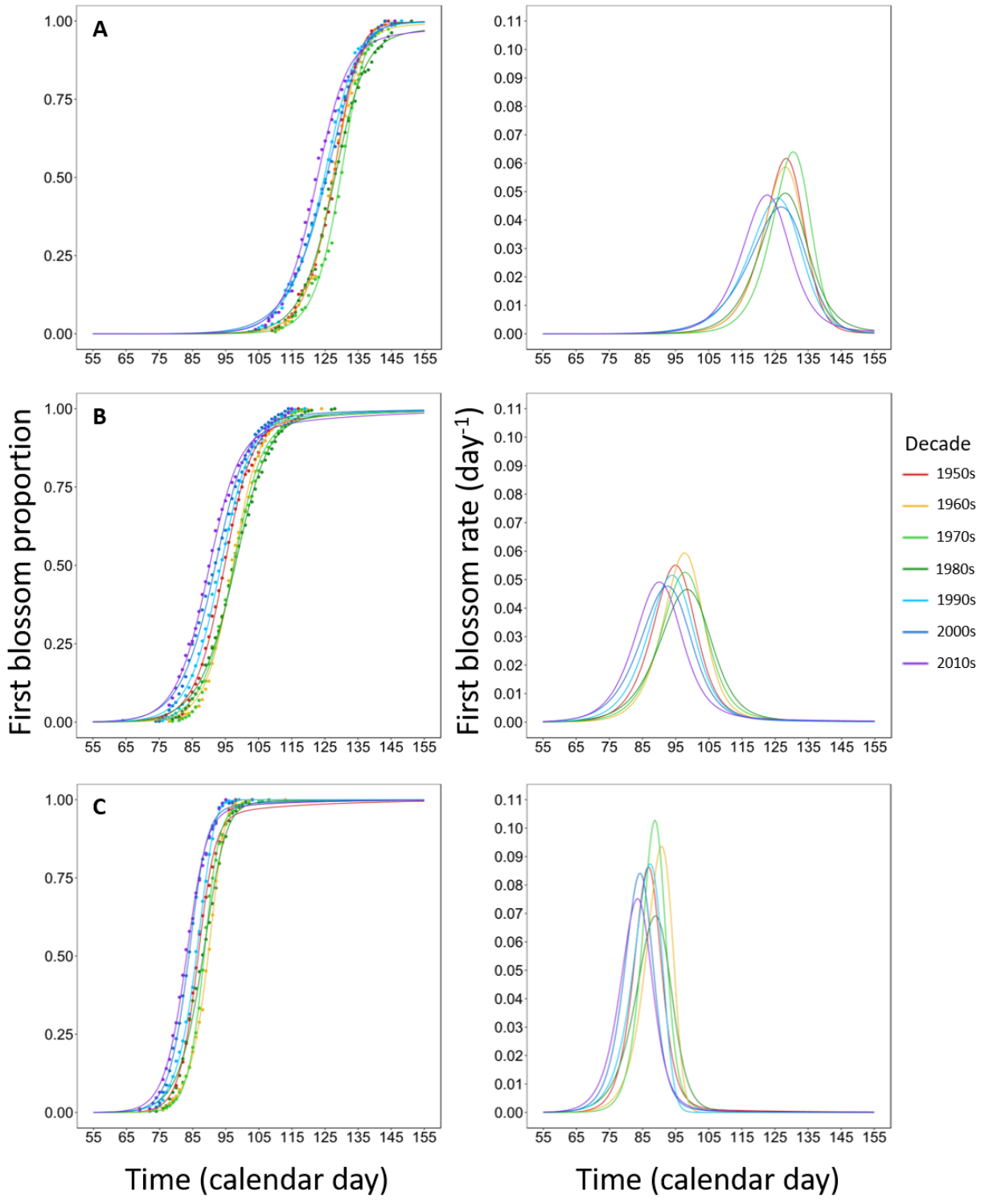

Figure 6.3. Cumulative distribution functions (left) and corresponding probability density functions (right) of Japanese cherry tree first blossoming across three latitudinal bands (A) high latitude sites between 40.500-45.415°N, (B) mid latitude sites between 35.013-39.717°N, and (C) low latitude sites between 30.574-34.975°N for each decade: 1953-59 (red), 1960-69 (yellow), 1970-79 (light green), 1980-89 (dark green), 1990-99 (light blue), 2000-2010 (dark blue), and 2010-2018 (purple). Probability density functions describe the rate of first blossoming through time.

in later flowering and where the period of cooling was more pronounced (low and mid latitudes), the shift towards later flowering was greater. Warmer periods resulted in earlier flowering and where warming occurred more rapidly (the high latitude band), the change to earlier flowering happened sooner. The curves reveal that the first flowering response of *Prunus* to periods of cooling and warming was similar at all three latitudes. The position of these curves characterises the sequence of flowering from the last week of March (low latitude) to the first week of May (high latitude) suggesting that first flowering at different latitudes is likely influenced by air temperatures at different points in the year. Changes in first flowering with time and air temperature are better described by the change in the values of the distributions' parameters (Appendix C: Table C2).

6.3.3 Relationships between parameters and both time and air temperature

No credible relationships were identified between parameter *r* (the proportional rate of occurrence) and time and only weak negative relationships were identified between parameters *c* (the rate/temporal concentration of the phenology) and *t* (its time lag), and time (Fig. 6.4; Appendix C: Table C3). Despite these low correlations, negative trends were consistent across all three latitudes suggesting that the temporal spread of first flowering across Japan has widened and its time lag has shortened with time, but the trends are weakened by the wide year-to-year variation in temperature. Strong quadratic relationships were identified between the statistical moment *median* and time for each latitudinal band (low: $F_{2,4} = 12.811$, $p = 0.018$, $R^2 = 0.865$; mid: $F_{2,4} = 15.403$, $p = 0.013$, $R^2 = 0.885$; high: $F_{2,4} = 8.547$, $p = 0.036$, $R^2 = 0.810$) reflecting the change from cooler (1960s-1980s) to warmer (1990s-2010s) air temperatures described in the Air temperature section above. Regression was also used to explore the relationships between the distribution's parameters and different aspects of air temperature to identify which had

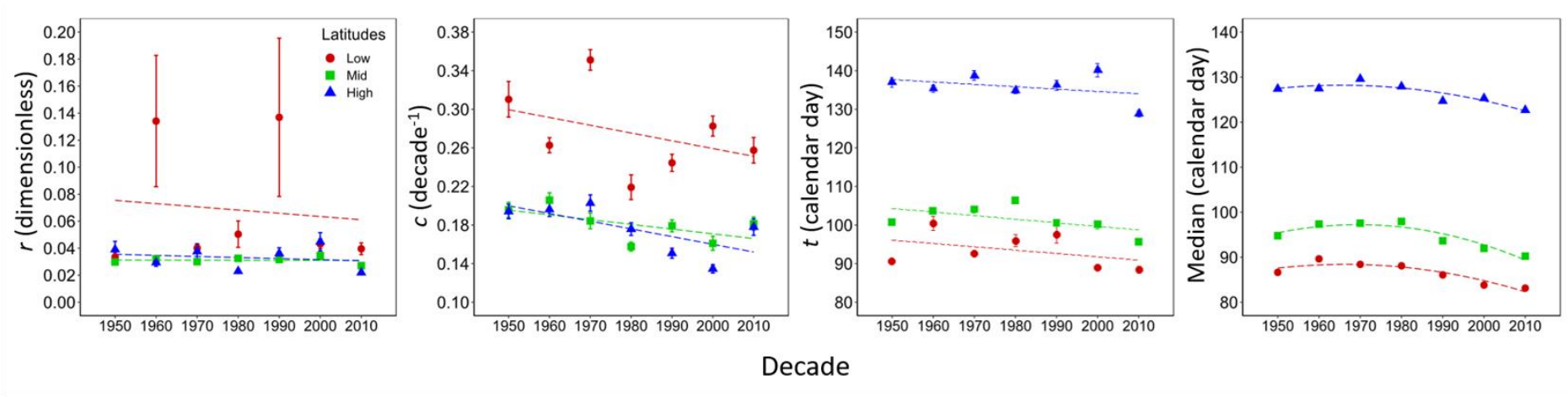

Figure 6.4. Relationships between the values of the parameter estimates (*r*, *c*, *t* and *median*) produced from each model fit and time (decades: 1953-1959, 1960-69, 1970-79, 1980-89, 1990-99, 2000-09, 2010-18) for low – 30.574-34.975°N (red circle), mid – 35.013-39.717°N (green square), and high – 40.500-45.415°N (blue triangle) latitudinal groups. The two estimates of *r* with wide standard errors at low latitude are due to multimodal distributions and are likely a consequence of small sample size. For regression analysis, see Appendix C: Table C3.

the greatest influence on them at each latitude. No correlations were identified between parameter *r* and the individual months of January, February, March, or April (Fig. 6.5). However, a negative correlation ($F_{1,5} = 7.476$, $p = 0.041$, $R = -0.774$) was identified between parameter *r* and the change in late winter/mid spring (February to April) air temperatures for the high latitudinal band (Appendix C: Table C3). This relationship suggests that the rate of first flowering at high latitudes may be determined by the difference between

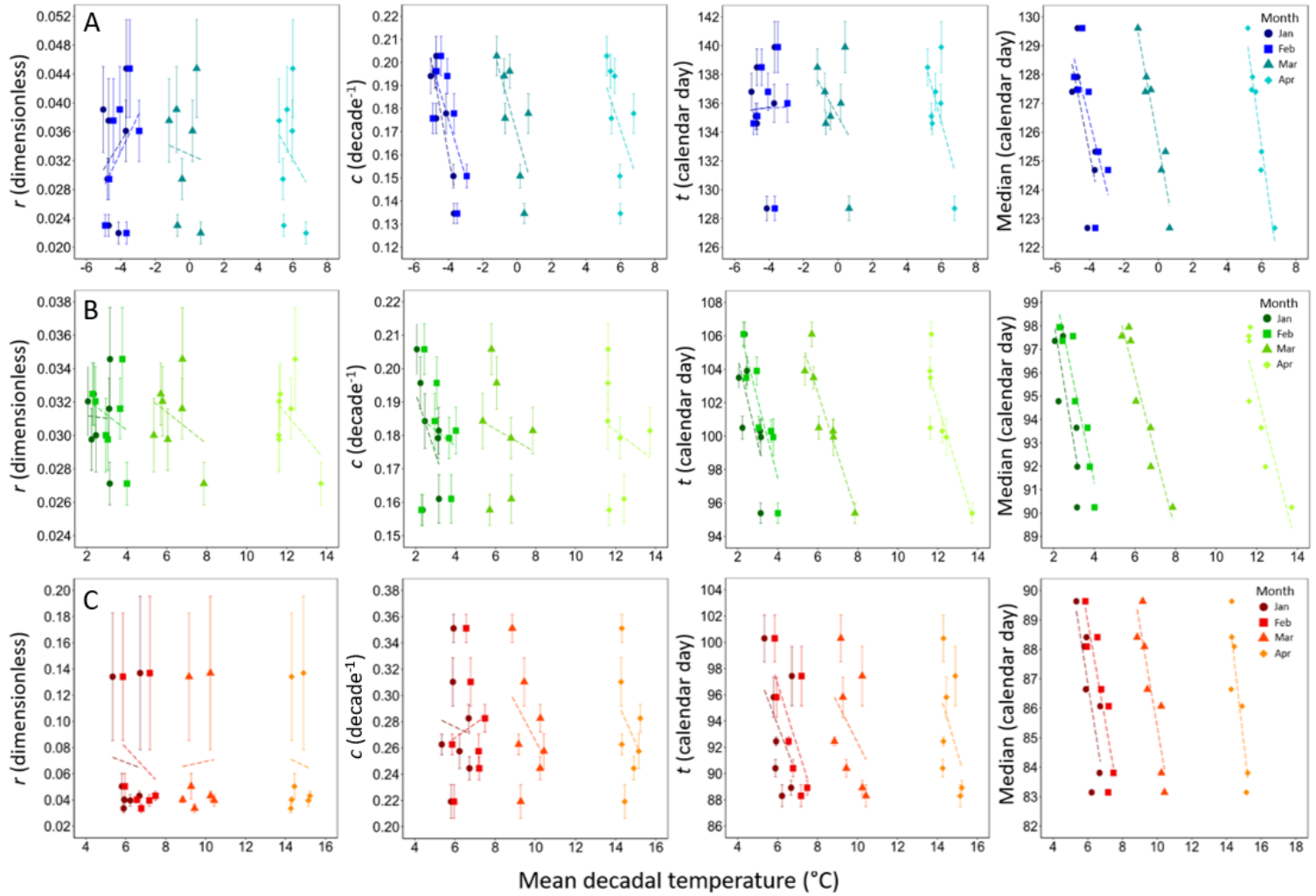

Figure 6.5. Linear relationships between the values of the parameter estimates (*r*, *c*, *t* and *median*) produced from each model fit and mean decadal temperatures for January (circle), February (square), March (triangle), and April (diamond) across three latitudinal bands (A) high latitude sites between 40.500-45.415°N (blue), mid latitude sites between 35.013-39.717°N (green), and (C) low latitude sites between 30.574-34.975°N (red). Error bars represent the standard error of the parameter estimates. For regression analysis, see Appendix C: Table C3.

winter and spring air temperatures. Strong negative relationships were also identified between parameter *c* and winter, and average late winter/early spring (February and March) air temperatures for the high latitudinal band (January: $F_{1,5} = 20.277$, $p = 0.006$, $R = -0.896$; February and March: $F_{1,5} = 6.964$, $p = 0.046$, $R = -0.763$) and suggest that warmer winter and early spring temperatures widen the first flowering distribution (Appendix C: Table C3).

No correlations were detected between parameter *c* and air temperature for the mid or low latitudinal bands. The change in air temperatures in the three months preceding first flowering was found to have a strong influence on parameter *t* at all three latitudes. Both high and mid latitudes displayed strong correlations (high: $F_{1,5} = 6.147$, $p = 0.056$, $R = -0.743$; mid: $F_{1,5} = 11.327$, $p = 0.020$, $R = -0.833$) with the change in mid-winter/early spring (January to March) air temperatures, and the low latitudinal band displayed a strong correlation ($F_{1,5} = 14.171$, $p = 0.013$, $R = -0.860$) with the change in winter (December to February) air temperatures. These relationships suggest that the advancement of first flowering at each latitude is determined, in part, by the extent of temperature change in the months prior to flowering.

All three latitudinal bands showed advancement in the median point of their temporal distribution with increasing air temperatures. As with parameter *t* above, the air temperature of the months preceding the date of first flowering, appear to have the greatest influence on the median point of *Prunus* flowering phenology. Strong linear relationships were identified between *median* and average February and March air temperatures ($F_{1,5} = 35.458$, $p = 0.002$, $R = -0.936$) for the low latitudinal band, both average February and March ($F_{1,5} = 139.844$, $p < 0.001$, $R = -0.908$) and March ($F_{1,5} =$

49.857, p = 0.001, R = -0.953) air temperatures for the mid latitudinal band, and both average March and April ($F_{1,5}$ = 202.166, p < 0.001, R = -0.988) and April ($F_{1,5}$ = 71.758, p < 0.001, R = -0.967) air temperatures for the high latitudinal band. Slope coefficients suggest that first flowering has advanced by 3.8 d/°C for the low latitudinal band, between 3.3 and 4.0 d/°C for the mid latitudinal band, and between 3.9 and 4.3 d/°C for the high latitudinal band.

6.4 Discussion

Using first occurrence data over a large area to make up for sample size, the model indicated that cherry tree first flowering trends closely matched the pattern of climatic cooling and warming at three latitudes. During the initial cooling phase, first flowering was delayed (relative to the 1950s) at all three latitudes. The model showed that where cooling was more pronounced (at low and mid latitudes) the delay in first flowering was greater. Following the cooling phase, warming accelerated significantly and increased more in the period 1981–2005 than at any other time in the previous 100 years (Schaefer & Domroes 2009; Higashino & Stefan 2014). The rapid increase of air temperatures from the 1980s onwards advanced first flowering at all three latitudes. The model revealed that the shift to advanced first flowering occurred shortly after each latitude had transitioned to a warming phase (this occurred earlier at the high latitudinal band where the transition to a warming phase happened sooner). The intensity of the warming phase resulted in an overall linear trend of warming between 1953 and 2018 and a general advancement of cherry tree first flowering for all three latitudinal bands.

This study found that cherry tree first flowering advanced by 5.0–6.1 days between 1953 and 2018. This figure is similar to that obtained in earlier analyses of Japanese cherry tree flowering phenology. For example, Miller-Rushing *et al.* (2007) reported an average advance of first flowering of 7.9 days over a 25-year period (1981-2005) for 17 *Prunus*/*Cerasus* taxa near Mt. Takao, Tokyo. Whilst Aono and Kazui (2008) found that average flowering dates of *P. jamasakura* in Kyoto had advanced by 7 days between 1971 and 2000 (in comparison to the average of all previous records of a 1200-year dataset). The larger estimations of advancement in these studies compared to our own are likely due to the location of the study sites and the greater warming trends recorded for urban and metropolitan areas (Primack, Higuchi & Miller-Rushing 2009; Higashino & Stefan 2014). Shorter and more recent time series also have a tendency to reveal greater rates of phenological advance (Post, Steinman & Mann 2018).

The advancement of cherry tree first flowering can be largely explained by the increase of the air temperatures in the two months preceding flowering. The importance of air temperatures in late winter and early spring for promoting spring phenophases is well-established (Kai *et al.* 1993; Chmielewski & Rötzer 2001; Chmielewski, Müller & Bruns 2004; Piao *et al.* 2006; Miller-Rushing *et al.* 2007; Doi & Katano 2008; Allen *et al.* 2014; Ge *et al.* 2014; Wang *et al.* 2017). At low and mid latitudes, strong correlations were identified between the median point of the decadal flowering distributions and average February and March temperatures, whereas flowering in the high latitudinal band was more closely correlated with average March and April, and April temperatures. These findings are in agreement with Kai *et al.* (1993) who showed that cherry trees that blossom before April 21st correlate strongly with mean March temperatures, whereas

trees that flower after this date, i.e. those in the high latitudinal band, correlate more strongly with mean April temperatures. The relationships with monthly temperatures described above reflect the latitudinal progression of flowering from south to north and similar latitudinal patterns in spring phenophases have been found in Europe (Rötzer & Chmielewski 2001) and in Eastern China and the USA (Wang *et al.* 2015).

Across all latitudes, cherry trees flowered 3.8–4.3 days earlier for each 1°C increase in February to April mean monthly temperatures. The level of sensitivity (the number of days change per 1°C) reported here corresponds well with the range described for Japanese cherry trees (3–5 days $°C^{-1}$ (Kai *et al.* 1993; Miller-Rushing *et al.* 2007; Wang *et al.* 2017)) and for fruit trees in different locations in the Northern Hemisphere (2.9–5 days $°C^{-1}$ (Chmielewski, Müller & Bruns 2004; Lu *et al.* 2006; Estrella, Sparks & Menzel 2007; Ge *et al.* 2014; Jochner *et al.* 2016)). The similarity between the results reported here and those of earlier studies suggest that the model can reliably estimate phenological responses to specific environmental stimuli using first occurrence data.

First flowering in the high latitudinal band displayed greater sensitivity to increasing temperatures than first flowering in the low and mid latitudinal bands. It was also the only band where significant relationships were detected between parameters *r* and *c*, and an aspect of pre-season temperature. Many fruit trees from temperate zones require both chilling and heating (forcing) during dormancy to restart growth and begin flowering in spring (Luedeling & Brown 2011; Luedeling *et al.* 2013; Allen *et al.* 2014; Guo *et al.* 2015; Shi *et al.* 2017). Evidence suggests that in cold-winter locations plant phenology is determined largely by temperatures during the forcing period, as chill requirements are fully satisfied during winter (Luedeling *et al.* 2013; Guo *et al.* 2015).

The high latitudinal band is an example of a cold-winter location. Specimen trees in this band comprised of both *P.* × *yedoensis* and *P. sargentii* and were located predominantly in the Hokkaido region of Japan. Hokkaido is the northernmost island of Japan and has a cool temperate to sub-arctic climate (Nakatsuji *et al.* 2021). Prevéy *et al.* (2017) have suggested that the phenology of plants adapted to colder, higher latitude sites may exhibit greater sensitivity to changes in temperature due to small changes having a greater effect on the plants thermal balance. The proper fulfilment of the chilling requirement and the greater sensitivity to forcing in the high latitudinal band may be why trends between the parameter estimates *r* and *c*, and temperature were identified at this latitude and not at others.

The negative relationship identified between parameter *r* and the change in late winter/early spring air temperatures shows that the proportional rate of first flowering slows when the difference between February and April temperatures is greater. Luedeling, Kunz and Blanke (2013) estimated that cherry trees require approximately 3,500 growing degree hours to initiate flowering in spring and it is possible that when the difference between winter and spring temperatures is greater, the forcing requirement takes longer to be fulfilled. Interestingly, this finding suggests that the rate of temperature change between winter and spring may be responsible for accelerating the rate of first flowering and not the absolute values of winter and spring temperatures. This conclusion was also reached by Kai *et al.* (1993) who showed that the temperature progression in the months preceding flowering was a determining factor for the timing of first blossom. The strong negative relationship between parameter *c* and January air temperatures shows that warming in mid-winter is

widening the first flowering distribution. The response to temperature changes in mid-winter suggests that warming is affecting the process of chill accumulation during dormancy. In cold-winter locations, freezing mid-winter temperatures halt the accumulation of winter chill (Luedeling, Kunz & Blanke 2013). However, Luedeling and Brown (2011) and Shi *et al.* (2017) suggest that winter warming in cold-winter locations may accelerate the accumulation of winter chill and advance flowering by reducing the number of days with sub-zero temperatures. The effect of winter warming on chill accumulation rates is likely greater in urban areas where warming trends exceed those of rural and coastal locations (Primack, Higuchi & Miller-Rushing 2009; Sato & Sasaki 2011; Higashino & Stefan 2014). It is this differential response to warming that is likely responsible for the widening of the first flowering distribution in the high latitudinal band.

Urbanisation and the heat island effect may also explain the general widening of the first flowering distribution with time observed across all three latitudes. Following the post-war period, Japan experienced rapid population growth and urbanisation (Sorensen 2002). The rapid development and industrialisation of Japan has resulted in a warming trend approximately three times higher in large metropolitan areas than in surrounding rural locations (Higashino & Stefan 2014). The effect of urbanisation on the timing of cherry tree flowering was reported by Aono (1997) who found that cherry trees flowered 4-8 days earlier in cities than in nearby rural locations. The proximity of cherry trees to urban centres has also been shown to affect the timing of flowering, with successively later flowering reported as distances from urban centres increased (Aono 1997; Ohashi *et al.* 2012). The opposite trend has been identified for coastal regions

where cooler temperatures were found to lessen the rate of advancement (Aono 1997; Ohashi *et al.* 2012). The general widening of the first flowering distribution with time can be adequately described by the response of cherry trees to different rates of warming in urban, rural and coastal locations over the last seven decades.

The lack of identifiable trends between parameter *r* and *c*, and temperature in the low and mid latitudinal bands may be due to the effect that winter warming has on chill accumulation in warmer-winter locations. In locations with warmer-winters, temperature increases during the chilling phase have been shown to be the dominant driver of spring phenophases (Luedeling *et al.* 2013; Guo *et al.* 2015). Warmer conditions during dormancy are reported to extend the chilling phase and delay the timing of spring events (Yu, Luedeling & Xu 2010; Elloumi *et al.* 2013; Luedeling *et al.* 2013; Guo *et al.* 2015). It is possible that the delaying effect of winter warming, which would be greater in urban areas where warming has increased the most, may counteract the advancing effect of higher forcing temperatures in the cooler areas of the latitudinal bands. The response of these two temperature dependent processes may confound each other and mask the effect that forcing alone has on the proportional rate (parameter *r*) and concentration (parameter *c*) of the first flowering distribution. Although the model was unable to distinguish trends for parameters *r* and *c* in the low and mid latitudinal bands, strong negative relationships were detected between the time delay (parameter *t*) and the median points of the decadal distributions, and temperature changes in the months preceding flowering for all three latitudinal bands. The identification of these relationships by the model, despite the confounding effects of winter warming, indicate that increasing spring temperatures have a dominant effect

on the overall timing of cherry tree flowering phenology.

This study has shown that the model can be used to detect phenological trends using first occurrence data across an environmental gradient. However, it has also shown that in order to identify meaningful relationships for all of the parameters in the model it may be necessary to refine the sampling area or the research question, or both. When using first occurrence data a trade-off occurs between choosing an area large enough so that there are sufficient data points for the model to reliably fit, and an area small enough that a more specific environmental variable can be investigated. If the sampling area is particularly large, as in this study, it may be possible to refine the research question to investigate the difference between, for example, urban and rural or inland and coastal regions. The fact that the model was able to capture the effects of warming on first-occurrence flowering events suggests it could be used on similar, point event historical phenological data.

7 General discussion

Phenological change is widely regarded as an important biological indicator of contemporary climate change (Parmesan & Yohe 2003; Root *et al.* 2003; Menzel *et al.* 2006; Scranton & Amarasekare 2017; Garonna *et al.* 2018). Numerous studies examining the impact of rising temperatures on the timing of phenological events have reported changes that are consistent with the observed pattern of warming (Menzel 2000; Fitter & Fitter 2002; Parmesan & Yohe 2003; Root *et al.* 2003; Menzel *et al.* 2006; Cleland *et al.* 2007; Parmesan 2007; Piao *et al.* 2019; Menzel *et al.* 2020). Estimates of phenological change are often based on long-term datasets that contain single measures of phenology, such as the date of the first flower to bloom or the first migrant of the season to arrive. However, changes in first dates have been shown to shift independently from peak and last dates and are therefore unlikely to be representative of the population as a whole (CaraDonna, Iler & Inouye 2014). A method of analysis that accounts for the variation in the response of individuals and focusses on the population-level response would provide a more complete picture of the extent of phenological change (Steer, Ramsay & Franco 2019).

The phenological responses presented here underline the fact that assessments of phenological change based on single measures alone mask their complexity. The present research demonstrates that a model capable of accommodating the wide range of distribution shapes, which characterise the diversity of phenological responses, provides more detailed information on three aspects of the process in addition to its

standard statistical moments. By quantifying the influence that temperature change has had on each of the three model parameters (rate, concentration and time lag), further insight may be afforded into the potential drivers of phenological change.

To facilitate the exploration of a diverse range of phenological phenomena, an R package was produced (Chapters 2 & 3). The rationale for the development of the R package was two-fold: to automate the fitting of the model to varied and often extensive datasets, and to provide a free to use, easily accessible method of time distribution analysis for other researchers. Phenological research has been criticised for its lack of comparable studies (Root *et al.* 2003; Parmesan 2007; Thackeray *et al.* 2010). This criticism often references the wide range of definitions and criteria for the identification of phenophases, the different sampling methods, and the different scales of observation that have been used to assess phenological change (Denny *et al.* 2014). By providing a conceptually simple, consistent method of phenological analysis, it is hoped that it would be used by researchers to facilitate standardised comparisons of phenological data.

To explore the accuracy of the model and its ability to quantify subtle responses to temperature, it was first applied to data produced under controlled laboratory conditions (Chapter 4). A detailed analysis of the germination response of three high-elevation, monocarpic perennial plant species revealed small but likely important differences in their response to temperature. These differences were attributed to the prevailing ecological conditions at their sites of origin. Higher elevation species had cooler minimum and optimal temperature ranges for germination than their lower elevation counterparts. The ability of the model to quantify subtle variations in the

shape of the temporal distribution of seed germination as a result of minor changes in experimental condition (in some cases less than 0.5°C) highlight its sensitivity. Confidence in the meaning and accuracy of the model was demonstrated by the capacity of all three parameters to describe an established biological process, namely the regulating effect that temperature-mediated metabolic processes have on seed germination (Kozlowski 1972; Bewley & Black 1982; Fenner & Thompson 2005). The germination response of each species, and the ecological characteristics of their respective habitats, suggest that *Puya* might be particularly susceptible to changing climatic conditions and that this vulnerability would likely be expressed through their regeneration niche. This chapter demonstrated the accuracy and sensitivity of the model and its ability to quantify variation in the phenological response of three closely related species. It also demonstrated the capacity of the model to assess the potential for climate-related species range shifts.

The model was next used to investigate phenological changes in marine plankton functional groups in response to rising sea surface temperatures (Chapter 5). The scale of the Continuous Plankton Recorder (CPR) survey provided an opportunity to use the model to examine the effects of climate change on the phenology of interacting marine plankton species over several decades. The extent of phenological advancement was found to differ considerably between functional groups and suggested that the mismatch between successive plankton trophic levels identified by Edwards and Richardson (2004) has continued to increase. Estimations of phenological advancement corresponded well with those of earlier studies (Edwards & Richardson 2004; Chivers, Edwards & Hays 2020). Importantly, the model allowed the description of phenological

change to go beyond that of a general measure of advancement and revealed that the parameters of each functional group's temporal distribution had responded differently to increases in sea surface temperature. The complexity of the phenological response is exemplified by the overall advancement of the dinoflagellate bloom despite a decrease in its proportional rate of occurrence and an increase in its temporal concentration, and by the advancement of the copepod bloom despite a decrease in its temporal concentration and an increase in its time lag. The variation in the response of individual parameters across the different functional groups indicates that they likely respond via different biological mechanisms or processes. Quantification of the model's parameters also identified which aspect of sea surface temperature was driving phenological change in each functional group. For example, increases in mean decadal March-May sea surface temperatures were found to have a strong influence on the dinoflagellate bloom, a finding supported by Chivers, Edwards and Hays (2020). This chapter revealed that information regarding the way phenological distributions are changing through time, and the drivers of phenological change, could provide assessments of trophic mismatch that offer a more thorough evaluation of the possible mechanisms operating in each functional group.

The ability of the model to use first occurrence data to identify phenological trends along an environmental gradient was next explored using data from the Japanese cherry tree flowering records (Chapter 6). The pooling together of first flowering dates by latitude and decade provided sufficient data for the model to estimate successfully the time distribution of first flowering dates. Estimates of advancement and sensitivity were similar to those described previously (Kai *et al.* 1993; Miller-Rushing *et al.* 2007;

Aono & Kazui 2008; Wang *et al.* 2017) with variations in the estimates of advancement attributed to the effects of urban warming in study locations and the length of the study period (Primack, Higuchi & Miller-Rushing 2009; Higashino & Stefan 2014; Post, Steinman & Mann 2018). The similarity between the results reported here and those of earlier studies suggest that the model can reliably estimate phenological responses to specific environmental stimuli using first occurrence data. The model correctly identified the established relationship between the advancement of first flowering and the increase of the air temperature in the few months preceding flowering (Kai *et al.* 1993; Miller-Rushing *et al.* 2007; Wang *et al.* 2017). In addition, the model also identified which aspect of pre-season temperature had the greatest influence on the parameters of the first flowering time distribution. Quantification of the model's parameters permitted exploration of the mechanisms that might be driving the advancement of cherry tree first flowering in each latitudinal band. For example, in the high latitudinal band, earlier fulfilment of the forcing requirement likely explained the relationship between the proportional rate of first flowering and the change in late winter/early spring temperatures. On the other hand, the faster accumulation of the chilling requirement likely explained the relationship between the temporal concentration and mid-winter temperatures. The combination of these temperature dependent processes are predicted to be driving the advancement of first flowering at higher latitudes. The effect of urban warming was also expected to have a strong influence on cherry tree first flowering phenology (Aono 1997; Ohashi *et al.* 2012). The response of cherry trees to different rates of warming in urban, rural and coastal locations adequately explained the general widening of the first flowering distribution described for all three latitudinal bands. This chapter demonstrated that the model

could be used to detect phenological trends using first occurrence data across an environmental gradient provided a large sample of observation sites is available. However, it also demonstrated that in order to identify meaningful relationships for all of the parameters in the model careful consideration should be given to defining the research question more precisely and selecting the appropriate sampling area to address the question.

The ability of the model to produce a reliable fit to phenological data was found to be dependent on the number of data points in a sample and the modality of the distribution. In Chapter 5, it was necessary to pool monthly abundance data from the Continuous Plankton Recorder (CPR) survey over ten-year periods to provide the model with enough data points to achieve a reliable fit. This was due to the low abundance observed in many species and samples. The CPR survey takes steps to standardise its sampling methodology (Warner & Hays 1994; Batten *et al.* 2003; Richardson *et al.* 2006a), however, the monthly sampling, shallow depth, and use of transects over a large geographic area inevitably results in the inconsistent sampling of some species. Although it was not possible to quantify the annual distribution of abundance of plankton at a lower taxonomic level, pooling the data together over ten-year periods likely provided a more accurate assessment of phenological change due to the smoothing of year to year variation in abundance, and the probable existence of unknown and varying time lags in the response of individual species to changing temperatures. The importance of sample size for the production of an accurate and therefore reliable model fit is also evident in Chapter 4. Less reliable model fits, as evidenced by larger standard errors of the parameter estimates, occurred in treatments

with fewer germinated seeds. These examples show that for the model to provide a detailed description of a phenology, i.e. to characterise the start, duration and overall shape of the phenological time distribution, a relatively large number of observations is required.

The modality of the distribution must also be considered when attempting to fit the model as it was designed to quantify monotonically increasing phenomena. Exploration of datasets during the early stages of this research showed that the model was unable to quantify the phenologies of organisms with complex life cycles such as aphids (which may have more than one overlapping cohort in good years) or pulsed events such as the staggered arrival of migrants following adverse weather conditions. Despite the model's applicability being limited to the quantification of unimodal phenologies, this research has established that the model can quantify phenologies at different scales of observation, i.e. behaviour at the individual, population, and ecosystem level, which makes it a useful tool for the analysis of phenological change.

The signal or “fingerprint” of climate change on phenology can be seen clearly in Chapters 5 & 6. Consistent temperature-related phenological shifts (later pre-1980s and earlier post-1980s) were observed in organisms as different as North Sea plankton and Japanese cherry trees. The model can be confidently used to describe historical shifts in phenology in response to changing climatic conditions. It could also be used to predict possible change in phenological distributions under future temperature scenarios. This extrapolation would have to proceed with caution and with a better understanding of the underlying biological processes being affected. This is because it is likely that the disruption of biological processes may have consequences beyond the simple seasonal

advance through the modification of the model's parameters. Although it is everybody's hope not to witness catastrophic effects of global climate change, these cannot be discounted.

Finally, the generality of the model permits its application to a wide variety of phenological events, including investigations of reproduction and development (e.g., pollination, gestation, egg-laying, egg-hatching, germination, cohort age distribution), seasonal population dynamics (of leaves, flowers, whole organisms), species interactions (trophic mismatch, predator-prey dynamics, competition, pest outbreaks), migration and dispersal (in relation to cues and invasion dynamics), and mortality in response to environmental challenge (climate change, ecotoxicology). This dissertation has only begun the investigation of the scope and significance of the model.

8 References

Abu-Asab, M., Peterson, P., Shetler, S. & Orli, S. (2001) Earlier plant flowering in spring as a response to global warming in the Washington, DC, area. *Biodiversity and Conservation,* **10,** 597-612.

Albano, V. (2000) The population structure of *Puya hamata*, a basal rosette species in the Andean paramo of the Northern Ecuador. BSc, Plymouth University.

Alexander, J.M., Chalmandrier, L., Lenoir, J., Burgess, T.I., Essl, F., Haider, S., Kueffer, C., McDougall, K., Milbau, A., Nuñez, M.A., Pauchard, A., Rabitsch, W., Rew, L.J., Sanders, N.J. & Pellissier, L. (2018) Lags in the response of mountain plant communities to climate change. *Global Change Biology,* **24,** 563-579.

Allen, J.M., Terres, M.A., Katsuki, T., Iwamoto, K., Kobori, H., Higuchi, H., Primack, R.B., Wilson, A.M., Gelfand, A. & Silander Jr, J.A. (2014) Modeling daily flowering probabilities: expected impact of climate change on Japanese cherry phenology. *Global Change Biology,* **20,** 1251-1263.

Anderson, E.P., Marengo, J., Villalba, R., Halloy, S., Young, B., Cordero, D., Gast, F., Jaimes, E. & Ruiz, D. (2011) Consequences of climate change for ecosystems and ecosystem services in the tropical Andes. *Climate Change and Biodiversity in the Tropical Andes* (ed. S.K. Herzog, Martínez, R., Jørgensen,P.M., Tiessen, H.). Inter-American Institute for Global Change Research and Scientific Committee on Problems of the Environment, San Jose dos Campos and Paris.

Aono, Y. (1997) Assessment of urban warming using plant phenology. *Proceedings of International Symposium on Monitoring and Management of Urban Heat Island*, pp. 111-123. Keio University, Fujisawa, Japan.

Aono, Y. & Kazui, K. (2008) Phenological data series of cherry tree flowering in Kyoto, Japan, and its application to reconstruction of springtime temperatures since the 9th century. *International Journal of Climatology,* **28,** 905-914.

Augspurger, C.K. (1985) Demography and life history variation of *Puya dasylirioides*, a long-lived rosette in tropical subalpine bogs. *Oikos,* **45,** 341–352.

Badeck, F.-W., Bondeau, A., Böttcher, K., Doktor, D., Lucht, W., Schaber, J. & Sitch, S. (2004) Responses of spring phenology to climate change. *New Phytologist,* **162,** 295-309.

Balslev, H. & Luteyn, J.L. (1992) *Páramo: An Andean Ecosystem Under Human Influence*. Academic Press, London.

Baskin, C.C. & Baskin, J.M. (1988) Germination ecophysiology of herbaceous plant species in a temperate region. *American Journal of Botany,* **75,** 286-305.

Baskin, C.C. & Baskin, J.M. (2014) *Seeds: Ecology, Biogeography, and Evolution of Dormancy and Germination,* 2nd Edition edn. Academic Press, San Diego.

Basler, D. & Körner, C. (2012) Photoperiod sensitivity of bud burst in 14 temperate forest tree species. *Agricultural and Forest Meteorology,* **165,** 73-81.

Batten, S.D., Clark, R., Flinkman, J., Hays, G., John, E., John, A.W.G., Jonas, T., Lindley, J.A., Stevens, D.P. & Walne, A. (2003) CPR sampling: the technical background, materials and methods, consistency and comparability. *Progress in Oceanography,* **58,** 193-215.

Baty, F., Ritz, C., Charles, S., Brutsche, M., Flandrois, J.-P. & Delignette-Muller, M.-L. (2015) A toolbox for nonlinear regression in R: the package nlstools. *Journal of Statistical Software,* **66,** 1-21.

Beard, K.H., Kelsey, K.C., Leffler, A.J. & Welker, J.M. (2019) The missing angle: Ecosystem consequences of phenological mismatch. *Trends in Ecology & Evolution,* **34,** 885-888.

Beaugrand, G. (2004) The North Sea regime shift: Evidence, causes, mechanisms and consequences. *Progress in Oceanography,* **60,** 245-262.

Beaugrand, G., Conversi, A., Chiba, S., Edwards, M., Fonda-Umani, S., Greene, C., Mantua, N., Otto, S.A., Reid, P.C., Stachura, M.M., Stemmann, L. & Sugisaki, H. (2015) Synchronous marine pelagic regime shifts in the Northern Hemisphere. *Philosophical Transactions of the Royal Society B: Biological Sciences,* **370,** 20130272.

Beaugrand, G. & Ibanez, F. (2004) Monitoring marine plankton ecosystems. II: Long-term changes in North Sea calanoid copepods in relation to hydro-climatic variability. *Marine Ecology Progress Series,* **284,** 35-47.

Beaugrand, G., Ibañez, F. & Lindley, J.A. (2003) An overview of statistical methods applied to CPR data. *Progress in Oceanography,* **58,** 235-262.

Benzing, D.H. (2000) *Bromeliaceae: Profile of an Adaptive Radiation*. Cambridge University Press, Cambridge.

Berry, G.J., Cawood, R.J. & Flood, R.G. (1988) Curve fitting of germination data using the Richards function. *Plant Cell and Environment,* **11,** 183-188.

Bewley, J.D. & Black, M. (1982) *Physiology and Biochemistry of Seeds in Relation to Germination,* 1 edn. Springer-Verlag Berlin Heidelberg.

Birch, C.P.D. (1999) A new generalized logistic sigmoid growth equation compared with the Richards growth equation. *Annals of Botany,* **83,** 713-723.

Bradbeer, J.W. (1988) *Seed Dormancy and Germination,* 1 edn. Blackie and Son Ltd, London & Glasgow.

Bradley, R.S., Vuille, M., Diaz, H.F. & Vergara, W. (2006) Threats to water supplies in the tropical Andes. *Science,* **312,** 1755-1756.

Brown, R. & Mayer, D. (1988) Representing cumulative germination. 2. The use of the Weibull function and other empirically derived curves. *Annals of Botany,* **61,** 127-138.

Buytaert, W., Cuesta-Camacho, F. & Tobón, C. (2011) Potential impacts of climate change on the environmental services of humid tropical alpine regions. *Global Ecology and Biogeography,* **20,** 19-33.

Buytaert, W., Vuille, M., Dewulf, A., Urrutia, R., Karmalkar, A. & Célleri, R. (2010) Uncertainties in climate change projections and regional downscaling in the tropical Andes: implications for water resources management. *Hydrology and Earth System Science,* **14,** 1247-1258.

Cameron, C.A. & Windmeijer, F.A.G. (1997) An R-squared measure of goodness of fit for some common nonlinear regression models. *Journal of Econometrics,* **77**.

Camill, P. (2010) Global Change. *Nature Education Knowledge,* **3,** 49.

CaraDonna, P.J., Iler, A.M. & Inouye, D.W. (2014) Shifts in flowering phenology reshape a subalpine plant community. *Proceedings of the National Academy of Sciences,* **111,** 4916-4921.

Carter, S.K., Saenz, D. & Rudolf, V.H.W. (2018) Shifts in phenological distributions reshape interaction potential in natural communities. *Ecology Letters,* **21,** 1143-1151.

Castro-Arellano, I., Lacher Jr, T.E., Willig, M.R. & Rangel, T.F. (2010) Assessment of assemblage-wide temporal niche segregation using null models. *Methods in Ecology and Evolution,* **1,** 311-318.

Cavieres, L.A., Badano, E.I., Sierra-Almeida, A. & Molina-Montenegro, M.A. (2007) Microclimatic modifications of cushion plants and their consequences for seedling survival of native and non-native herbaceous species in the high Andes of central Chile. *Arctic, Antarctic, and Alpine Research,* **39,** 229-236.

Cheng, W., Li, Z. & Yan, L. (2021) Uniforming spring phenology under non-uniform climate warming across latitude in China. *Science of The Total Environment,* **762,** 143177.

Chiba, S., Batten, S., Sasaoka, K., Sasai, Y. & Sugisaki, H. (2012) Influence of the Pacific Decadal Oscillation on phytoplankton phenology and community structure in the western North Pacific. *Geophysical Research Letters,* **39**.

Chiba, S., Tadokoro, K., Sugisaki, H. & Saino, T. (2006) Effects of decadal climate change on zooplankton over the last 50 years in the western subarctic North Pacific. *Global Change Biology,* **12,** 907-920.

Chivers, W.J., Edwards, M. & Hays, G.C. (2020) Phenological shuffling of major marine phytoplankton groups over the last six decades. *Diversity and Distributions,* **26,** 536-548.

Chivers, W.J., Walne, A.W. & Hays, G.C. (2017) Mismatch between marine plankton range movements and the velocity of climate change. *Nature Communications,* **8,** 14434.

Chmielewski, F.-M., Müller, A. & Bruns, E. (2004) Climate changes and trends in phenology of fruit trees and field crops in Germany, 1961–2000. *Agricultural and Forest Meteorology,* **121,** 69-78.

Chmielewski, F.-M. & Rötzer, T. (2001) Response of tree phenology to climate change across Europe. *Agricultural and Forest Meteorology,* **108,** 101-112.

Choquecahua Morales, N.L. (2013) Germinación de semillas de *Puya raimondii* Harms en condiciones de laboratorio. Universidad Nacional del Altiplano.

Clark, R.M. & Thompson, R. (2011) Sampling bias in the determination of first and last occurrences. *Plant Ecology & Diversity,* **4,** 201-211.

Cleland, E.E., Chuine, I., Menzel, A., Mooney, H.A. & Schwartz, M.D. (2007) Shifting plant phenology in response to global change. *Trends in Ecology & Evolution,* **22,** 357-365.

Cole, E.F. & Sheldon, B.C. (2017) The shifting phenological landscape: Within- and between-species variation in leaf emergence in a mixed-deciduous woodland. *Ecology and Evolution,* **7,** 1135-1147.

Cotton, P.A. (2003) Avian migration phenology and global climate change. *Proceedings of the National Academy of Sciences,* **100,** 12219-12222.

Crick, H.Q.P. & Sparks, T.H. (1999) Climate change related to egg-laying trends. *Nature,* **399,** 423-423.

Cushing, D. (1990) Plankton production and year-class strength in fish populations: an update of the match/mismatch hypothesis. *Advances in marine biology*, pp. 249-293. Elsevier.

Dahlberg, J. & Andersson, G. (2018) Changing seasonal variation in births by sociodemographic factors: a population-based register study. *Human Reproduction Open,* **2018,** hoy015.

Damgaard, C. & Weiner, J. (2008) Modeling the growth of individuals in crowded plant populations. *Journal of Plant Ecology,* **1,** 111-116.

Denny, E.G., Gerst, K.L., Miller-Rushing, A.J., Tierney, G.L., Crimmins, T.M., Enquist, C.A.F., Guertin, P., Rosemartin, A.H., Schwartz, M.D., Thomas, K.A. & Weltzin, J.F. (2014) Standardized phenology monitoring methods to track plant and animal activity for science and resource management applications. *International Journal of Biometeorology,* **58,** 591-601.

deYoung, B., Barange, M., Beaugrand, G., Harris, R., Perry, R.I., Scheffer, M. & Werner, F. (2008) Regime shifts in marine ecosystems: detection, prediction and management. *Trends in Ecology & Evolution,* **23,** 402-409.

Dickey, M.-H., Gauthier, G. & Cadieux, M.-C. (2008) Climatic effects on the breeding phenology and reproductive success of an arctic-nesting goose species. *Global Change Biology,* **14,** 1973-1985.

Doi, H. & Katano, I. (2008) Phenological timings of leaf budburst with climate change in Japan. *Agricultural and Forest Meteorology,* **148,** 512-516.

Durant, J.M., Hjermann, D.Ø., Ottersen, G. & Stenseth, N.C. (2007) Climate and the match or mismatch between predator requirements and resource availability. *Climate Research,* **33,** 271-283.

Dvorský, M., Macek, M., Kopecký, M., Wild, J. & Doležal, J. (2017) Niche asymmetry of vascular plants increases with elevation. *Journal of Biogeography,* **44,** 1418-1425.

Edwards, M., Bresnan, E., Cook, K., Heath, M., Helaouet, P., Lynam, C., Raine, R. & Widdicombe, C. (2013) Impacts of climate change on plankton. *MCCIP Science Review,* **2013,** 98-112.

Edwards, M. & Richardson, A.J. (2004) Impact of climate change on marine pelagic phenology and trophic mismatch. *Nature,* **430,** 881.

Ellis, R.H., Hong, T.D. & Roberts, E.H. (1985) *Handbook of Seed Technology for Genebanks. Volume I. Principles and Methodology*. International Board for Plant Genetic Resources. Handbooks for Genebanks, No. 2, Rome.

Elloumi, O., Ghrab, M., Kessentini, H. & Ben Mimoun, M. (2013) Chilling accumulation effects on performance of pistachio trees cv. Mateur in dry and warm area climate. *Scientia Horticulturae,* **159,** 80-87.

Elzhov, T.V., Mullen, K.M., Spiess, A.-N. & Bolker, B. (2016) Minpack.lm: R Interface to the Levenberg-Marquardt Nonlinear Least-Squares Algorithm Found in Minpack, Plus Support for Bounds.

Emery, S.E. & Mills, N.J. (2018) Sources of Variation in the Adult Flight of Walnut Husk Fly (Diptera: Tephritidae): A Phenology Model for California Walnut Orchards. *Environmental Entomology,* **48,** 234-244.

Estrella, N., Sparks, T.H. & Menzel, A. (2007) Trends and temperature response in the phenology of crops in Germany. *Global Change Biology,* **13,** 1737-1747.

Fenner, M. (1991) The effects of the parent environment on seed germinability. *Seed Science Research,* **1,** 75-84.

Fenner, M. & Thompson, K. (2005) *The Ecology of Seeds*. Cambridge University Press, Cambridge.

Fernández-Pascual, E., Mattana, E. & Pritchard, H.W. (2019) Seeds of future past: climate change and the thermal memory of plant reproductive traits. *Biological Reviews,* **94,** 439-456.

Fitter, A.H. & Fitter, R.S.R. (2002) Rapid changes in flowering time in British plants. *Science,* **296,** 1689-1691.

Flantua, S.G.A., O'Dea, A., Onstein, R.E., Giraldo, C. & Hooghiemstra, H. (2019) The flickering connectivity system of the north Andean páramos. *Journal of Biogeography,* **46,** 1808-1825.

Fleming, T.H. & Partridge, B.L. (1984) On the analysis of phenological overlap. *Oecologia,* **62,** 344-350.

Flynn, D. & Wolkovich, E. (2018) Temperature and photoperiod drive spring phenology across all species in a temperate forest community. *New Phytologist,* **219,** 1353-1362.

Forbis, T.A. (2003) Seedling demography in an alpine ecosystem. *American Journal of Botany,* **90,** 1197-1206.

Forcella, F., Benech Arnold, R.L., Sanchez, R. & Ghersa, C.M. (2000) Modeling seedling emergence. *Field Crops Research,* **67,** 123-139.

Forrest, J. & Miller-Rushing, A.J. (2010) Toward a synthetic understanding of the role of phenology in ecology and evolution. *Philosophical Transactions of the Royal Society B-Biological Sciences,* **365,** 3101-3112.

Forrest, J.R.K. & Thomson, J.D. (2011) An examination of synchrony between insect emergence and flowering in Rocky Mountain meadows. *Ecological Monographs,* **81,** 469-491.

Franco, M. (2018) The time distribution of biological phenomena – illustrated with the London marathon. *PeerJ Preprints 6:e27175v1*.

Franco, M., Ramsay, P. & Steer, N. (2019) nlstimedist: Non-linear model fitting of time distribution of biological phenomena. R package version 1.1.4. https://CRAN.R-project.org/package=nlstimedist.

Frei, E.S., Scheepens, J. & Stöcklin, J. (2012) Dispersal and microsite limitation of a rare alpine plant. *Plant ecology,* **213,** 395-406.

Frenken, T., Velthuis, M., de Senerpont Domis, L.N., Stephan, S., Aben, R., Kosten, S., van Donk, E. & Van de Waal, D.B. (2016) Warming accelerates termination of a phytoplankton spring bloom by fungal parasites. *Global Change Biology,* **22,** 299-309.

Fu, Y.H., Piao, S., Delpierre, N., Hao, F., Hänninen, H., Liu, Y., Sun, W., Janssens, I.A. & Campioli, M. (2018) Larger temperature response of autumn leaf senescence than spring leaf-out phenology. *Global Change Biology,* **24,** 2159-2168.

Fuller, M.P. & Fuller, F.M. (1995) Plant tissue culture using Brassico seedlings. *Journal of Biological Education,* **29,** 53-59.

Gabriel y Galán, J.M., Prada, C., Martínez-Calvo, C. & R., L.-B. (2015) A Gompertz regression model for fern spores germination. *Anales del Jardín Botánico de Madrid,* **72,** 1-8.

García-Meneses, P.M. (2012) Landscape-scale population dynamics: field observations and modelling of *Puya hamata*, a flagship plant from the Andes. PhD, Plymouth University.

Garcia-Meneses, P.M. & Ramsay, P.M. (2012) Pollinator response to within-patch spatial context determines reproductive output of a giant rosette plant. *Basic and Applied Ecology,* **13,** 516-523.

Garcia-Meneses, P.M. & Ramsay, P.M. (2014) Puya hamata demography as an indicator of recent fire history in the páramo of El Ángel amd Volcán Chiles, Ecuador-Colombia. *Caldasia,* **36,** 53-69.

García-Camacho, R., Iriondo, J.M. & Escudero, A. (2010) Seedling dynamics at elevation limits: complex interactions beyond seed and microsite limitations. *American Journal of Botany,* **97,** 1791-1797.

Garonna, I., de Jong, R., Stöckli, R., Schmid, B., Schenkel, D., Schimel, D. & Schaepman, M.E. (2018) Shifting relative importance of climatic constraints on land surface phenology. *Environmental Research Letters,* **13,** 024025.

Gavin, H.P. (2013) The Levenberg-Marquardt method for nonlinear least squares curve-fitting problems. *Department of Civil and Environmental Engineering, Duke University***,** 1-19.

Ge, Q., Wang, H., Zheng, J., This, R. & Dai, J. (2014) A 170 year spring phenology index of plants in eastern China. *Journal of Geophysical Research: Biogeosciences,* **119,** 301-311.

Gehrke, B. & Linder, H.P. (2009) The scramble for Africa: pan-temperate elements on the African high mountains. *Proceedings of the Royal Society B: Biological Sciences,* **276,** 2657-2665.

Goldstein, G., Meinzer, F.C. & Rada, F. (1994) Environmental biology of a tropical treeline species, Polylepis sericea. *Tropical Alpine Environments: Plant Form and Function* (eds A.P. Smith, F.C. Meinzer & P.W. Rundel), pp. 129-150. Cambridge University Press, Cambridge.

Gordo, O. (2007) Why are bird migration dates shifting? A review of weather and climate effects on avian migratory phenology. *Climate Research,* **35,** 37-58.

Gordo, O. & Sanz, J.J. (2006) Climate change and bird phenology: a long-term study in the Iberian Peninsula. *Global Change Biology,* **12,** 1993-2004.

Grabherr, G., Gottfried, M. & Pauli, H. (2010) Climate change impacts in alpine environments. *Geography Compass,* **4,** 1133-1153.

Grime, J.P. (2002) *Plant Strategies, Vegetation Processes, and Ecosystem Properties*. John Wiley & Sons, New York.

Grubb, P.J. (1977) The maintenance of species-richness in plant communities: The importance of the regeneration niche. *Biological Reviews,* **52,** 107-145.

Guo, L., Dai, J., Wang, M., Xu, J. & Luedeling, E. (2015) Responses of spring phenology in temperate zone trees to climate warming: A case study of apricot flowering in China. *Agricultural and Forest Meteorology,* **201,** 1-7.

Hays, G.C., Richardson, A.J. & Robinson, C. (2005) Climate change and marine plankton. *Trends in Ecology & Evolution,* **20,** 337-344.

Hedberg, O. (1969) Evolution and speciation in a tropical high mountain flora. *Biological Journal of the Linnean Society,* **1,** 135-148.

Higashino, M. & Stefan, H.G. (2014) Hydro-climatic change in Japan (1906-2005): Impacts of global warming and urbanization. *Air, Soil and Water Research,* **7,** 19-34.

Hills, P.N., Van Staden, J. & Thomas, T.H. (2003) Thermoinhibition of seed germination. *South African Journal of Botany,* **69,** 455-461.

Hinder, S.L., Hays, G.C., Edwards, M., Roberts, E.C., Walne, A.W. & Gravenor, M.B. (2012) Changes in marine dinoflagellate and diatom abundance under climate change. *Nature Climate Change,* **2,** 271-275.

Hjerne, O., Hajdu, S., Larsson, U., Downing, A.S. & Winder, M. (2019) Climate driven changes in timing, composition and magnitude of the Baltic Sea phytoplankton spring bloom. *Frontiers in Marine Science,* **6**.

Hornung-Leoni, C. & Sosa, V. (2005) Morphological variation in Puya (Bromeliaceae): an allometric study. *Plant Systematics and Evolution,* **256,** 35-53.

Hornung-Leoni, C.T., Gonzalez-Gomez, P.L. & Troncoso, A.J. (2013) Morphology, nectar characteristics and avian pollinators in five Andean Puya species (Bromeliaceae). *Acta Oecologica-International Journal of Ecology,* **51,** 54-61.

Hornung-Leoni, C.T., Sosa, V., Simpson, J. & Gil, K. (2013) Genetic variation in the emblematic Puya raimondii (Bromeliaceae) from Huascaran National Park, Peru. *Crop Breeding and Applied Biotechnology,* **13,** 67-74.

Huang, Z., Footitt, S., Tang, A. & Finch-Savage, W.E. (2018) Predicted global warming scenarios impact on the mother plant to alter seed dormancy and germination behaviour in Arabidopsis. *Plant, Cell & Environment,* **41,** 187-197.

Innan, H., Terauchi, R., Miyashita, N.T. & Tsunewaki, K. (1995) DNA fingerprinting study on the intraspecific variation and the origin of Prunus yedoensis (Someiyoshino). *Jpn J Genet,* **70,** 185-196.

IPCC (2014) Climate Change 2014: Synthesis Report, Contribution of Working Groups I, II and III to the Fifth Assessment Report of the Intergovernmental Panel on Climate Change (eds Core Writing Team, R.K. Pachauri & L.A. Meyer), pp. 151 pp. IPCC, Geneva, Switzerland.

IPCC (2021) Summary for Policymakers. *Climate Change 2021: The Physical Science Basis. Contribution of Working Group I to the Sixth Assessment Report of the Intergovernmental Panel on Climate Change* (eds V. Masson-Delmotte, P. Zhai, A. Pirani, S.L. Connors, C. Péan, S. Berger, N. Caud, Y. Chen, L. Goldfarb, M.I. Gomis, M. Huang, K. Leitzell, E. Lonnoy, J.B.R. Matthews, T.K. Maycock, T. Waterfield, O. Yelekçi, R. Yu & B. Zhou). Cambridge University Press. In Press.

Jabaily, R.S. & Sytsma, K.J. (2010) Phylogenetics of Puya (Bromeliaceae): placement, major lineages, and evolution of Chilean species. *American Journal of Botany,* **97,** 337-356.

Jabaily, R.S. & Sytsma, K.J. (2013) Historical biogeography and life-history evolution of Andean Puya (Bromeliaceae). *Botanical Journal of the Linnean Society,* **171,** 201-224.

Japanese Meteorological Agency (1988) Phenological observation in Japan. *Technical Report of the Japanese Meteorological Agency,* **No. 110,** 233 (in Japanese).

Ji, R., Edwards, M., Mackas, D.L., Runge, J.A. & Thomas, A.C. (2010) Marine plankton phenology and life history in a changing climate: current research and future directions. *Journal of Plankton Research,* **32,** 1355-1368.

Jochner, S., Sparks, T.H., Laube, J. & Menzel, A. (2016) Can we detect a nonlinear response to temperature in European plant phenology? *International Journal of Biometeorology,* **60,** 1551-1561.

Johns, D. & Reid, P. (2001) An overview of plankton ecology in the North Sea.

Kai, K., Kainuma, M., Murakoshi, N. & Omasa, K. (1993) Potential effects on the phenological observation of plants by global warming in Japan. *Journal of Agricultural Meteorology,* **48,** 771-774.

Keppel, G. (1991) *Design and Analysis: A Researcher's Handbook,* 3rd ed. edn. Prentice-Hall, Inc.

Kigel, J. (1995) Seed germination in arid and semiarid regions. *Seed Development and Germination* (eds J. Kigel & G. Galili), pp. 645-699. Marcel Dekker, New York.

Kirby, R.R., Beaugrand, G., Lindley, J.A., Richardson, A.J., Edwards, M. & Reid, P.C. (2007) Climate effects and benthic–pelagic coupling in the North Sea. *Marine Ecology Progress Series,* **330,** 31-38.

Klimeš, L. & Doležal, J. (2010) An experimental assessment of the upper elevational limit of flowering plants in the western Himalayas. *Ecography,* **33,** 590-596.

Knox, E.B. & Palmer, J.D. (1998) Chloroplast DNA evidence on the origin and radiation of the giant lobelias in eastern Africa. *Systematic Botany***,** 109-149.

Körner, C. (2003) *Alpine Plant Life: Functional Plant Ecology of High Mountain Ecosystems,* 2nd edn. Springer-Verlag, Berlin.

Körner, C. & Paulsen, J. (2004) A world-wide study of high altitude treeline temperatures. *Journal of Biogeography,* **31,** 713-732.

Kozlowski, T.T. (1972) *Seed Biology: Germination, Control, Metabolism and Pathology*. Academic Press, New York.

Kroiss, S.J. & HilleRisLambers, J. (2015) Recruitment limitation of long-lived conifers: implications for climate change responses. *Ecology,* **96,** 1286-1297.

Kudo, G. & Ida, T.Y. (2013) Early onset of spring increases the phenological mismatch between plants and pollinators. *Ecology,* **94,** 2311-2320.

Kvålseth, T.O. (1985) Cautionary Note about R2. *The American Statistician,* **39,** 279-285.

Laegaard, S. (1992) Influence of fire in the grass páramo vegetation of Ecuador. *Páramo: An Andean Ecosystem under Human Influence* (eds H. Balslev & J.L. Luteyn), pp. 151–170. Academic Press, London.

Lam, D.A. & Miron, J.A. (1991) Seasonality of births in human populations. *Soc Biol,* **38,** 51-78.

Lam, D.A. & Miron, J.A. (1994) Global patterns of seasonal variation in human fertility. *Annals of the New York Academy of Sciences,* **709,** 9-28.

Lambe, A. (2009) Puya raimondii. The IUCN Red List of Threatened Species.

Lambert, A.M., Miller-Rushing, A.J. & Inouye, D.W. (2010) Changes in snowmelt date and summer precipitation affect the flowering phenology of Erythronium grandiflorum (glacier lily; Liliaceae). *American Journal of Botany,* **97,** 1431-1437.

Larsen, T.H., Brehm, G., Navarrete, H., Franco, P., Gomez, H., Mena, J.L., Morales, V., Argollo, J., Blacutt, L. & Canhos, V. (2011) Range shifts and extinctions driven by climate change in the tropical Andes: synthesis and directions. *Climate Change and Biodiversity in the Tropical Andes* (ed. S.K. Herzog, Martínez, R., Jørgensen,P.M., Tiessen, H.), pp. 47-67. Inter-American Institute for Global Change Research and Scientific Committee on Problems of the Environment, San Jose dos Campos and Paris.

Li, W.K.W. & Glen Harrison, W. (2008) Propagation of an atmospheric climate signal to phytoplankton in a small marine basin. *Limnology and Oceanography,* **53,** 1734-1745.

Lieth, H. (1974) *Phenology and Seasonality Modeling*. Springer-Verlag, Berlin.

Lindley, J. & Batten, S. (2002) Long-term variability in the diversity of North Sea zooplankton. *Journal of the Marine Biological Association of the United Kingdom,* **82,** 31-40.

Linkosalo, T., Carter, T.R., Häkkinen, R. & Hari, P. (2000) Predicting spring phenology and frost damage risk of Betula spp. under climatic warming: a comparison of two models. *Tree Physiology,* **20,** 1175-1182.

Lourakis, M.I.A. (2005) A brief description of the Levenberg-Marquardt algorithm implemented by levmar. *Foundation of Research and Technology,* **4,** 1-6.

Lu, P., Yu, Q., Liu, J. & Lee, X. (2006) Advance of tree-flowering dates in response to urban climate change. *Agricultural and Forest Meteorology,* **138,** 120-131.

Luedeling, E. & Brown, P.H. (2011) A global analysis of the comparability of winter chill models for fruit and nut trees. *International Journal of Biometeorology,* **55,** 411-421.

Luedeling, E., Guo, L., Dai, J., Leslie, C. & Blanke, M.M. (2013) Differential responses of trees to temperature variation during the chilling and forcing phases. *Agricultural and Forest Meteorology,* **181,** 33-42.

Luedeling, E., Kunz, A. & Blanke, M.M. (2013) Identification of chilling and heat requirements of cherry trees—a statistical approach. *International Journal of Biometeorology,* **57,** 679-689.

Mackas, D.L., Goldblatt, R. & Lewis, A.G. (1998) Interdecadal variation in developmental timing of Neocalanus plumchrus populations at Ocean Station P in the subarctic North Pacific. *Canadian Journal of Fisheries and Aquatic Sciences,* **55,** 1878-1893.

Mackas, D.L., Greve, W., Edwards, M., Chiba, S., Tadokoro, K., Eloire, D., Mazzocchi, M.G., Batten, S., Richardson, A.J., Johnson, C., Head, E., Conversi, A. & Peluso, T. (2012) Changing zooplankton seasonality in a changing ocean: Comparing time series of zooplankton phenology. *Progress in Oceanography,* **97-100,** 31-62.

Madriñán, S., Cortés, A. & Richardson, J. (2013) Páramo is the world's fastest evolving and coolest biodiversity hotspot. *Frontiers in Genetics,* **4**.

Mann, K.H. & Lazier, J.R. (2013) *Dynamics of marine ecosystems: biological-physical interactions in the oceans*. John Wiley & Sons.

Marquardt, D.W. (1963) An algorithm for least-squares estimation of nonlinear parameters. *Journal of the Society for Industrial and Applied Mathematics,* **11,** 431-441.

Martinez-Bakker, M., Bakker, K.M., King, A.A. & Rohani, P. (2014) Human birth seasonality: latitudinal gradient and interplay with childhood disease dynamics. *Proceedings of the Royal Society B: Biological Sciences,* **281,** 20132438.

Masao, C.A. (2012) Evolutionary history, genetic diversity and conservation implications of selected afro-alpine taxa. Sokoine University of Agriculture.

Mayer, A.M. & Poljakoff-Mayber, A. (1982) *The Germination of Seeds,* 3rd Edition edn. Pergamon Press, New York.

Mayor, D.J., Sommer, U., Cook, K.B. & Viant, M.R. (2015) The metabolic response of marine copepods to environmental warming and ocean acidification in the absence of food. *Scientific Reports,* **5,** 13690.

Mbeau-Ache, C. & Franco, M. (2013) The time distribution of reproductive value measures the pace of life. *Journal of Ecology,* **101,** 1273-1280.

McQuatters-Gollop, A., Edwards, M., Helaouët, P., Johns, D.G., Owens, N.J.P., Raitsos, D.E., Schroeder, D., Skinner, J. & Stern, R.F. (2015) The Continuous Plankton Recorder survey: How can long-term phytoplankton datasets contribute to the assessment of Good Environmental Status? *Estuarine, Coastal and Shelf Science,* **162,** 88-97.

Meier, U. (2001) Growth stages of mono- and dicotyledonous plants: BBCH-Monograph. *Federal Biological Research Centre for Agriculture and Forestry*.

Melaas, E.K., Sulla-Menashe, D. & Friedl, M.A. (2018) Multidecadal changes and interannual variation in springtime phenology of North American temperate and boreal deciduous forests. *Geophysical Research Letters,* **45,** 2679-2687.

Menzel, A. (2000) Trends in phenological phases in Europe between 1951 and 1996. *International Journal of Biometeorology,* **44,** 76-81.

Menzel, A., Sparks, T.H., Estrella, N., Koch, E., Aasa, A., Ahas, R., Alm-Kübler, K., Bissolli, P., Braslavská, O.g., Briede, A., Chmielewski, F.M., Crepinsek, Z., Curnel, Y., Dahl, Å., Defila, C., Donnelly, A., Filella, Y., Jatczak, K., Måge, F., Mestre, A., Nordli, Ø., Peñuelas, J., Pirinen, P., Remišová, V., Scheifinger, H., Striz, M., Susnik, A., Van Vliet, A.J.H., Wielgolaski, F.-E., Zach, S. & Zust, A. (2006) European phenological response to climate change matches the warming pattern. *Global Change Biology,* **12,** 1969-1976.

Menzel, A., Yuan, Y., Matiu, M., Sparks, T., Scheifinger, H., Gehrig, R. & Estrella, N. (2020) Climate change fingerprints in recent European plant phenology. *Global Change Biology,* **26,** 2599-2612.

Miller-Rushing, A.J., Høye, T.T., Inouye, D.W. & Post, E. (2010) The effects of phenological mismatches on demography. *Philosophical Transactions of the Royal Society B: Biological Sciences,* **365,** 3177-3186.

Miller-Rushing, A.J., Katsuki, T., Primack, R.B., Ishii, Y., Lee, S.D. & Higuchi, H. (2007) Impact of global warming on a group of related species and their hybrids: cherry tree (Rosaceae) flowering at Mt. Takao, Japan. *American Journal of Botany,* **94,** 1470-1478.

Miller-Rushing, A.J. & Primack, R.B. (2008) Global warming and flowering times in Thoreau's Concord: A community perspective. *Ecology,* **89,** 332-341.

Miller, G.A. (1986) Pubescence, floral temperature and fecundity in species of *Puya* (Bromeliaceae) in the Ecuadorian Andes. *Oecologia,* **70,** 155–160.

Miller, G.A. & Silander, J.A., Jr. (1991) Control of the distribution of giant rosette species of *Puya* (Bromeliaceae) in the Ecuadorian páramos. *Biotropica,* **23,** 124–133.

Montesinos-Tubee, D.B., Cleef, A.M. & Sykora, K.V. (2015) The Puna vegetation of Moquegua, South Peru: Chasmophytes, grasslands and Puya raimondii stands. *Phytocoenologia,* **45,** 365-397.

Nakatsuji, T., Shiga, H., Takeuchi, H., Tsukamoto, Y., Gotou, E., Watanabe, Y., Sakurai, M., Fueki, N., Hikasa, Y. & Hayashi, T. (2021) Hokkaido Region. *The Soils of Japan*, pp. 135-184. Springer, Singapore.

Nevado, B., Wong, E.L.Y., Osborne, O.G. & Filatov, D.A. (2019) Adaptive evolution is common in rapid evolutionary radiations. *Current Biology,* **29,** 3081-3086.e3085.

O'Neill, M.E., Thomson, P.C., Jacobs, B.C., Brain, P., Butler, R.C., Turner, H. & Mitakda, B. (2004) Fitting and comparing seed germination models with a focus on the inverse normal distribution. *Australian & New Zealand Journal of Statistics,* **46,** 349-366.

Ohashi, Y., Kawakami, H., Shigeta, Y., Ikeda, H. & Yamamoto, N. (2012) The phenology of cherry blossom (*Prunus yedoensis* "Somei-yoshino") and the geographic features contributing to its flowering. *International Journal of Biometeorology,* **56,** 903-914.

Olejnik, S.F. & Algina, J. (1984) Parametric ANCOVA and the rank transform ANCOVA when the data are conditionally non-normal and heteroscedastic. *Journal of Educational Statistics,* **9,** 129-149.

Omoto, Y. & Aono, Y. (1989) Estimation of blooming date for *Prunus yedoensis* by means of kinetic method. *Journal of Agricultural Meteorology,* **45,** 25-31.

Orellana Macías, J.M., Bautista Sopelana, L.M., Merchán Elena, D., Causapé Valenzuela, J.A. & Alonso, J.C. (2020) Shifts in crane migration phenology associated with climate change in southwestern Europe. *Avian Conservation and Ecology,* **15,** 16.

Paine, C.E.T., Marthews, T.R., Vogt, D.R., Purves, D., Rees, M., Hector, A. & Turnbull, L.A. (2012) How to fit nonlinear plant growth models and calculate growth rates: an update for ecologists. *Methods in Ecology and Evolution,* **3,** 245-256.

Parmesan, C. (2007) Influences of species, latitudes and methodologies on estimates of phenological response to global warming. *Global Change Biology,* **13,** 1860-1872.

Parmesan, C. & Yohe, G. (2003) A globally coherent fingerprint of climate change impacts across natural systems. *Nature,* **421,** 37-42.

Peng, D., Chen, Z., Hu, X., Li, Z., Song, B. & Sun, H. (2017) Seed dormancy and germination characteristics of two Rheum species in the Himalaya-Hengduan Mountains. *Plant Diversity,* **39,** 180-186.

Peng, D., Sun, L., Pritchard, H.W., Yang, J., Sun, H. & Li, Z. (2019) Species distribution modelling and seed germination of four threatened snow lotus (Saussurea), and their implication for conservation. *Global Ecology and Conservation,* **17,** e00565.

Perez, F.L. (1987) Soil moisture and the upper altitudinal limit of giant paramo rosettes. *Journal of Biogeography,* **14,** 173-186.

Piao, S., Fang, J., Zhou, L., Ciais, P. & Zhu, B. (2006) Variations in satellite-derived phenology in China's temperate vegetation. *Global Change Biology,* **12,** 672-685.

Piao, S., Liu, Q., Chen, A., Janssens, I.A., Fu, Y., Dai, J., Liu, L., Lian, X., Shen, M. & Zhu, X. (2019) Plant phenology and global climate change: Current progresses and challenges. *Global Change Biology,* **25,** 1922-1940.

Pleasants, J.M. (1980) Competition for bumblebee pollinators in Rocky Mountain plant communities. *Ecology,* **61,** 1446-1459.

Poloczanska, E.S., Hoegh-Guldberg, O., Cheung, W., Pörtner, H.-O. & Burrows, M. (2014) Cross-chapter box on observed global responses of marine biogeography, abundance, and phenology to climate change. *Climate Change 2014: Impacts, Adaptation, and Vulnerability. Part A: Global and Sectoral Aspects. Contribution of Working Group II to the Fifth Assessment Report of the Intergovernmental Panel on Climate Change* (eds C.B. Field, V.R. Barros, D.J. Dokken, K.J. Mach, M.D. Mastrandrea, T.E. Bilir, M. Chatterjee, K.L. Ebi, Y.O. Estrada, R.C. Genova, B. Girma, E.S. Kissel, A.N. Levy, S. MacCracken, P.R. Mastrandrea & L.L. White), pp. 123-127. Cambridge University Press, Cambridge, UK and New York, USA.

Post, E., Steinman, B.A. & Mann, M.E. (2018) Acceleration of phenological advance and warming with latitude over the past century. *Scientific Reports,* **8,** 3927.

Prevéy, J., Vellend, M., Rüger, N., Hollister, R.D., Bjorkman, A.D., Myers-Smith, I.H., Elmendorf, S.C., Clark, K., Cooper, E.J., Elberling, B., Fosaa, A.M., Henry, G.H.R., Høye, T.T., Jónsdóttir, I.S., Klanderud, K., Lévesque, E., Mauritz, M., Molau, U., Natali, S.M., Oberbauer, S.F., Panchen, Z.A., Post, E., Rumpf, S.B., Schmidt, N.M., Schuur, E.A.G., Semenchuk, P.R., Troxler, T., Welker, J.M. & Rixen, C. (2017) Greater temperature sensitivity of plant phenology at colder sites: implications for convergence across northern latitudes. *Global Change Biology,* **23,** 2660-2671.

Primack, R.B., Higuchi, H. & Miller-Rushing, A.J. (2009) The impact of climate change on cherry trees and other species in Japan. *Biological Conservation,* **142,** 1943-1949.

Rada, F., García-Núñez, C. & Rangel, S. (2011) Microclimate and regeneration patterns of *Polylepis sericea* in a treeline forest of the Venezuelan Andes. *Ecotropicos,* **24,** 113-122.

Rafferty, N.E., Caradonna, P.J., Burkle, L.A., Iler, A.M. & Bronstein, J.L. (2013) Phenological overlap of interacting species in a changing climate: an assessment of available approaches. *Ecology and Evolution,* **3,** 3183-3193.

Ramsay, P. & Oxley, E. (1996) Fire temperatures and postfire plant community dynamics in Ecuadorian grass páramo. *Vegetatio,* **124,** 129-144.

Ramsay, P.M. (2001) Diurnal temperature variation in major growth forms of an Ecuadorian páramo plant community. *The Ecology of Volcán Chiles. High-Altitude Ecosystems on the Ecuador-Colombia Border* (ed. P.M. Ramsay). Pebble & Shell Publications, Plymouth.

Ranganathan, A. (2004) The levenberg-marquardt algorithm. *Tutoral on LM algorithm,* **11,** 101-110.

Ratkowsky, D. (1983) Nonlinear Regression Modeling: a Unified Practical Approach. Marcel Dekker, Inc., New York.

Rayner, N.A., Parker, D.E., Horton, E.B., Folland, C.K., Alexander, L.V., Rowell, D.P., Kent, E.C. & Kaplan, A. (2003) Global analyses of sea surface temperature, sea ice, and night marine air temperature since the late nineteenth century. *Journal of Geophysical Research: Atmospheres,* **108**.

Régnier, T., Gibb, F.M. & Wright, P.J. (2019) Understanding temperature effects on recruitment in the context of trophic mismatch. *Scientific Reports,* **9,** 15179.

Reid, P.C., Edwards, M., Beaugrand, G., Skogen, M. & Stevens, D. (2003) Periodic changes in the zooplankton of the North Sea during the twentieth century linked to oceanic inflow. *Fisheries Oceanography,* **12,** 260-269.

Renner, S.S. & Zohner, C.M. (2018) Climate change and phenological mismatch in trophic interactions among plants, insects, and vertebrates. *Annual Review of Ecology, Evolution, and Systematics,* **49,** 165-182.

Richards, F.J. (1959) A Flexible Growth Function for Empirical Use. *Journal of Experimental Botany,* **10,** 290-300.

Richardson, A., Walne, A., John, A., Jonas, T., Lindley, J., Sims, D., Stevens, D. & Witt, M. (2006a) Using continuous plankton recorder data. *Progress in Oceanography,* **68,** 27-74.

Richardson, A.D., Bailey, A.S., Denny, E.G., Martin, C.W. & O'Keefe, J. (2006b) Phenology of a northern hardwood forest canopy. *Global Change Biology,* **12,** 1174-1188.

Root, T.L., Price, J.T., Hall, K.R., Schneider, S.H., Rosenzweig, C. & Pounds, J.A. (2003) Fingerprints of global warming on wild animals and plants. *Nature,* **421,** 57-60.

Rötzer, T. & Chmielewski, F.-M. (2001) Phenological maps of Europe. *Climate Research,* **18,** 249-257.

Roy, D. & Sparks, T. (2000) Phenology of British butterflies and climate change. *Global Change Biology,* **6,** 407-416.

Ruckstuhl, A. (2010) Introduction to nonlinear regression. *IDP Institut fur Datenanalyse und Prozessdesign, Zurcher Hochschule fur Angewandte Wissenschaften*.

Ruiz, H.d. (1978) A propósito de la mayor de las bromeliaceas. *Boletín de la Sociedad Geográfica de Lima,* **97,** 35-41.

Salisbury, F.B. & Ross, C.W. (1992) *Plant Physiology, Hormones and Plant Regulators: Auxins and Gibberellins,* 4th Edition edn. Wadsworth Publishing, Belmont.

Sato, T. & Sasaki, T. (2011) Impact of historical deforestation and urbanization on regional climate in north Japan. *AGU Fall Meeting Abstracts*, pp. A23C-0180.

Saumweber, W.J. & Durbin, E.G. (2006) Estimating potential diapause duration in Calanus finmarchicus. *Deep Sea Research Part II: Topical Studies in Oceanography,* **53,** 2597-2617.

Schaefer, D. & Domroes, M. (2009) Recent climate change in Japan - spatial and temporal characteristics of trends of temperature. *Climate of the Past,* **5,** 13-19.

Scherrer, D. & Körner, C. (2011) Topographically controlled thermal-habitat differentiation buffers alpine plant diversity against climate warming. *Journal of Biogeography,* **38,** 406-416.

Schwartz, M.D. (2003) *Phenology: An Integrative Environmental Science,* 2 edn. Springer, Netherlands.

Schwartz, M.D., Ahas, R. & Aasa, A. (2006) Onset of spring starting earlier across the Northern Hemisphere. *Global Change Biology,* **12,** 343-351.

Scranton, K. & Amarasekare, P. (2017) Predicting phenological shifts in a changing climate. *Proceedings of the National Academy of Sciences,* **114,** 13212-13217.

Sedmak, R. & Scheer, L. (2015) Properties and prediction accuracy of a sigmoid function of time-determinate growth. *iForest - Biogeosciences and Forestry,* **8,** 631-637.

Sharples, J., Ross, O.N., Scott, B.E., Greenstreet, S.P.R. & Fraser, H. (2006) Inter-annual variability in the timing of stratification and the spring bloom in the North-western North Sea. *Continental Shelf Research,* **26,** 733-751.

Shen, M., Piao, S., Cong, N., Zhang, G. & Jassens, I.A. (2015) Precipitation impacts on vegetation spring phenology on the Tibetan Plateau. *Global Change Biology,* **21,** 3647-3656.

Shi, P., Chen, Z., Reddy, G.V.P., Hui, C., Huang, J. & Xiao, M. (2017) Timing of cherry tree blooming: Contrasting effects of rising winter low temperatures and early spring temperatures. *Agricultural and Forest Meteorology,* **240-241,** 78-89.

Sklenář, P., Dušková, E. & Balslev, H. (2011) Tropical and temperate: evolutionary history of páramo flora. *The Botanical Review,* **77,** 71-108.

Smith, L.B. & Downs, R.J. (1974) *Flora Neotropica, Volume 14: Pitcairnioideae (Bromeliaceae)*. Hafner Press, New York.

Sorensen, A. (2002) *The Making of Urban Japan: Cities and Planning from Edo to the Twenty First Century* 1st ed. edn. Routledge, London.

Sparks, T.H. & Tryjanowski, P. (2010) Regression and causality. *Phenological Research* (eds I. Hudson & M. Keatley), pp. 123-145. Springer, Dordrecht.

Spiess, A.-N. & Neumeyer, N. (2010) An evaluation of R^2 as an inadequate measure for nonlinear models in pharmacological and biochemical research: a Monte Carlo approach. *BMC pharmacology,* **10,** 6-6.

Squeo, F.A., Rada, F., Azocar, A. & Goldstein, G. (1991) Freezing tolerance and avoidance in high tropical Andean plants: Is it equally represented in species with different plant height? *Oecologia,* **86,** 378-382.

Steer, N.C., Ramsay, P.M. & Franco, M. (2019) nlstimedist: An R package for the biologically meaningful quantification of unimodal phenology distributions. *Methods in Ecology and Evolution,* **10,** 1934-1940.

Straile, D., Kerimoglu, O. & Peeters, F. (2015) Trophic mismatch requires seasonal heterogeneity of warming. *Ecology,* **96,** 2794-2805.

Stukel, T.A. (1988) Generalized logistic models. *Journal of the American Statistical Association,* **83,** 426-431.

Sun, S. & Frelich, L.E. (2011) Flowering phenology and height growth pattern are associated with maximum plant height, relative growth rate and stem tissue mass density in herbaceous grassland species. *Journal of Ecology,* **99,** 991-1000.

Tang, J., Körner, C., Muraoka, H., Piao, S., Shen, M., Thackeray, S.J. & Yang, X. (2016) Emerging opportunities and challenges in phenology: a review. *Ecosphere,* **7,** e01436.

Thackeray, S.J., Henrys, P.A., Hemming, D., Bell, J.R., Botham, M.S., Burthe, S., Helaouet, P., Johns, D.G., Jones, I.D., Leech, D.I., Mackay, E.B., Massimino, D., Atkinson, S., Bacon, P.J., Brereton, T.M., Carvalho, L., Clutton-Brock, T.H., Duck, C., Edwards, M., Elliott, J.M., Hall, S.J.G., Harrington, R., Pearce-Higgins, J.W., Høye, T.T., Kruuk, L.E.B., Pemberton, J.M., Sparks, T.H., Thompson, P.M., White, I., Winfield, I.J. & Wanless, S. (2016) Phenological sensitivity to climate across taxa and trophic levels. *Nature,* **535,** 241-245.

Thackeray, S.J., Sparks, T.H., Frederiksen, M., Burthe, S., Bacon, P.J., Bell, J.R., Botham, M.S., Brereton, T.M., Bright, P.W., Carvalho, L., Clutton-Brock, T., Dawson, A., Edwards, M., Elliott, J.M., Harrington, R., Johns, D., Jones, I.D., Jones, J.T., Leech, D.I., Roy, D.B., Scott, W.A., Smith, M., Smithers, R.J., Winfield, I.J. & Wanless, S. (2010) Trophic level asynchrony in rates of phenological change for marine, freshwater and terrestrial environments. *Global Change Biology,* **16,** 3304-3313.

Thompson, K. & Ceriani, R.M. (2003) No relationship between range size and germination niche width in the UK herbaceous flora. *Functional Ecology,* **17,** 335-339.

Thompson, P.A. (1970) Characterization of the germination response to temperature of species and ecotypes. *Nature,* **225,** 827-831.

Thornley, J.H. & Johnson, I.R. (1990) *Plant and crop modelling: a mathematical approach to plant and crop physiology*. Clarendon, Oxford.

Tinker, J., Howes, E., Wakelin, S., Menary, M., Kent, E. & Berry, D. (2020) The impacts of climate change on temperature (air and sea), relevant to the coastal and marine environment around the UK. *MCCIP Science Reviews,* **2020,** 1-3.

Totland, Ø. (1993) Pollination in alpine Norway: flowering phenology, insect visitors, and visitation rates in two plant communities. *Canadian Journal of Botany,* **71,** 1072-1079.

Tudela-Isanta, M., Fernández-Pascual, E., Wijayasinghe, M., Orsenigo, S., Rossi, G., Pritchard, H.W. & Mondoni, A. (2018a) Habitat-related seed germination traits in alpine habitats. *Ecology and Evolution,* **8,** 150-161.

Tudela-Isanta, M., Ladouceur, E., Wijayasinghe, M., Pritchard, H.W. & Mondoni, A. (2018b) The seed germination niche limits the distribution of some plant species in calcareous or siliceous alpine bedrocks. *Alpine Botany,* **128,** 83-95.

Urrutia, R. & Vuille, M. (2009) Climate change projections for the tropical Andes using a regional climate model: Temperature and precipitation simulations for the end of the 21st century. *Journal of Geophysical Research: Atmospheres,* **114**.

Vadillo, G., Suni, M. & Cano, A. (2004) Viabilidad y germinación de semillas de *Puya raimondii* Harms (Bromeliaceae). *Rev. peru. biol.,* **11,** 71–78

van der Hammen, T. (1974) The Pleistocene changes of vegetation and climate in tropical South America. *Journal of Biogeography,* **1,** 3-26.

Varadarajan, G.S. (1990) Patterns of geographic distribution and their implications on the phylogeny of Puya (Bromeliaceae). *Journal of the Arnold Arboretum,* **71,** 527-552.

Verma, M., Friedl, M.A., Finzi, A. & Phillips, N. (2016) Multi-criteria evaluation of the suitability of growth functions for modeling remotely sensed phenology. *Ecological Modelling,* **323,** 123-132.

Visser, M.E. & Gienapp, P. (2019) Evolutionary and demographic consequences of phenological mismatches. *Nature Ecology & Evolution,* **3,** 879-885.

Vuille, M., Francou, B., Wagnon, P., Juen, I., Kaser, G., Mark, B.G. & Bradley, R.S. (2008) Climate change and tropical Andean glaciers: Past, present and future. *Earth-Science Reviews,* **89,** 79-96.

Vuille, M., Franquist, E., Garreaud, R., Casimiro, W.S.L. & Cáceres, B. (2015) Impact of the global warming hiatus on Andean temperature. *Journal of Geophysical Research: Atmospheres,* **120,** 3745-3757.

Waite, B.A. (1978) *Puya raimondii*: Wonder of the Bolivian Andes. *Journal of the Bromeliad Society,* **28,** 200-208.

Walck, J.L., Hidayati, S.N., Dixon, K.W., Thompson, K. and Poschlod, P. (2011) Climate change and plant regeneration from seed. *Global Change Biology,* **17,** 2145-2161.

Walder, T. & Erschbamer, B. (2015) Temperature and drought drive differences in germination responses between congeneric species along altitudinal gradients. *Plant ecology,* **216,** 1297-1309.

Walther, G.-R., Post, E., Convey, P., Menzel, A., Parmesan, C., Beebee, T.J.C., Fromentin, J.-M., Hoegh-Guldberg, O. & Bairlein, F. (2002) Ecological responses to recent climate change. *Nature,* **416,** 389.

Wang, H., Ge, Q., Dai, J. & Tao, Z. (2015) Geographical pattern in first bloom variability and its relation to temperature sensitivity in the USA and China. *International Journal of Biometeorology,* **59,** 961-969.

Wang, L., Ning, Z., Wang, H. & Ge, Q. (2017) Impact of climate variability on flowering phenology and its implications for the schedule of blossom festivals. *Sustainability,* **9,** 1127.

Warner, A.J. & Hays, G.C. (1994) Sampling by the continuous plankton recorder survey. *Progress in Oceanography,* **34,** 237-256.

Wenden, B., Campoy, J.A., Lecourt, J., Ortega, G.L., Blanke, M., Radičević, S., Schüller, E., Spornberger, A., Christen, D., Magein, H., Giovannini, D., Campillo, C., Malchev, S., Peris, J.M., Meland, M., Stehr, R., Charlot, G. & Quero-García, J. (2016) A collection of European sweet cherry phenology data for assessing climate change. *Scientific data,* **3,** 1-10.

Wickham, H. (2009) *ggplot2: Elegant Graphics for Data Analysis*. Springer, New York.

Wilson, R.J., Banas, N.S., Heath, M.R. & Speirs, D.C. (2016) Projected impacts of 21st century climate change on diapause in Calanus finmarchicus. *Global Change Biology,* **22,** 3332-3340.

Wilson, R.J., Speirs, D.C. & Heath, M.R. (2015) On the surprising lack of differences between two congeneric calanoid copepod species, Calanus finmarchicus and C. helgolandicus. *Progress in Oceanography,* **134,** 413-431.

Winder, M., Berger, S.A., Lewandowska, A., Aberle, N., Lengfellner, K., Sommer, U. & Diehl, S. (2012) Spring phenological responses of marine and freshwater plankton to changing temperature and light conditions. *Marine Biology,* **159,** 2491-2501.

Winder, M. & Sommer, U. (2012) Phytoplankton response to a changing climate. *Hydrobiologia,* **698,** 5-16.

Winkler, D.E., Butz, R.J., Germino, M.J., Reinhardt, K. & Kueppers, L.M. (2018) Snowmelt timing regulates community composition, phenology, and physiological performance of alpine plants. *Frontiers in plant science,* **9**.

Wipf, S. (2010) Phenology, growth, and fecundity of eight subarctic tundra species in response to snowmelt manipulations. *Plant Ecology,* **207,** 53-66.

Wu, D., Zhao, X., Liang, S., Zhou, T., Huang, K., Tang, B. & Zhao, W. (2015) Time-lag effects of global vegetation responses to climate change. *Global Change Biology,* **21,** 3520-3531.

Xie, Y., Tilstone, G.H., Widdicombe, C., Woodward, E.M.S., Harris, C. & Barnes, M.K. (2015) Effect of increases in temperature and nutrients on phytoplankton community structure and photosynthesis in the western English Channel. *Marine Ecology Progress Series,* **519,** 61-73.

Yin, X.Y., Goudriaan, J., Lantinga, E.A., Vos, J. & Spiertz, H.J. (2003) A flexible sigmoid function of determinate growth. *Annals of Botany,* **91,** 361-371.

Young, B., Young, K.R. & Josse, C. (2011) Vulnerability of tropical Andean ecosystems to climate change. *Climate Change and Biodiversity in the Tropical Andes* (ed. S.K.

Herzog, Martínez, R., Jørgensen,P.M., Tiessen, H.), pp. 170-181. Inter-American Institute for Global Change Research and Scientific Committee on Problems of the Environment, San Jose dos Campos and Paris.

Yu, H., Luedeling, E. & Xu, J. (2010) Winter and spring warming result in delayed spring phenology on the Tibetan Plateau. *Proceedings of the National Academy of Sciences,* **107,** 22151-22156.

Zeide, B. (1993) Analysis of growth equations. *Forest Science,* **39,** 594-616.

Zhang, G., Zhang, Y., Dong, J. & Xiao, X. (2013) Green-up dates in the Tibetan Plateau have continuously advanced from 1982 to 2011. *Proceedings of the National Academy of Sciences,* **110,** 4309-4314.

Zhang, X., Friedl, M.A., Schaaf, C.B., Strahler, A.H., Hodges, J.C., Gao, F., Reed, B.C. & Huete, A. (2003) Monitoring vegetation phenology using MODIS. *Remote Sensing of Environment,* **84,** 471-475.

Zhao, S.-Y., Chen, L.-Y., Muchuku, J.K., Hu, G.-W. & Wang, Q.-F. (2016) Genetic adaptation of giant lobelias (*Lobelia aberdarica* and *Lobelia telekii*) to different altitudes in East African mountains. *Frontiers in plant science,* **7,** 488-488.

Zhou, Y.-Z. & Jia, G.-S. (2016) Precipitation as a control of vegetation phenology for temperate steppes in China. *Atmospheric and Oceanic Science Letters,* **9,** 162-168.

9 Appendices

Appendix A:

Table A1. Number of seeds germinated (N), percentage of germination (y_{max}) and germination time (days) at each temperature, estimated parameter values (with standard errors in parenthesis), "significance" of each parameter estimate (* P<0.05, ** p<0.01, *** p < 0.001), proportion of variance explained by the model (R^2) and statistical moments for each of the predicted distributions. Each species is presented separately.

Puya hamata

Temp. (°C)	N	y_{max} (%)	Germ. time (days)			*r* (s.e.)	Sig.	*c* (s.e.)	Sig.	*t* (s.e.)	Sig.	R^2	Mean	SD	Skew	Kurtosis	Entropy
			Start	End	Duration												
10.8	0	-	-	-	-	-	-	-	-	-	-	-	-	-	-	-	-
11.4	0	-	-	-	-	-	-	-	-	-	-	-	-	-	-	-	-
12.0	0	-	-	-	-	-	-	-	-	-	-	-	-	-	-	-	-
12.6	0	-	-	-	-	-	-	-	-	-	-	-	-	-	-	-	-

13.3	0	-	-	-	-	-	-	-	-	-	-	-	-	-	-	-	-
13.9	9	45.0	18	26	9	-	-	-	-	-	-	-	-	-	-	-	-
14.5	8	40.0	17	26	10	-	-	-	-	-	-	-	-	-	-	-	-
15.1	13	65.0	17	26	10	0.110 (0.043)	.	0.436 (0.126)	*	22.973 (1.955)	***	98.3	21.359	4.847	2.507	17.596	4.044
15.7	18	90.0	17	25	9	0.123 (0.076)		0.467 (0.204)	.	21.718 (2.932)	***	95.8	19.949	4.235	2.221	16.156	3.893
16.3	18	90.0	17	24	8	0.124 (0.027)	*	0.784 (0.184)	*	18.977 (0.646)	***	99.0	18.401	3.750	4.089	31.672	3.382
16.9	18	90.0	14	14	1	-	-	-	-	-	-	-	-	-	-	-	-
17.5	17	85.0	14	15	2	-	-	-	-	-	-	-	-	-	-	-	-
18.1	19	95.0	14	15	2	-	-	-	-	-	-	-	-	-	-	-	-
18.7	17	85.0	14	14	1	-	-	-	-	-	-	-	-	-	-	-	-
19.4	16	80.0	14	14	1	-	-	-	-	-	-	-	-	-	-	-	-
20.0	16	80.0	9	16	8	0.209 (0.015)	***	1.094 (0.086)	***	10.901 (0.162)	***	99.9	10.419	2.253	3.279	24.085	2.813
20.6	20	100.0	9	11	3	-	-	-	-	-	-	-	-	-	-	-	-
21.2	16	80.0	9	14	6	-	-	-	-	-	-	-	-	-	-	-	-
21.8	19	95.0	9	12	4	-	-	-	-	-	-	-	-	-	-	-	-
22.4	18	90.0	9	11	3	-	-	-	-	-	-	-	-	-	-	-	-
23.0	20	100.0	9	15	7	0.189 (0.036)	**	1.011 (0.224)	**	11.188 (0.474)	***	98.9	10.851	2.650	3.384	23.312	2.996
23.6	19	95.0	9	16	8	-	-	-	-	-	-	-	-	-	-	-	-
24.2	16	80.0	9	15	7	0.171 (0.019)	***	1.101 (0.229)	**	10.249 (0.286)	***	99.1	10.472	3.235	3.654	22.386	3.100

24.8	16	80.0	9	17	9	0.188 (0.034)	**	0.938 (0.302)	*	9.952 (0.497)	***	99.1	9.852	2.949	3.134	19.194	3.159
25.5	16	80.0	9	18	11	0.167 (0.013)	**	1.454 (0.412)	*	9.151 (0.147)	***	99.7	9.833	3.475	3.830	21.969	2.959
26.1	13	65.0	12	23	12	0.176 (0.125)		0.667 (0.180)	**	18.757 (1.849)	***	97.3	16.938	2.575	1.480	13.673	3.259
26.7	12	60.0	11	21	11	0.145 (0.061)	*	0.459 (0.128)	**	18.371 (1.925)	***	98.2	16.558	3.923	1.648	11.172	3.850
27.3	10	50.0	12	19	8	-	-	-	-	-	-	-	-	-	-	-	-
27.9	5	25.0	11	19	9	-	-	-	-	-	-	-	-	-	-	-	-
28.5	5	20.0	14	15	2	-	-	-	-	-	-	-	-	-	-	-	-
29.1	0	-	-	-	-	-	-	-	-	-	-	-	-	-	-	-	-
29.7	0	-	-	-	-	-	-	-	-	-	-	-	-	-	-	-	-
30.3	0	-	-	-	-	-	-	-	-	-	-	-	-	-	-	-	-
30.9	0	-	-	-	-	-	-	-	-	-	-	-	-	-	-	-	-
31.6	0	-	-	-	-	-	-	-	-	-	-	-	-	-	-	-	-

Puya clava-herculis

Temp. (°C)	N	y_{max} (%)	Germ. time (days)			*r* (s.e.)	Sig.	*c* (s.e.)	Sig.	*t* (s.e.)	Sig.	R^2	Mean	SD	Skew	Kurtosis	Entropy
			Start	End	Duration												
0.3	0	-	-	-	-	-	-	-	-	-	-	-	-	-	-	-	-
1.2	0	-	-	-	-	-	-	-	-	-	-	-	-	-	-	-	-
3.6	0	-	-	-	-	-	-	-	-	-	-	-	-	-	-	-	-

5.4	0	-	-	-	-	-	-	-	-	-	-	-	-	-	-	-	-
7.5	13	13.0	-	-	-	-	-	-	-	-	-	-	-	-	-	-	-
9.1	42	42.0	30	43	14	0.079 (0.040)	.	0.349 (0.103)	**	39.598 (3.031)	***	97.1	36.535	5.713	2.608	22.898	4.295
11.0	51	51.0	32	43	12	0.105 (0.012)	***	1.079 (0.088)	***	26.849 (0.221)	***	99.8	26.220	3.338	6.305	66.361	2.891
11.7	49	49.0	20	31	12	-	-	-	-	-	-	-	-	-	-	-	-
14.1	50	50.0	17	24	8	0.218 (0.155)		0.830 (0.173)	**	20.978 (1.459)	***	99.4	18.912	1.786	0.194	6.909	2.808
14.5	54	54.0	13	24	12	0.160 (0.038)	**	0.701 (0.108)	***	18.964 (0.705)	***	99.5	17.447	2.740	2.323	20.340	3.266
16.8	49	49.0	14	26	13	-	-	-	-	-	-	-	-	-	-	-	-
17.5	48	48.0	14	25	12	0.129 (0.019)	***	1.689 (0.440)	**	15.266 (0.268)	***	98.2	15.683	3.688	5.120	37.722	2.660
19.8	47	47.0	12	20	9	0.192 (0.029)	***	0.948 (0.119)	***	14.522 (0.366)	***	99.6	13.555	2.221	2.906	24.856	2.891
20.1	46	46.0	11	27	17	0.186 (0.039)	**	1.201 (0.184)	***	14.182 (0.383)	***	99.4	13.547	2.132	4.134	36.990	2.650
22.8	49	49.0	12	19	8	0.176 (0.065)	.	1.436 (0.452)	*	14.082 (0.598)	***	98.2	13.715	2.242	5.018	44.806	2.502
23.2	51	51.0	11	17	7	0.224 (0.111)		1.032 (0.255)	**	15.114 (0.949)	***	98.8	13.881	1.712	1.887	19.520	2.638
25.5	40	40.0	13	22	10	0.170 (0.030)	**	0.825 (0.082)	***	19.455 (0.440)	***	99.8	17.983	2.283	2.432	24.319	3.003
26.2	48	48.0	17	34	18	0.113 (0.041)	*	0.750 (0.266)	*	21.176 (1.123)	***	96.0	20.562	16.308	4.038	34.037	3.453

Puya raimondii

Temp. (°C)	N	y_{max} (%)	Germ. time (days)			*r* (s.e.)	Sig.	*c* (s.e.)	Sig.	*t* (s.e.)	Sig.	R^2	Mean	SD	Skew	Kurtosis	Entropy
			Start	End	Duration												

3.4	0	-	-	-	-	-	-	-	-	-	-	-	-	-	-	-	-	-
4.6	9	4.5	47	54	8	-	-	-	-	-	-	-	-	-	-	-	-	-
8.4	148	74.0	29	52	24	0.073 (0.005)	***	0.447 (0.025)	***	37.368 (0.345)	***	99.7	35.661	5.892	4.156	36.205	4.097
9.3	156	78.0	23	45	23	0.075 (0.003)	***	0.653 (0.032)	***	29.532 (0.158)	***	99.8	29.461	6.334	4.848	37.191	3.823
12.5	161	80.5	17	47	31	0.112 (0.008)	***	0.806 (0.062)	***	22.018 (0.230)	***	99.6	21.421	3.925	4.621	38.424	3.354
13.6	166	83.0	16	27	12	0.158 (0.018)	***	0.696 (0.050)	***	20.449 (0.339)	***	99.8	18.772	2.667	2.177	20.343	3.247
13.8	164	82.0	13	39	27	0.129 (0.004)	***	1.485 (0.083)	***	16.133 (0.071)	***	99.9	16.360	3.571	5.188	39.817	2.748
14.7	160	80.0	13	43	31	0.126 (0.006)	***	1.418 (0.117)	***	15.113 (0.104)	***	99.7	15.580	3.988	4.774	33.338	2.911
16.7	147	73.5	11	45	35	0.134 (0.003)	***	2.230 (0.108)	***	13.992 (0.037)	***	99.9	14.597	3.639	5.116	36.541	2.393
17.6	157	78.5	11	31	21	0.139 (0.005)	***	1.917 (0.158)	***	14.028 (0.074)	***	99.8	14.452	3.418	5.144	37.802	2.500
19.5	159	79.5	13	47	35	0.121 (0.008)	***	0.801 (0.080)	***	15.970 (0.226)	***	99.3	16.061	4.431	3.893	25.498	3.526
20.0	155	77.5	14	41	28	0.090 (0.004)	***	0.487 (0.041)	***	17.896 (0.259)	***	99.4	18.775	7.089	3.218	17.477	4.307
21.7	146	73.0	16	50	35	0.080 (0.003)	***	0.504 (0.025)	***	25.638 (0.212)	***	99.8	25.516	6.712	3.898	26.187	4.154
22.4	144	72.0	19	57	39	0.058 (0.003)	***	0.283 (0.024)	***	30.436 (0.560)	***	99.1	30.989	10.882	3.133	17.629	4.992
23.7	88	44.0	25	57	33	0.052 (0.005)	***	0.201 (0.015)	***	43.426 (0.992)	***	99.2	41.159	11.452	2.641	16.558	5.242
24.3	24	12.0	29	58	30	0.045 (0.020)	*	0.194 (0.060)	**	51.420 (4.938)	***	95.4	49.021	12.614	2.980	19.719	5.325
25.8	0	-	-	-	-	-	-	-	-	-	-	-	-	-	-	-	-	-
26.3	0	-	-	-	-	-	-	-	-	-	-	-	-	-	-	-	-	-

Appendix B:

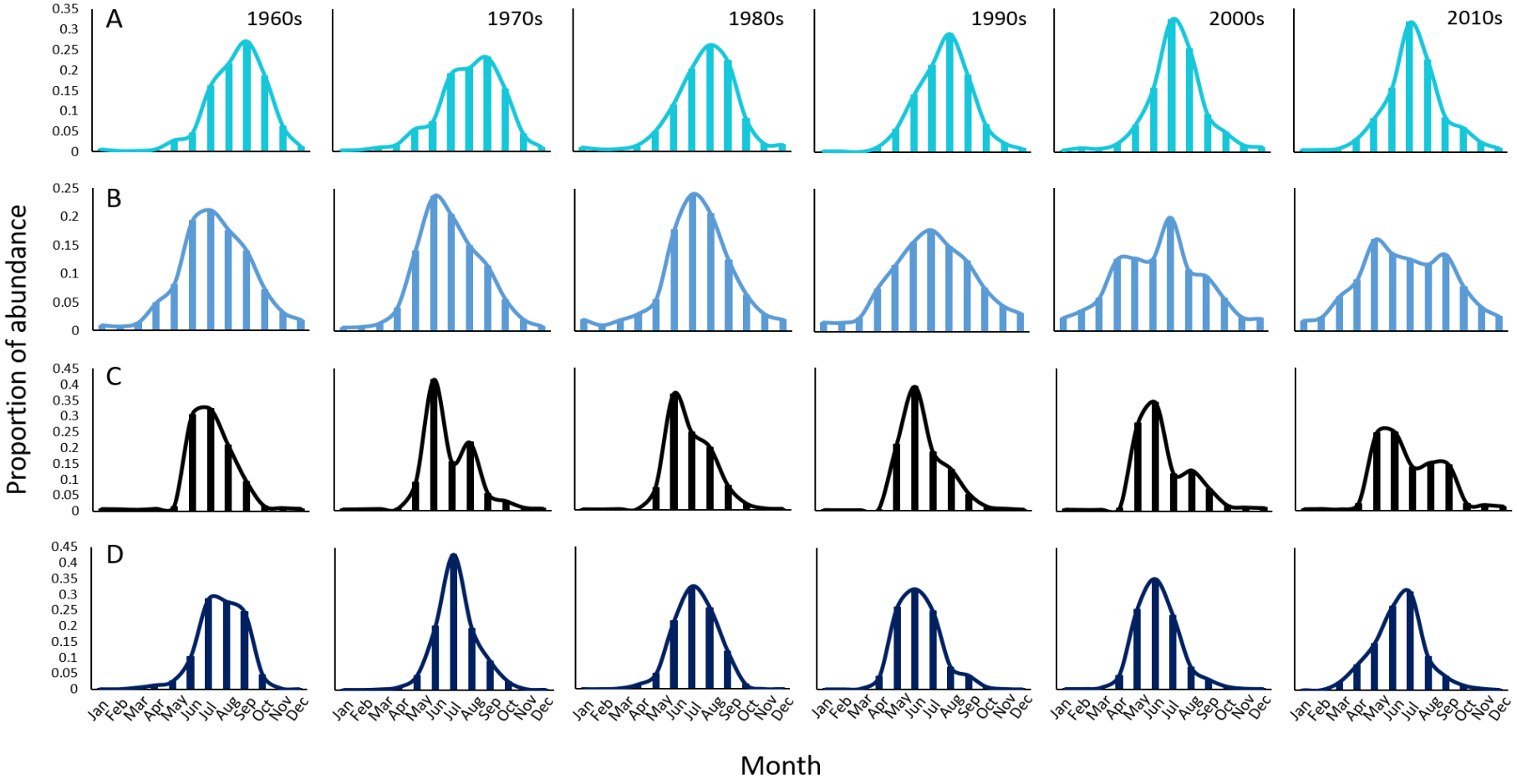

Figure B1. Pooled monthly species data by functional groups (A) dinoflagellates, (B) copepods, (C) non-copepod holozooplankton, (D) meroplankton for each decade (1960s–2010s).

Table B1. Individual taxa and total functional group abundance for each decade (1960-69, 1970-79, 1980-89, 1990-99, 2000-09, 2010-2015) identified from 20,985 Continuous Plankton Recorder samples collected between January 1960 and December 2015.

FUNCTIONAL GROUP	SPECIES	ABUNDANCE					
		1960s	1970s	1980s	1990s	2000s	2010s
Dinoflagellate	*Ceratium furca*	2,918,967	2,744,125	5,516,189	3,710,747	959,360	378,635
	Ceratium fusus	4,020,930	2,707,376	5,555,695	3,026,266	1,487,511	1,023,548
	Ceratium horridum	819,940	562,330	795,265	705,696	270,061	265,502
	Ceratium lineatum	2,064,289	1,314,951	1,513,687	1,352,350	574,162	251,940
	Ceratium longipes	1,142,239	662,927	471,623	176,242	127,536	195,695
	Ceratium macroceros	3,257,565	1,301,595	201,752	420,309	577,938	470,435
	Ceratium tripos	2,149,523	1,796,461	1,884,924	1,471,594	668,730	970,923
	Dinophysis spp.	239,320	720,876	1,247,125	727,193	346,237	246,898
	Prorocentrum spp.	6,867	43,999	257,441	235,977	113,725	64,533
	Protoperidinium spp.	393,446	517,222	610,774	533,957	247,616	217,539
TOTAL DINOFLAGELLATE		**17,013,086**	**12,371,862**	**18,054,475**	**12,360,331**	**5,372,876**	**4,085,648**
Copepod	*Acartia* spp. (unidentified)	29,928	31,707	31,801	39,131	16,542	7,610
	Calanus finmarchicus	4,318	3,430	1,529	860	619	475
	Calanus helgolandicus	586	630	732	1,035	1,844	965
	Candacia armata	8	4	13	19	38	27
	Centropages hamatus	859	786	4,005	1,187	439	424
	Corycaeus spp.	251	64	802	2,289	518	144
	Harpacticoida Total Traverse	188	267	269	278	151	48
	Labidocera wollastoni	4	8	5	13	2	3

	Metridia lucens	90	36	139	172	133	105
	Oithona spp.	22,001	11,364	14,107	9,020	3,870	2,579
	Para-Pseudocalanus spp.	51,532	40,248	31,770	36,153	16,254	8,324
	Pseudocalanus spp. Adult Atl.	10,354	10,357	9,272	7,090	4,431	2,144
	Temora longicornis	8,786	10,252	18,117	14,000	11,430	9,026
TOTAL COPEPOD		**128,905**	**109,153**	**112,561**	**111,247**	**56,271**	**31,874**
Non-copepod holozooplankton	*Chaetognatha*	730	375	374	630	446	327
	Clione limacina	44	13	7	7	4	2
	Cumacea	1	2	3	13	6	9
	Euphausiacea (Total)	967	1,015	558	360	285	113
	Evadne spp.	15,580	11,843	19,605	20,684	8,348	3,583
	Gammaridea	44	6	12	18	10	5
	Hyperiidea (Total)	171	101	184	132	203	115
	Podon spp.	2,821	5,276	8,566	8,528	4,572	3,413
	Polychaete larvae	6	5	5	8	5	6
	Tomopteris spp.	13	15	10	13	5	5
TOTAL HOLOZOOPLANKTON		**20,378**	**18,651**	**29,323**	**30,392**	**13,884**	**7,579**
Meroplankton	Cirripede larvae	496	558	545	675	799	1,064
	Cyphonautes	1,965	1,137	819	948	1,522	1,583
	Decapoda larvae	276	339	319	489	450	277
	Echinoderm larvae	37,769	32,613	58,735	107,632	124,694	73,637
	Fish eggs	65	58	25	27	84	97
	Fish larvae	105	83	109	139	113	72
TOTAL MEROPLANKTON		**40,677**	**34,788**	**60,551**	**109,909**	**127,661**	**76,730**

Table B2. Number of individual taxa (N) recorded in each decade for each functional group, estimated parameter values (with standard errors in parenthesis), ** p < 0.01, *** p < 0.001, proportion of variance explained by the model (R2) and statistical moments for each of the predicted distributions.

Functional group	Decade	N	*r* (s.e.)	Sig.	*c* (s.e.)	Sig.	*t* (s.e.)	Sig.	R^2	Mean	Median	SD	Skew	Kurtosis	Entropy
Dinoflagellates	1960	17,013,086	0.524 (0.087)	***	0.754 (0.032)	***	10.344 (0.360)	***	99.97	7.956	8.109	1.582	-0.588	0.884	2.668
	1970	12,371,862	0.649 (0.151)	**	0.615 (0.029)	***	10.786 (0.584)	***	99.97	7.539	7.729	1.771	-0.608	0.588	2.827
	1980	18,054,475	0.464 (0.052)	***	0.749 (0.029)	***	9.291 (0.266)	***	99.98	7.261	7.381	1.625	-0.391	0.836	2.720
	1990	12,360,331	0.387 (0.024)	***	0.870 (0.027)	***	8.598 (0.266)	***	99.98	7.186	7.247	1.564	0.039	2.307	2.655
	2000	5,372,876	0.325 (0.019)	***	1.055 (0.051)	***	7.570 (0.127)	***	99.95	6.816	6.764	1.612	1.322	9.043	2.603
	2010	4,085,648	0.316 (0.022)	***	0.972 (0.056)	***	7.511 (0.161)	***	99.93	6.762	6.695	1.742	1.316	8.449	2.717
Copepods	1960	128,905	0.325 (0.026)	***	0.665 (0.036)	***	8.044 (0.251)	***	99.94	6.781	6.765	2.080	0.533	3.108	3.055
	1970	109,153	0.305 (0.028)	***	0.766 (0.064)	***	7.211 (0.275)	***	99.86	6.435	6.342	2.066	1.115	5.976	2.992
	1980	112,561	0.334 (0.039)	***	0.716 (0.055)	***	8.058 (0.339)	***	99.88	6.813	6.809	1.957	0.504	3.276	2.966
	1990	111,247	0.336 (0.027)	***	0.490 (0.025)	***	8.386 (0.341)	***	99.96	6.622	6.619	2.412	0.301	1.257	3.293
	2000	56,271	0.415 (0.071)	***	0.379 (0.034)	***	8.554 (0.869)	***	99.91	5.884	5.897	2.476	0.140	0.055	3.337

	2010	31,874	0.419 (0.120)	**	0.348 (0.047)	***	9.411 (1.555)	***	99.80	6.230	6.259	2.618	0.095	-0.067	3.418
Non-copepod holozooplankton	1960	20,378	0.314 (0.033)	***	1.340 (0.140)	***	7.078 (0.189)	***	99.79	6.632	6.521	1.531	2.329	16.126	2.406
	1970	18,651	0.284 (0.040)	***	1.239 (0.232)	***	6.551 (0.301)	***	99.30	6.365	6.143	1.890	2.630	15.884	2.638
	1980	29,323	0.310 (0.040)	***	1.270 (0.177)	***	6.836 (0.251)	***	99.64	6.432	6.301	1.625	2.282	14.958	2.494
	1990	30,392	0.294 (0.024)	***	1.492 (0.178)	***	6.095 (0.149)	***	99.73	6.017	5.779	1.756	3.013	18.632	2.449
	2000	13,884	0.262 (0.022)	***	1.399 (0.221)	***	5.798 (0.184)	***	99.50	6.023	5.630	2.188	3.065	16.888	2.690
	2010	7,579	0.283 (0.046)	***	0.825 (0.153)	***	6.724 (0.486)	***	99.29	6.300	6.120	2.188	1.645	8.595	3.010
Meroplankton	1960	40,677	0.496 (0.131)	**	0.978 (0.084)	***	8.840 (0.468)	***	99.91	7.199	7.306	1.299	-0.480	1.170	2.388
	1970	34,788	0.327 (0.021)	***	1.528 (0.092)	***	7.127 (0.100)	***	99.93	6.678	6.589	1.353	2.504	18.783	2.212
	1980	60,551	0.396 (0.039)	***	1.125 (0.062)	***	7.701 (0.175)	***	99.95	6.682	6.713	1.304	0.364	4.358	2.369
	1990	109,909	0.352 (0.030)	***	1.280 (0.106)	***	6.188 (0.157)	***	99.88	5.715	5.632	1.448	1.765	11.439	2.398
	2000	127,661	0.361 (0.023)	***	1.344 (0.082)	***	6.127 (0.112)	***	99.94	5.653	5.579	1.376	1.766	11.750	2.325
	2010	76,730	0.428 (0.040)	***	0.934 (0.050)	***	7.019 (0.203)	***	99.96	5.855	5.896	1.441	0.130	2.207	2.540

Table B3. Regression analysis of the relationship between parameter estimates *r*, *c*, *t* and *median* and four different aspects of sea surface temperature (mean decadal SST, mean decadal spring SST, change in mean decadal March to May SST, and mean decadal summer SST), and time (decade) for four plankton functional groups (dinoflagellates, copepods, non-copepod holozooplankton, and meroplankton), * $p < 0.05$, ** $p < 0.01$, *** $p < 0.001$.

Sea Surface Temperature	Parameter Estimate	Functional Group	Sum of Squares	df1	df2	F	Sig.	R^2	Pearson's R	Unstandardised coefficients B
Mean decadal SST	r	Dinoflagellate	0.055	1	4	7.934	0.048*	0.665	0.815	-0.232
		Copepod	0.009	1	4	14.044	0.020*	0.778	0.882	0.095
		Holozooplankton	0.001	1	4	9.637	0.036*	0.707	0.848	-0.036
		Meroplankton	0.001	1	4	0.292	0.617	0.068	0.261	-0.036
	c	Dinoflagellate	0.112	1	4	23.994	0.008**	0.857	0.926	0.331
		Copepod	0.138	1	4	24.215	0.008**	0.858	0.926	-0.367
		Holozooplankton	0.003	1	4	0.051	0.833	0.012	0.115	-0.057
		Meroplankton	0.001	1	4	0.014	0.911	0.003	0.059	0.030
	t	Dinoflagellate	7.436	1	4	14.395	0.019*	0.783	0.885	-2.696
		Copepod	1.212	1	4	3.459	0.136	0.464	0.681	1.088
		Holozooplankton	0.675	1	4	5.623	0.077	0.584	0.764	-0.812
		Meroplankton	2.973	1	4	5.468	0.080	0.578	0.760	-1.705
	Median	Dinoflagellate	1046.300	1	4	12.436	0.024*	0.757	0.870	-31.984
		Copepod	415.760	1	4	10.123	0.033*	0.717	0.847	-20.161
		Holozooplankton	348.922	1	4	9.238	0.038*	0.678	0.835	-18.470
		Meroplankton	1663.101	1	4	12.483	0.024*	0.764	0.870	-40.324

Mean decadal spring SST	r	Dinoflagellate	0.054	1	4	7.607	0.051	0.655	0.810	-0.221
		Copepod	0.008	1	4	9.085	0.039*	0.694	0.833	0.086
		Holozooplankton	0.001	1	4	9.061	0.040*	0.694	0.833	-0.034
		Meroplankton	0.002	1	4	0.476	0.528	0.106	0.326	-0.043
	c	Dinoflagellate	0.108	1	4	19.462	0.012*	0.830	0.911	0.312
		Copepod	0.133	1	4	19.814	0.011*	0.832	0.912	-0.346
		Holozooplankton	0.000	1	4	0.004	0.955	0.001	0.030	-0.015
		Meroplankton	0.004	1	4	0.055	0.826	0.014	0.116	0.056
	t	Dinoflagellate	7.282	1	4	13.118	0.022*	0.766	0.875	-2.558
		Copepod	1.092	1	4	2.873	0.165	0.418	0.647	0.991
	Median	Holozooplankton	0.777	1	4	8.216	0.046*	0.673	0.820	-0.836
		Meroplankton	3.407	1	4	7.828	0.049*	0.662	0.814	-1.750
		Dinoflagellate	1028.206	1	4	11.598	0.027*	0.744	0.862	-30.401
		Copepod	388.383	1	4	8.108	0.047*	0.670	0.818	-18.685
		Holozooplankton	391.978	1	4	14.515	0.019*	0.784	0.885	-18.771
		Meroplankton	1815.005	1	4	19.055	0.012*	0.827	0.909	-40.392
Change in mean decadal March to May SST	r	Dinoflagellate	0.068	1	4	19.131	0.012*	0.827	0.909	-0.364
		Copepod	0.011	1	4	78.565	0.001**	0.952	0.975	0.148
		Holozooplankton	0.001	1	4	3.015	0.158	0.430	0.656	-0.039
		Meroplankton	0.000	1	4	0.007	0.937	0.002	0.042	-0.008
	c	Dinoflagellate	0.118	1	4	36.575	0.004**	0.901	0.949	0.478
		Copepod	0.129	1	4	16.308	0.016*	0.803	0.896	-0.500
		Holozooplankton	0.025	1	4	0.415	0.555	0.094	0.307	-0.222
		Meroplankton	0.014	1	4	0.222	0.662	0.052	0.229	-0.163
	t	Dinoflagellate	8.730	1	4	45.209	0.003**	0.919	0.958	-4.120
		Copepod	1.759	1	4	8.238	0.045*	0.673	0.820	1.849

		Holozooplankton	0.314	1	4	1.493	0.289	0.272	0.521	-0.781
		Meroplankton	1.610	1	4	1.820	0.249	0.313	0.559	-1.769
	Median	Dinoflagellate	1166.251	1	4	21.539	0.010*	0.843	0.918	-47.620
		Copepod	285.813	1	4	3.886	0.120	0.493	0.702	-23.574
		Holozooplankton	189.458	1	4	2.440	0.193	0.379	0.616	-19.193
		Meroplankton	1144.857	1	4	4.357	0.105	0.521	0.722	-47.181
Mean decadal summer SST	r	Dinoflagellate	0.054	1	4	7.465	0.052	0.651	0.807	-0.166
		Copepod	0.009	1	4	10.916	0.030*	0.732	0.855	0.067
		Holozooplankton	0.001	1	4	10.861	0.030*	0.731	0.855	-0.026
		Meroplankton	0.003	1	4	0.614	0.477	0.133	0.365	-0.036
	c	Dinoflagellate	0.105	1	4	16.085	0.016*	0.801	0.895	0.232
		Copepod	0.132	1	4	18.595	0.013*	0.823	0.907	-0.260
		Holozooplankton	0.004	1	4	0.062	0.816	0.015	0.124	-0.046
		Meroplankton	0.004	1	4	0.058	0.821	0.014	0.120	0.044
	t	Dinoflagellate	7.573	1	4	15.698	0.017*	0.797	0.893	-1.971
		Copepod	1.146	1	4	3.124	0.152	0.439	0.662	0.767
		Holozooplankton	0.732	1	4	6.915	0.058	0.634	0.796	-0.613
		Meroplankton	3.561	1	4	8.973	0.040*	0.692	0.832	-1.352
	Median	Dinoflagellate	1149.290	1	4	19.684	0.011*	0.831	0.912	-24.286
		Copepod	407.291	1	4	9.433	0.037*	0.702	0.838	-14.458
		Holozooplankton	381.166	1	4	12.830	0.023*	0.762	0.873	-13.986
		Meroplankton	1875.214	1	4	23.383	0.008**	0.854	0.924	-31.022
Time (decade)	r	Dinoflagellate	0.062	1	4	12.325	0.025*	0.755	0.869	-0.006
		Copepod	0.009	1	4	13.378	0.022*	0.770	0.877	0.002
		Holozooplankton	0.001	1	4	2.900	0.164	0.420	0.648	-0.001
		Meroplankton	0.001	1	4	0.264	0.635	0.062	0.249	-0.001

c	Dinoflagellate	0.091	1	4	9.372	0.038*	0.701	0.837	0.007
	Copepod	0.126	1	4	14.722	0.019*	0.786	0.887	-0.008
	Holozooplankton	0.050	1	4	0.915	0.393	0.186	0.431	-0.005
	Meroplankton	0.005	1	4	0.085	0.785	0.021	0.144	-0.002
t	Dinoflagellate	8.578	1	4	37.137	0.004**	0.903	0.950	-0.070
	Copepod	1.789	1	4	8.688	0.042*	0.685	0.827	0.032
	Holozooplankton	0.325	1	4	1.565	0.279	0.281	0.530	-0.014
	Meroplankton	2.650	1	4	4.244	0.108	0.515	0.717	-0.039
Median	Dinoflagellate	1346.414	1	4	147.880	< 0.001***	0.974	0.987	-0.877
	Copepod	234.057	1	4	2.706	0.175	0.404	0.635	-0.366
	Holozooplankton	219.657	1	4	3.134	0.151	0.439	0.663	-0.354
	Meroplankton	1632.057	1	4	11.576	0.027*	0.743	0.862	-0.966

Table B4. One-way analysis of covariance (ANCOVA) examining the main effects of functional group (dinoflagellates, copepods, non-copepod holozooplankton, and meroplankton) and four different aspects of sea surface temperature (mean decadal SST, mean decadal spring SST, change in mean decadal March to May SST, and mean summer SST), along with their interaction, on the parameter estimates *r*, *c*, *t*, and *median*, * p <0.05, ** p < 0.01, *** p < 0.001. The denominator degrees of freedom was 16 for all effects in the Table.

Covariate	Effect	Dependent Variable	Sum of Squares (Type III)	df	Mean Square	F	Sig.	Partial η^2
Mean decadal SST	Functional group	*r*	0.059	3	0.020	6.483	0.004**	0.549
		c	1.933	3	0.644	14.941	< 0.001***	0.702
		t	8.143	3	2.714	7.093	0.003**	0.571
		Median	5020.125	3	1673.375	21.030	< 0.001***	0.769
	Mean decadal SST	*r*	0.011	1	0.011	3.668	0.074	0.186
		c	0.001	1	0.001	0.024	0.879	0.001
		t	4.352	1	4.352	11.371	0.004**	0.415
		Median	3147.019	1	3147.019	39.551	< 0.001***	0.675
	Functional group * Mean decadal SST	*r*	0.056	3	0.019	6.119	0.006**	0.534
		c	0.253	3	0.084	2.377	0.108	0.308
		t	7.944	3	2.648	6.920	0.003**	0.565
		Median	327.033	3	109.011	1.472	0.260	0.216
Mean decadal spring SST	Functional group	*r*	0.058	3	0.019	6.252	0.005**	0.540
		c	1.933	3	0.644	14.922	< 0.001***	0.702
		t	8.024	3	2.675	7.302	0.003**	0.578
		Median	5020.125	3	1673.375	22.712	< 0.001***	0.782

	Mean decadal spring SST	*r*	0.012	1	0.012	4.018	0.062	0.201
		c	0.000	1	0.000	0.000	0.986	0.000
		t	4.798	1	4.798	13.099	0.002**	0.450
		Median	3258.949	1	3258.949	44.232	< 0.001***	0.700
	Functional group * Mean decadal spring SST	*r*	0.053	3	0.018	5.727	0.007**	0.518
		c	0.245	3	0.082	2.275	0.119	0.299
		t	7.760	3	2.587	7.062	0.003**	0.570
		Median	364.624	3	121.541	1.878	0.174	0.260
Change in mean decadal spring SST	Functional group	*r*	0.080	3	0.027	12.198	< 0.001***	0.696
		c	1.933	3	0.644	15.319	< 0.001***	0.708
		t	10.244	3	3.415	9.097	0.001**	0.630
		Median	5020.125	3	1673.375	14.286	< 0.001***	0.693
	Change in mean decadal spring SST	*r*	0.009	1	0.009	4.135	0.059	0.205
		c	0.021	1	0.021	0.506	0.486	0.026
		t	2.989	1	2.989	7.962	0.012*	0.332
		Median	2433.279	1	2433.279	20.773	< 0.001***	0.522
	Functional Group * Change in mean decadal spring SST	*r*	0.071	3	0.024	10.945	< 0.001***	0.672
		c	0.264	3	0.088	2.631	0.086	0.330
		t	9.424	3	3.141	8.368	0.001**	0.611
		Median	353.101	3	117.700	1.006	0.416	0.159
Mean decadal summer SST	Functional group	*r*	0.057	3	0.019	6.200	0.005**	0.538
		c	1.933	3	0.644	14.930	< 0.001***	0.702
		t	8.297	3	2.766	8.184	0.002**	0.605
		Median	5020.125	3	1673.375	25.602	< 0.001***	0.802
	Mean decadal summer SST	*r*	0.013	1	0.013	4.188	0.058	0.207
		c	0.000	1	0.000	0.011	0.919	0.001

		t	4.893	1	4.893	14.478	0.002**	0.475
		Median	3416.977	1	3416.977	52.279	< 0.001***	0.733
	Functional group * Mean decadal summer SST	*r*	0.054	3	0.018	5.84	0.007**	0.523
		c	0.244	3	0.081	2.256	0.121	0.297
		t	8.118	3	2.706	8.007	0.002**	0.600
		Median	395.983	3	131.994	2.497	0.097	0.319
Time (decade)	Functional group	*r*	0.062	3	0.021	7.971	0.002**	0.599
		c	1.933	3	0.644	15.501	< 0.001***	0.710
		t	9.812	3	3.271	10.309	0.001**	0.659
		Median	5020.125	3	1673.375	17.810	< 0.001***	0.738
	Time (decade)	*r*	0.012	1	0.012	4.504	0.050	0.066
		c	0.031	1	0.031	0.874	0.401	0.037
		t	3.590	1	3.590	11.315	0.004**	0.414
		Median	2873.604	1	2873.604	30.583	< 0.001***	0.617
	Functional group * Time (decade)	*r*	0.062	3	0.021	7.872	0.002**	0.596
		c	0.242	3	0.081	2.361	0.110	0.307
		t	9.753	3	3.251	10.247	0.001**	0.658
		Median	558.582	3	186.194	2.429	0.103	0.313

Table B5. Pairwise comparisons (Bonferroni adjustment for multiple comparisons) between plankton functional groups (dinoflagellates, copepods, non-copepod holozooplankton, and meroplankton) based on the estimated marginal means of the parameter estimates *r*, *c*, *t*, and *median*, whilst controlling for the mean value of the covariate change in mean decadal March to May sea surface temperature, * p <0.05, ** p < 0.01, *** p < 0.001.

Dependent Variable	Functional Group (I)	Functional Group (J)	Mean Difference (I-J)	95% Confidence Interval		SE	Sig.
				Lower Bound	Upper Bound		
Median	Dinoflagellates	Copepods	26.833	8.044	45.623	6.246	0.003**
		Holozooplankton	37.833	19.044	56.623	6.246	< 0.001***
		Meroplankton	31.833	13.044	50.623	6.246	0.001**
	Copepods	Holozooplankton	11.000	-7.789	29.789	6.246	0.584
		Meroplankton	5.000	-13.789	23.789	6.246	1.000
	Holozooplankton	Meroplankton	-6.000	-24.789	12.789	6.246	1.000
r	Dinoflagellates	Copepods	0.089	0.008	0.170	0.027	0.027*
		Holozooplankton	0.153	0.072	0.234	0.027	< 0.001***
		Meroplankton	0.051	-0.030	0.132	0.027	0.464
	Copepods	Holozooplankton	0.064	-0.017	0.145	0.027	0.178
		Meroplankton	-0.038	-0.119	0.043	0.027	1.000
	Holozooplankton	Meroplankton	-0.102	-0.183	-0.021	0.027	0.010*
c	Dinoflagellates	Copepods	0.275	-0.042	0.593	0.106	0.114
		Holozooplankton	-0.425	-0.743	-0.107	0.106	0.006**
		Meroplankton	-0.362	-0.680	-0.045	0.106	0.020*
	Copepods	Holozooplankton	-0.700	-1.018	-0.383	0.106	< 0.001***

		Meroplankton	-0.638	-0.956	-0.320	0.106	< 0.001***
	Holozooplankton	Meroplankton	0.062	-0.255	0.380	0.106	1.000
t	Dinoflagellates	Copepods	0.739	-0.325	1.804	0.354	0.317
		Holozooplankton	2.503	1.439	3.567	0.354	< 0.001***
		Meroplankton	1.850	0.786	2.914	0.354	< 0.001***
	Copepods	Holozooplankton	1.764	0.699	2.828	0.354	0.001**
		Meroplankton	1.110	0.046	2.174	0.354	0.038*
	Holozooplankton	Meroplankton	-0.653	-1.717	0.411	0.354	0.500

Table B6. Pairwise comparisons (Bonferroni adjustment for multiple comparisons) between plankton functional groups (dinoflagellates, copepods, non-copepod holozooplankton, and meroplankton) based on the estimated marginal means of the parameter estimates *r*, *c*, *t*, and *median*, whilst controlling for the mean value of the covariate mean decadal summer sea surface temperature, * p <0.05, ** p < 0.01, *** p < 0.001.

Dependent Variable	Functional Group (I)	Functional Group (J)	Mean Difference (I-J)	95% Confidence Interval		SE	Sig.
				Lower Bound	Upper Bound		
Median	Dinoflagellates	Copepods	26.833	14.205	39.462	4.198	< 0.001***
		Holozooplankton	37.833	25.205	50.462	4.198	< 0.001***
		Meroplankton	31.833	19.205	44.462	4.198	< 0.001***
	Copepods	Holozooplankton	11.000	-1.629	23.629	4.198	0.111
		Meroplankton	5.000	-7.629	17.629	4.198	1.000
	Holozooplankton	Meroplankton	-6.000	-18.629	6.629	4.198	1.000
r	Dinoflagellates	Copepods	0.089	-0.007	0.185	0.032	0.080
		Holozooplankton	0.153	0.057	0.249	0.032	0.001**
		Meroplankton	0.051	-0.045	0.147	0.032	0.784
	Copepods	Holozooplankton	0.064	-0.032	0.160	0.032	0.367
		Meroplankton	-0.038	-0.134	0.058	0.032	1.000
	Holozooplankton	Meroplankton	-0.102	-0.198	-0.006	0.032	0.033*
c	Dinoflagellates	Copepods	0.275	-0.054	0.605	0.110	0.138
		Holozooplankton	-0.425	-0.754	-0.095	0.110	0.008**
		Meroplankton	-0.362	-0.692	-0.033	0.110	0.027*
	Copepods	Holozooplankton	-0.700	-1.030	-0.371	0.110	< 0.001***

		Meroplankton	-0.638	-0.967	-0.308	0.110	< 0.001***
	Holozooplankton	Meroplankton	0.062	-0.267	0.392	0.110	1.000
t	Dinoflagellates	Copepods	0.739	-0.270	1.749	0.336	0.256
		Holozooplankton	2.503	1.493	3.513	0.336	< 0.001***
		Meroplankton	1.85	0.840	2.859	0.336	< 0.001***
	Copepods	Holozooplankton	1.764	0.754	2.773	0.336	< 0.001***
		Meroplankton	1.11	0.101	2.120	0.336	0.027*
	Holozooplankton	Meroplankton	-0.653	-1.663	0.356	0.336	0.416

Appendix C:

Table C1. Location (latitude and longitude) of Japanese Meteorological Agency WMO stations and the species of *Prunus* index specimens present at each location.

Latitudinal Group	Location	Latitude (°N)	Longitude (°E)	Island	Species
High (40.500-45.415°N)	Hachinohe	40.5000	141.4833	Honshu	*Prunus × yedoensis*
	Aomori	40.8217	140.7683	Honshu	*Prunus × yedoensis*
	Hakodate	41.8167	140.7533	Hokkaido	*Prunus × yedoensis*
	Esashi	41.8667	140.1333	Hokkaido	*Prunus × yedoensis*
	Urakawa	42.1667	142.7667	Hokkaido	*Prunus sargentii*
	Muroran	42.3117	140.9750	Hokkaido	*Prunus × yedoensis*
	Kutchan	42.9000	140.7667	Hokkaido	*Prunus × yedoensis*
	Obihiro	42.9217	143.2117	Hokkaido	*Prunus sargentii*
	Sapporo	43.0600	141.3283	Hokkaido	*Prunus × yedoensis*
	Nemuro	43.1924	145.3429	Hokkaido	*Prunus nipponica var. kurilensis*
	Iwamizawa	43.2000	141.7833	Hokkaido	*Prunus sargentii*
	Asahikawa	43.7567	142.3717	Hokkaido	*Prunus sargentii*
	Rumoi	43.9333	141.6333	Hokkaido	*Prunus sargentii*
	Abashiri	44.0167	144.2783	Hokkaido	*Prunus sargentii*
	Monbetsu	44.3500	143.3500	Hokkaido	*Prunus sargentii*
	Wakkanai	45.4150	141.6783	Hokkaido	*Prunus sargentii*
Mid (35.013-39.717°N)	Kyoto	35.0133	135.7317	Honshu	*Prunus × yedoensis*

Nagoya	35.1667	136.9650	Honshu	*Prunus × yedoensis*
Hikone	35.2750	136.2433	Honshu	*Prunus × yedoensis*
Tsuruga	35.3843	136.0320	Honshu	*Prunus × yedoensis*
Gifu	35.4000	136.7617	Honshu	*Prunus × yedoensis*
Yonago	35.4333	133.3333	Honshu	*Prunus × yedoensis*
Yokohama	35.4383	139.6517	Honshu	*Prunus × yedoensis*
Matsue	35.4567	133.0650	Honshu	*Prunus × yedoensis*
Maizuru	35.4667	135.3833	Honshu	*Prunus × yedoensis*
Tottori	35.4867	134.2383	Honshu	*Prunus × yedoensis*
Iida	35.5167	137.8167	Honshu	*Prunus × yedoensis*
Toyooka	35.5333	134.8333	Honshu	*Prunus × yedoensis*
Kofu	35.6667	138.5533	Honshu	*Prunus × yedoensis*
Tokyo	35.6917	139.7500	Honshu	*Prunus × yedoensis*
Choshi	35.7383	140.8567	Honshu	*Prunus × yedoensis*
Fukue	35.9833	136.1833	Goto	*Prunus × yedoensis*
Fukui	36.0550	136.2217	Honshu	*Prunus × yedoensis*
Aikawa	36.0833	136.0333	Honshu	*Prunus × yedoensis*
Saigo	36.1200	133.1960	Okinoshima	*Prunus × yedoensis*
Takayama	36.1500	137.2500	Honshu	*Prunus × yedoensis*
Kumagai	36.1500	139.3800	Honshu	*Prunus × yedoensis*
Matsumoto	36.2333	137.9667	Honshu	*Prunus × yedoensis*
Mito	36.3800	140.4667	Honshu	*Prunus × yedoensis*
Maebashi	36.4050	139.0600	Honshu	*Prunus × yedoensis*
Utsunomiya	36.5483	139.8683	Honshu	*Prunus × yedoensis*
Onahama	36.5700	140.5400	Honshu	*Prunus × yedoensis*
Kanazawa	36.5883	136.6333	Honshu	*Prunus × yedoensis*

	Nagano	36.6617	138.1917	Honshu	*Prunus × yedoensis*
	Toyama	36.7083	137.2017	Honshu	*Prunus × yedoensis*
	Takada	37.0630	138.1500	Honshu	*Prunus × yedoensis*
	Wajima	37.3833	136.9000	Honshu	*Prunus × yedoensis*
	Fukushima	37.7583	140.4700	Honshu	*Prunus × yedoensis*
	Niigata	37.8933	139.0183	Honshu	*Prunus × yedoensis*
	Yamagata	38.2550	140.3450	Honshu	*Prunus × yedoensis*
	Sendai	38.2617	140.8967	Honshu	*Prunus × yedoensis*
	Sakata	38.9167	139.8333	Honshu	*Prunus × yedoensis*
	Miyako	39.6333	141.9500	Honshu	*Prunus × yedoensis*
	Morioka	39.6983	141.1650	Honshu	*Prunus × yedoensis*
	Akita	39.7167	140.0983	Honshu	*Prunus × yedoensis*
Low (30.574-34.975°N)	Tanegashima	30.5739	130.9811	Tanegashima	*Prunus × yedoensis*
	Kagoshima	31.5550	130.5467	Kyushu	*Prunus × yedoensis*
	Nagasaki	32.7333	129.8667	Kyushu	*Prunus × yedoensis*
	Kumamoto	32.8133	130.7067	Kyushu	*Prunus × yedoensis*
	Hachijojima	33.1094	139.7914	Hachijojima	*Prunus × yedoensis*
	Oita	33.2350	131.6183	Kyushu	*Prunus × yedoensis*
	Saga	33.2650	130.3050	Kyushu	*Prunus × yedoensis*
	Shionomisaki	33.4500	135.7500	Honshu	*Prunus × yedoensis*
	Kochi	33.5667	133.5483	Shikoku	*Prunus × yedoensis*
	Fukuoka	33.5817	130.3750	Kyushu	*Prunus × yedoensis*
	Matsuyama	33.8433	132.7767	Shikoku	*Prunus × yedoensis*
	Shimonoseki	33.9483	130.9250	Honshu	*Prunus × yedoensis*
	Owase	34.0667	136.1833	Honshu	*Prunus × yedoensis*
	Tokushima	34.0667	134.5733	Shikoku	*Prunus × yedoensis*

Izuhara	34.1134	129.1729	Tsushima	*Prunus × yedoensis*
Wakayama	34.2283	135.1633	Honshu	*Prunus × yedoensis*
Takamatsu	34.3167	134.0533	Shikoku	*Prunus × yedoensis*
Sumoto	34.3500	134.9000	Honshu	*Prunus × yedoensis*
Hiroshima	34.3983	132.4617	Honshu	*Prunus × yedoensis*
Oshima	34.4400	139.4200	Oshima	*Prunus × yedoensis*
Osaka	34.6817	135.5183	Honshu	*Prunus × yedoensis*
Okayama	34.6850	133.9250	Honshu	*Prunus × yedoensis*
Nara	34.6933	135.8267	Honshu	*Prunus × yedoensis*
Kobe	34.6967	135.2117	Honshu	*Prunus × yedoensis*
Hamamatsu	34.7108	137.7261	Honshu	*Prunus × yedoensis*
Tsu	34.7333	136.5183	Honshu	*Prunus × yedoensis*
Hamada	34.9000	132.0833	Honshu	*Prunus × yedoensis*
Shizuoka	34.9750	138.4033	Honshu	*Prunus × yedoensis*

Table C2. Number of cherry trees (N) recorded in each decade for each latitudinal group, estimated parameter values (with standard errors in parenthesis), * $p < 0.05$, ** $p < 0.01$, *** $p < 0.001$, proportion of variance explained by the model (R^2) and statistical moments for each of the predicted distributions.

Latitude	Decade	N	*r* (s.e.)	Sig.	*c* (s.e.)	Sig.	*t* (s.e.)	Sig.	R^2	Mean	Median	SD	Skew	Kurtosis	Entropy
High (40.500-45.415°N)	1950	95	0.039 (0.006)	***	0.194 (0.008)	***	136.800 (1.285)	***	99.768	126.918	127.401	7.893	0.735	16.061	4.921
	1960	152	0.029 (0.003)	***	0.196 (0.007)	***	135.100 (0.912)	***	99.735	127.622	127.469	10.395	4.162	55.189	5.074
	1970	155	0.038 (0.006)	***	0.203 (0.008)	***	138.500 (1.265)	***	99.721	129.189	129.609	7.760	1.181	22.291	4.875
	1980	160	0.023 (0.001)	***	0.176 (0.007)	***	134.600 (0.765)	***	99.668	129.337	127.915	16.199	5.366	55.986	5.425
	1990	158	0.036 (0.004)	***	0.151 (0.005)	***	136.000 (1.323)	***	99.778	124.171	124.684	10.254	0.712	12.670	5.301
	2000	147	0.045 (0.007)	***	0.135 (0.004)	***	139.900 (1.760)	***	99.807	124.408	125.320	10.329	-0.439	2.907	5.359
	2010	73	0.022 (0.002)	***	0.178 (0.009)	***	128.700 (0.840)	***	99.484	124.778	122.672	18.356	5.415	51.686	5.495
Mid (35.013-39.717°N)	1950	272	0.030 (0.002)	***	0.196 (0.008)	***	100.500 (0.680)	***	99.626	95.950	94.777	13.571	4.616	44.305	5.265
	1960	390	0.032 (0.002)	***	0.206 (0.008)	***	103.500 (0.650)	***	99.711	98.032	97.356	11.533	4.454	47.412	5.114
	1970	390	0.030 (0.002)	***	0.184 (0.008)	***	103.900 (0.834)	***	99.544	98.514	97.561	13.297	4.288	42.008	5.308
	1980	390	0.032 (0.002)	***	0.158 (0.005)	***	106.100 (0.723)	***	99.785	98.354	97.943	12.670	2.920	28.895	5.425
	1990	390	0.032 (0.002)	***	0.179 (0.006)	***	100.300 (0.671)	***	99.710	94.447	93.644	12.873	3.875	37.475	5.321

	2000	366	0.035 (0.003)	***	0.161 (0.007)	***	99.941 (1.099)	***	99.530	92.331	91.978	12.148	2.710	26.463	5.385
	2010	222	0.027 (0.001)	***	0.181 (0.007)	***	95.386 (0.598)	***	99.619	92.348	90.240	16.963	4.519	37.434	5.493
Low (30.574-34.975°N)	1950	186	0.034 (0.003)	***	0.310 (0.018)	***	90.404 (0.668)	***	99.521	87.727	86.644	10.630	6.172	66.614	4.649
	1960	273	0.134 (0.049)	*	0.263 (0.008)	***	100.300 (1.776)	***	99.931	88.963	89.631	4.913	-0.955	1.926	4.255
	1970	279	0.040 (0.002)	***	0.351 (0.011)	***	92.456 (0.336)	***	99.881	88.735	88.412	7.125	6.222	85.331	4.304
	1980	280	0.050 (0.010)	***	0.219 (0.013)	***	95.815 (1.518)	***	99.522	87.757	88.096	7.128	0.846	14.213	4.769
	1990	280	0.137 (0.059)	*	0.245 (0.009)	***	97.428 (2.264)	***	99.889	85.359	86.071	5.255	-0.950	1.907	4.353
	2000	263	0.043 (0.004)	***	0.283 (0.010)	***	88.917 (0.562)	***	99.809	83.959	83.807	7.331	4.132	52.453	4.561
	2010	171	0.040 (0.004)	***	0.258 (0.013)	***	88.298 (0.832)	***	99.630	83.535	83.145	8.768	4.403	50.104	4.754

Table C3. Regression analysis of the relationship between parameter estimates *r*, *c*, *t* and *median* and nine categories of air temperature (mean decadal January, mean decadal February, mean decadal March, mean decadal April, change in mean decadal December to February, change in mean decadal January to March, change in mean decadal February to April, average February & March, and average March & April), and time (decade) for three latitudinal groupings of cherry tree first blossoming (low - 30.574-34.975°N, mid - 35.013-39.717°N, and high - 40.500-45.415°N), * $p < 0.05$, ** $p < 0.01$, *** $p < 0.001$.

Mean decadal temperature (°C)	Parameter Estimate	Latitude	Sum of Squares	df1	df2	F	Sig.	R^2	Pearson's R	Unstandardised coefficients B
January	r	High	0.000	1	5	0.320	0.596	0.060	0.245	0.004
		Mid	0.000	1	5	0.004	0.953	0.001	-0.028	0.000
		Low	0.000	1	5	0.019	0.896	0.004	-0.061	-0.006
	c	High	0.003	1	5	20.277	0.006**	0.802	-0.896	-0.041
		Mid	0.000	1	5	1.726	0.246	0.257	-0.507	-0.018
		Low	0.000	1	5	0.036	0.857	0.007	-0.084	-0.007
	t	High	0.083	1	5	0.005	0.944	0.001	0.033	0.215
		Mid	35.882	1	5	4.825	0.079	0.491	-0.701	-5.102
		Low	23.907	1	5	1.175	0.328	0.190	-0.436	-4.034
	Median	High	16.561	1	5	5.118	0.073	0.506	-0.711	-3.042
		Mid	38.033	1	5	11.817	0.018*	0.703	-0.838	-5.252
		Low	20.218	1	5	6.977	0.046*	0.583	-0.763	-3.709
February	r	High	0.000	1	5	1.013	0.360	0.169	0.411	0.005
		Mid	0.000	1	5	0.363	0.573	0.068	-0.260	-0.001
		Low	0.001	1	5	0.267	0.628	0.051	-0.225	-0.016

	c	High	0.002	1	5	4.585	0.085	0.478	-0.692	-0.025
		Mid	0.000	1	5	0.177	0.692	0.034	-0.185	-0.005
		Low	0.000	1	5	0.127	0.736	0.025	0.157	0.011
	t	High	0.027	1	5	0.002	0.968	0.000	0.019	0.095
		Mid	58.781	1	5	20.577	0.006**	0.805	-0.897	-4.659
		Low	56.543	1	5	4.091	0.099	0.450	-0.671	-4.857
	Median	High	17.161	1	5	5.508	0.066	0.524	-0.724	-2.402
		Mid	47.788	1	5	37.708	0.002**	0.883	-0.940	-4.201
		Low	26.951	1	5	17.375	0.009**	0.777	-0.881	-3.353
March	r	High	0.000	1	5	0.035	0.858	0.007	-0.084	-0.001
		Mid	0.000	1	5	0.671	0.450	0.118	-0.344	-0.001
		Low	0.000	1	5	0.010	0.924	0.002	0.045	0.003
	c	High	0.002	1	5	5.387	0.068	0.519	-0.720	-0.027
		Mid	0.000	1	5	0.152	0.713	0.029	-0.172	-0.003
		Low	0.002	1	5	1.025	0.358	0.170	-0.412	-0.029
	t	High	12.661	1	5	0.979	0.368	0.164	-0.405	-2.126
		Mid	61.959	1	5	27.898	0.003**	0.848	-0.921	-3.733
		Low	21.520	1	5	1.033	0.356	0.171	-0.414	-3.019
	Median	High	30.148	1	5	58.167	0.001**	0.921	-0.960	-3.280
		Mid	49.192	1	5	49.857	0.001**	0.909	-0.953	-3.326
		Low	28.059	1	5	21.104	0.006**	0.808	-0.899	-3.448
April	r	High	0.000	1	5	0.344	0.583	0.064	-0.254	-0.004
		Mid	0.000	1	5	1.359	0.296	0.214	-0.462	-0.001
		Low	0.000	1	5	0.022	0.887	0.004	-0.067	-0.007
	c	High	0.001	1	5	1.373	0.294	0.215	-0.464	-0.022
		Mid	0.000	1	5	0.221	0.658	0.042	-0.206	-0.005

		Low	0.001	1	5	0.599	0.474	0.107	-0.327	-0.034
	t	High	31.386	1	5	3.415	0.124	0.406	-0.637	-4.400
		Mid	55.202	1	5	15.452	0.011*	0.756	-0.869	-3.914
		Low	28.493	1	5	1.466	0.280	0.227	-0.476	-5.176
	Median	High	30.607	1	5	71.758	< 0.001***	0.935	-0.967	-4.345
		Mid	42.031	1	5	17.376	0.009**	0.777	-0.881	-3.415
		Low	27.842	1	5	20.276	0.006**	0.802	-0.896	-5.116
Change in December to February	r	High	0.000	1	5	2.202	0.198	0.306	0.553	0.009
		Mid	0.000	1	5	0.005	0.949	0.001	-0.030	0.001
		Low	0.004	1	5	2.607	0.167	0.343	-0.585	-0.094
	c	High	0.002	1	5	4.773	0.081	0.488	-0.699	-0.032
		Mid	0.000	1	5	0.080	0.788	0.016	-0.126	-0.007
		Low	0.002	1	5	1.139	0.335	0.186	0.431	0.066
	t	High	2.807	1	5	0.188	0.682	0.036	0.191	1.252
		Mid	22.368	1	5	2.206	0.198	0.306	-0.553	-6.468
		Low	92.879	1	5	14.171	0.013*	0.739	-0.860	-13.646
	Median	High	12.947	1	5	3.271	0.130	0.395	-0.629	-2.688
		Mid	19.436	1	5	2.802	0.155	0.359	-0.599	-6.029
		Low	20.241	1	5	6.996	0.046*	0.583	-0.764	-6.370
Change in January to March	r	High	0.000	1	5	1.518	0.273	0.233	-0.483	-0.010
		Mid	0.000	1	5	1.814	0.236	0.266	-0.516	-0.002
		Low	0.000	1	5	0.117	0.746	0.023	0.151	0.018
	c	High	0.000	1	5	0.000	0.987	0.000	-0.008	0.000
		Mid	0.000	1	5	0.155	0.710	0.030	0.173	0.005
		Low	0.004	1	5	2.287	0.191	0.314	-0.560	-0.064
	t	High	42.648	1	5	6.147	0.056	0.551	-0.743	-6.725

		Mid	50.689	1	5	11.327	0.020*	0.694	-0.833	-5.300
		Low	1.601	1	5	0.065	0.810	0.013	-0.113	-1.334
	Median	High	14.889	1	5	4.170	0.097	0.455	-0.674	-3.973
		Mid	31.569	1	5	6.998	0.046*	0.583	-0.764	-4.183
		Low	8.030	1	5	1.505	0.275	0.231	-0.481	-2.987
Change in February to April	r	High	0.000	1	5	7.476	0.041*	0.599	-0.774	-0.012
		Mid	0.000	1	5	0.911	0.384	0.154	-0.393	-0.002
		Low	0.001	1	5	0.469	0.524	0.086	0.293	0.035
	c	High	0.001	1	5	1.284	0.309	0.204	0.452	0.021
		Mid	0.000	1	5	0.028	0.873	0.006	-0.075	-0.003
		Low	0.004	1	5	2.944	0.147	0.371	-0.609	-0.069
	t	High	30.994	1	5	3.344	0.127	0.401	-0.633	-4.180
		Mid	1.689	1	5	0.118	0.745	0.023	-0.152	-1.135
		Low	41.367	1	5	2.454	0.178	0.329	0.574	6.741
	Median	High	0.006	1	5	0.001	0.977	0.000	0.013	0.058
		Mid	0.662	1	5	0.062	0.813	0.012	-0.111	-0.711
		Low	7.401	1	5	1.355	0.297	0.213	0.462	2.851
February & March	r	High	0.000	1	5	0.169	0.698	0.033	0.181	0.002
		Mid	0.000	1	5	0.565	0.486	0.102	-0.319	-0.001
		Low	0.000	1	5	0.046	0.839	0.009	-0.095	-0.007
	c	High	0.002	1	5	6.964	0.046*	0.582	-0.763	-0.030
		Mid	0.000	1	5	0.175	0.693	0.034	-0.184	-0.004
		Low	0.000	1	5	0.090	0.776	0.018	-0.133	-0.010
	t	High	3.257	1	5	0.220	0.659	0.042	-0.205	-1.148
		Mid	65.147	1	5	41.141	0.001**	0.892	-0.944	-4.460
		Low	40.952	1	5	2.418	0.181	0.326	-0.571	-4.364

	Median	High	27.004	1	5	23.541	0.005**	0.825	-0.908	-3.306
		Mid	52.257	1	5	139.844	< 0.001***	0.965	-0.983	-3.994
		Low	30.418	1	5	35.458	0.002**	0.876	-0.936	-3.761
March & April	r	High	0.000	1	5	0.134	0.730	0.026	-0.161	-0.002
		Mid	0.000	1	5	0.982	0.367	0.164	-0.405	-0.001
		Low	0.000	1	5	0.000	1.000	0.000	0.000	0.000
	c	High	0.001	1	5	3.213	0.133	0.391	-0.625	-0.027
		Mid	0.000	1	5	0.187	0.683	0.036	-0.190	-0.004
		Low	0.002	1	5	0.869	0.394	0.148	-0.385	-0.033
	t	High	20.767	1	5	1.835	0.233	0.269	-0.518	-3.173
		Mid	60.206	1	5	23.412	0.005**	0.824	-0.908	-3.922
		Low	25.059	1	5	1.246	0.315	0.199	-0.447	-3.967
	Median	High	31.950	1	5	202.166	< 0.001***	0.976	-0.988	-3.936
		Mid	46.895	1	5	32.430	0.002**	0.866	-0.931	-3.461
		Low	28.961	1	5	25.197	0.004**	0.834	-0.913	-4.265
Decade	r	High	0.000	1	5	0.207	0.668	0.040	-0.200	0.000
		Mid	0.000	1	5	0.009	0.929	0.002	-0.042	0.000
		Low	0.000	1	5	0.063	0.811	0.013	-0.112	0.000
	c	High	0.002	1	5	4.433	0.089	0.470	-0.686	-0.001
		Mid	0.001	1	5	3.035	0.142	0.378	-0.042	0.000
		Low	0.002	1	5	0.925	0.380	0.156	-0.395	-0.001
	t	High	10.566	1	5	0.791	0.414	0.137	-0.370	-0.061
		Mid	24.255	1	5	2.485	0.176	0.332	-0.576	-0.093
		Low	20.761	1	5	0.990	0.365	0.165	-0.406	-0.086
	Median	High	19.573	1	5	7.433	0.041*	0.598	-0.773	-0.084
		Mid	28.569	1	5	5.589	0.064	0.528	-0.727	-0.101

	Low	21.415	1	5	8.056	0.036*	0.617	-0.786	-0.087